IDENTIFICATION OF MODEL AIRCRAFT DYNAMIC USING FLIGHT TESTING

by

Edi Sofyan

Thesis submitted in accordance with the regulation

for the degree of master engineering.

Supervised by Robert Danaher

Aerospace Engineering Department

Royal Melbourne Institute of Technology

Victoria, Australia

September 1996

Declaration

I, Edi sofyan, declare that this thesis is my own work, except where dully acknowledged to others, and has not been submitted previously, in whole or in part, in respect to any other award.

All work has been carried out since the official date of commencement of this research program.

Trade of manufacture's names are used where essentials to this applied research. Endorsement of those names is not intended.

E. Sofyan

September, 1996

Acknowledgements

The author wishes to express sincere appreciation to the following people for their inspiration and help during the work of this thesis:

Robert Danaher

Dr Cees Bil

Associate Professor John Kneen

Mal Wilson

Lachlan Thompson

Professor Vladislav Klein

and the MAFV personnel,

and for their support, tolerance and understanding,

my wife Andhika Purnamasari and my daughter Amanda Haruminori Sofyan.

TABLE OF CONTENTS

LIST OF FIGURES

LIST OF TABLES

Abstract

The project involves estimating stability and control derivatives of a remote control aircraft model from flight test data using parameter identification techniques. The stability and control derivatives are inferred based on the modelled vehicle's dynamic equations and the measured inputs and aircraft responses during a predetermined manoeuvre.

Computer programs necessary to perform the identification processes have been developed using Matlab, a matrix manipulation software. The identification from simulated data has been carried out to assess the effectiveness of the identification algorithms. In addition, instrumentation and data acquisition systems for conducting the flight test program have also been developed in collaboration with the Computer System Engineering Department, RMIT. Implementation challenges encountered during the development of the whole flight test systems are presented.

The capability of the whole system was then demonstrated by conducting a dynamic flight test program on the Telemaster T240 aircraft model. Six longitudinal and fifteen lateral derivatives have been extracted from several recorded flight test data. The estimated derivatives will then be used in the design of flight control system for the aircraft.

The project has shown that the dynamic of a model aircraft can be estimated with a reasonable confidence using flight testing procedure.

Nomenclature:

$\dot{a}$	= angle of attack rate (rad/s)
$\dot{q}_0$	= initial pitch rate (rad/s)
$\dot{p}, \dot{r}$	= roll and pitch accelerations (rad/s^2)
$\dot{b}$	= sideslip rate, roll rate and pitch rate (rad/s)
ρ	= air density (kg/m^3)
α	= angle of attack (rad)
δ	= control surface deflection
ψ	= initial yaw angle (rad)
θ	= pitch angle (rad)
ϕ	= roll angle (rad)
β	= sideslip angle (rad)
$\dot{p}, \dot{q}, \dot{r}$	= roll, pitch and yaw acceleration (rad/s^2)
a	= acceleration (m/s^2)
A, B, C, D	= system matrices
b	= wingspan (m)
c	= wing chord (m)
Cl_β, Cl_p, Cl_r, $Cl_{\delta aileron}$, $Cl_{\delta rudder}$	= non-dimensional roll derivatives
Cm_α, Cm_q, $Cm_{\delta Elevator}$	= non-dimensional pitch derivatives
Cn_β, Cn_p, Cn_r, $Cn_{\delta aileron}$, $Cn_{\delta rudder}$	= non-dimensional yaw derivatives
C_t	= thrust coefficient = thrust/(ρ n^2 D$^{4)}$
Cy_β, Cy_p, Cy_r, $Cy_{\delta aileron}$, $Cy_{\delta rudder}$	= non-dimensional side-force derivatives
Cz_α, Cz_q, $Cz_{\delta Elevator}$	= non-dimensional lift derivatives
D	= propeller diameter (m)
g	= gravity constant (9.81 kg/m^3)
I_x, I_y, I_z, I_{xz}	= moment of inertia (kgm^2)
J	= advance ratio = nV/D
L	= aircraft length.
l	= length of the string (meter)
l_x	= vertical distance between cg and pivot point in bifilar suspension experiment
l_y	= vertical distance between cg and pivot point in knife edge experiment
m	= mass (kg)
m	= number of degree of freedom
M	= mass of the model (Kg)
n	= engine rotational speed (rev/s)
N	= number of time points
p	= angular rate about X-body axis (rad/s)
p,q,r	= roll, pitch and yaw rates (rad/s)
r	= angular rate about Z-body axis (rad/s)
R	= distance of the strings from the centre of gravity
Rx,Ry and Rz	= radius of gyrations.
S	= wing area (m^2)
t	= time (s)
T	= period of oscillation (seconds)

V_0	= airspeed (m/s)
w	= weight (N)
X_{ax}, X_{ay}, X_{az}, $X_{a\alpha}$, $X_{a\beta}$	= distances of instruments forward of the centre of gravity (m)
X_{cg}, Y_{cg}, Z_{cg}	= centre of gravity locations (m)
$\tilde{z}$	= measurement vector
$\overline{Rx} = \frac{2Rx}{b}, \overline{Ry} = \frac{2Ry}{L}, \overline{Rz} = \frac{2Rz}{(b+L)/2}$	= non-dimensional moment of inertias

Subscripts

a	= aileron
al	= left aileron
am	= apparent mass
ar	= right aileron
e	= elevator
i	= time index
m	= measured
o	= bias or initial condition
p,q,r,α, $\dot{a}$,β, $\dot{b}$,δ,δ_a,δ_e,δ_r	= derivatives with respect to indicated quantity
r	= rudder

Superscript

T	= matrix transpose

Dimensional Stability and Control Derivatives Definitions:

$$X_u = \frac{rUS}{2m} Cx_u \qquad Z_u = \frac{rUS}{2m} Cz_u \qquad M_u = \frac{rUSc}{2I_{yy}} Cm_u$$

$$X_a = \frac{rU^2 S}{2m} Cx_a \qquad Z_a = \frac{rU^2 S}{2m} Cz_a \qquad M_a = \frac{rU^2 Sc}{2I_{yy}} Cm_a$$

$$X_q = \frac{rUSc}{4m} Cx_q \qquad Z_q = \frac{rUSc}{4m} Cz_q \qquad M_q = \frac{rUSc^2}{4I_{yy}} Cm_q$$

$$X_{\P Elevator} = \frac{rU^2 S}{2m} Cx_{\P Elevator} \qquad Z_{\P Elevator} = \frac{rU^2 S}{2m} Cz_{\P Elevator} \qquad M_{\P Elevator} = \frac{rU^2 Sc}{2I_{yy}} Cm_{\P Elevator}$$

$$Y_b = \frac{rU^2 S}{2m} Cy_b \qquad L_b = \frac{rU^2 Sb}{2I_{xx}} Cl_b \qquad N_b = \frac{rU^2 Sb}{2I_{zz}} Cn_b$$

$$Y_p = \frac{rUSb}{4m} Cy_p \qquad L_p = \frac{rUSb^2}{4I_{xx}} Cl_p \qquad N_p = \frac{rUSb^2}{4I_{zz}} Cn_p$$

$$Y_r = \frac{rUSb}{4m} Cy_r \qquad L_r = \frac{rUSb^2}{4I_{xx}} Cl_r \qquad N_{rb} = \frac{rUSb^2}{4I_{zzz}} Cn_r$$

$$Y_{\P Aileron} = \frac{rU^2 S}{2m} Cy_{\P Aileron} \qquad L_{\P Aileron} = \frac{rU^2 Sb}{2I_{xx}} Cl_{\P Aileron} \qquad N_{\P Aileron} = \frac{rU^2 Sb}{2I_{zzz}} Cn_{\P Aileron}$$

$$Y_{\P Rudder} = \frac{rU^2 S}{2m} Cy_{\P Rudder} \qquad L_{\P Rudder} = \frac{rU^2 Sb}{2I_{xx}} Cl_{\P Rudder} \qquad N_{\P Rudder} = \frac{rU^2 Sb}{2I_{zzz}} Cn_{\P Rudder}$$

where:

$$Cx_u = \frac{\P Cx}{\P\left(\frac{u}{U}\right)} \qquad Cz_u = \frac{\P Cz}{\P\left(\frac{u}{U}\right)} \qquad Cm_u = \frac{\P Cm}{\P\left(\frac{u}{U}\right)}$$

$$Cx_a = \frac{\P Cx}{\P\left(\frac{w}{U}\right)} \qquad Cz_a = \frac{\P Cz}{\P\left(\frac{w}{U}\right)} \qquad Cm_a = \frac{\P Cm}{\P\left(\frac{w}{U}\right)}$$

$$Cx_q = \frac{\P Cx}{\P\left(qc/2U\right)} \qquad Cz_q = \frac{\P Cz}{\P\left(qc/2U\right)} \qquad Cm_q = \frac{\P Cm}{\P\left(qc/2U\right)}$$

$$Cx_{\P Elevator} = \frac{\P Cx}{\P_{Elevator}} \qquad Cz_{\P Elevator} = \frac{\P Cz}{\P_{Elevator}} \qquad Cm_{\P Elevator} = \frac{\P Cm}{\P_{Elevator}}$$

$$Cy_b = \frac{\P Cy}{\P\left(\frac{v}{U}\right)} \qquad Cl_b = \frac{\P Cl}{\P\left(\frac{v}{U}\right)} \qquad Cn_b = \frac{\P Cn}{\P\left(\frac{v}{U}\right)}$$

$$Cy_p = \frac{\P Cy}{\P\left(pb/2U\right)} \qquad Cl_p = \frac{\P Cl}{\P\left(pb/2U\right)} \qquad Cn_p = \frac{\P Cn}{\P\left(pb/2U\right)}$$

$$Cy_r = \frac{\P Cy}{\P\left(\frac{rb}{2U}\right)} \qquad Cl_r = \frac{\P Cl}{\P\left(\frac{rb}{2U}\right)} \qquad Cn_r = \frac{\P Cn}{\P\left(\frac{rb}{2U}\right)}$$

$$Cy_{\P Aileron} = \frac{\P Cx}{\P Aileron} \qquad Cl_{\P Aileron} = \frac{\P Cl}{\P Aileron} \qquad Cn_{\P Aileron} = \frac{\P Cn}{\P Aileron}$$

$$Cy_{\P Rudder} = \frac{\P Cx}{\P Rudder} \qquad Cl_{\P Rudder} = \frac{\P Cl}{\P Rudder} \qquad Cn_{\P Rudder} = \frac{\P Cn}{\P Rudder}$$

1. Introduction

Dynamic characteristics of an aircraft are normally described in terms of its stability and control derivative values. These values are determined either theoretically (empirical or semi-empirical, computational fluid dynamics) or experimentally (wind tunnel or flight test).

This project involves estimating stability and control derivatives of a model aircraft from flight data using parameter identification (PI) techniques. The unknown stability and control derivatives are inferred from the modelled vehicle dynamic equations and the measured inputs and system responses during flight manoeuvres. In contrast to conventional estimation, the PI technique provides for reduced test time, *more flexibility* in manoeuvre requirements and more parameters (including those unobtainable using conventional techniques) are obtained from a single manoeuvre.

The significance aspects of the project are: First, the obtained derivatives will be used in the design of an autonomous flight control system. The design of the control system is currently carried out by another post-graduate student (Valentinis, 1996). Second, the project will assess the capability of the flight test instrumentation systems designed in collaboration with the Computer System Department at RMIT (Kneen, 1994). Third, this project will provide a statistical stability and control derivative data base extracted from flight test measurements which will extend the confidence in existing stability and control derivative estimation techniques when applied to UAV's (Unmanned Air Vehicles) and other small flight vehicles.

There are many potential benefits in using UAV as aerial platforms for either commercial or research applications. UAVs have a low operating cost as compared to manned aircraft operations. UAVs can perform hazardous tasks such as close monitoring of fires, hurricane tracking, observation of radiation-contaminated areas and volcano eruptions. UAVs are suited to long endurance tasks that

are generally tiring and strenuous on aircraft crew. The present state of technology allows the development of relatively small, lightweight and accurate remote sensing equipment that will provide a wide range of different payload packages suitable for incorporation into UAVs.

With the advent of a reliable and low cost GPS (Global Positioning System), an autonomous unmanned air vehicle becomes technically and economically feasible for survey or surveillance missions. With self-contained navigation and control systems these vehicles have the potential to carry out their mission according to a pre-programmed set of instructions. Future developments on built-in intelligence open the way to true autonomous missions, whereby the on-board equipment senses anomalies and can take independent action. The potential benefit of UAV technology has prompted The Sir Lawrence Wackett Centre for Aerospace Design Technology to initiate a project with the objective to develop an unmanned autonomous flight vehicle, referred to as Multi-Purpose Autonomous Flight Vehicle (MAFV). The vehicle will be designed to suit a wide range of missions, such as aerial photography, coastal surveillance, geological and agricultural survey, atmospheric research and weather soundings (Thompson, Abanteriba and Bill, 1993). The Division of Atmospheric Research of the CSIRO in Australia has expressed particular interest in the MAFV as a potential platform for their equipment for monitoring of atmospheric pollution. With a typical payload of 20 Kg the aim is to achieve mission endurance ranging from 3 hours at 60,000ft to 5 days at 7,500ft. The design of the MAFV will be in close co-operation with CSIRO to accommodate their mission requirements. One of their specific missions is to measure the atmospheric abundance of $C0_2$ and its stable isotopes (The Wackett Centre, 1995).

In its development stage, a Telemaster T240 model aircraft has been purchased and assembled for use as an electronic test bed for the full scale MAFV. The model will perform several flight trials for

dynamic flight testing and autonomous flight testing. This project deals with the dynamic flight testing of the T240 model aircraft to obtain the stability and control derivatives of the vehicle.

The specific objectives of this project are:

- To provide stability and control derivative values for the aircraft model.
- To determine the necessary measurements and flight manoeuvre required in estimating the stability derivatives.
- To prepare the instrumentation and data acquisition system.
- To determine inertial characteristics (mass, centre of gravity and inertia).
- To select an appropriate model structure and parameter identification algorithms.
- To develop a computer program to extract stability and control derivatives from recorded flight test data.
- To determine the accuracy or confidence of the parameters obtained.

The project has several limitations that include:

- Only dominant linear stability and control derivatives are to be estimated.
- No coupling between longitudinal and lateral modes are considered.
- Limited accuracy and number of sensors are available.
- Limited time and budget for conducting the experiments.

Parts of the thesis have been presented at the IASE'95 (Sofyan, 1995) and ISASTI'96 (Sofyan, 1996) seminars.

The content of the thesis is divided into 3 major sections. The first section provides an introduction to the project (chapter 1), literature review (chapter 2) and method of flight testing (chapter 3). The next section addresses the works undertaken prior to the actual flight test (chapter 4 to 6) and some hardware problems encountered during the course of this project (chapter 7). The last section presents the simulation and flight test results (chapter 8 and 9), followed by discussion and conclusion. All the raw data from the pre-flight, flight and post-flight are collected in the appendices and computer files. A computer disc that is included with the thesis contains a number of Matlab script programs necessary to process the flight data.

2. Literature review

In the past, the role of model aircraft in dynamic flight testing was not so popular. The instrumentation was either too heavy or too large to be housed in the RPV (Reed, 1974). Also, the technology in the *off the shelf* aircraft modelling was not as advanced as today. Now however, an inexpensive and a reliable small RPV can be easily built in which necessary flight test instrumentation can be incorporated. Hamony (1994) reported on a state of the art, light-weight, low power, miniaturised instrumentation system, which is used to gather information during flight test.

Beside the progress in the instrumentation systems, several common problems in using a radio controlled model aircraft to conduct dynamic flight testing, still remain (Budd, 1993). These problems include:

- Inability of the model to perform a required manoeuvre (Coleman, 1981).
- Limited visual range and lack of flying conditions (Wong, 1989).
- Signal interferences (Hamory, 1994)
- Errors in the obtained sensor data (Coleman, 1981). Typical errors in the sensor mostly originate from engine and other structural vibration, cg offsets and misalignments, transducer errors, coupled longitudinal and lateral motions, and the presence of air turbulence (Budd, 1993).

Despite the above problems, some have reported successful flight test programs in determining several dominant stability and control derivatives. NASA has been using RPV's extensively to study the dynamic behaviour of their research aircraft, such as the X-29 drop model (Klein, 1975), F-15 model (Iliff, 1976) and HIMAT (Mathew, 1981). The US-NAVY was also researching with their

RPV (Howard, 1991). In England, British Aerospace conducted a similar flight test program to extract stability and control derivatives of their STABILEYE RPV (Coleman, 1981). In Australia, Sydney University has developed a series of small RPV for aerodynamic research (Wong 1989, and Newman 1995).

Present and future research in this field concentrates on 3 different key areas. First, the development in the instrumentation systems (Hamory, 1994); second, the development of system modelling and various estimation techniques for the extraction of the derivatives (Iliff, 1989). A recent research topic in the estimation technique is in the application of computational neural networks to identify several aerodynamic derivatives (Linse, 1993); and third, the search for an optimal input design and a more practical flight test manoeuvres (Plaetschke, 1979).

The following sections survey the above three key areas, namely instrumentation, flight data analysis and input forms.

2.1 Instrumentation

The flight test instrumentation includes sensors, data acquisition system (DAS) and Telemetry systems. With the present technology, it is possible to have a flight test instrumentation system that is small and light. Most components are commercially available for model aircraft hobbiers to construct their models. These components have been used by the University of Sydney (Wong, 1989) and NASA (Hamory, 1994).

2.1.1 (Sensors)

Parameters to be measured in flight can be categorised in to two groups; inertial (or dynamic) data and air data. Typical sensors needed to extract stability and control derivatives are given in Table 2-1. This table is summarised from Maine (1986), Wong (1989), and Yip (1992).

Table 2-1: Sensors frequently used in the extraction of stability & control derivatives.

No	Quantity measured	Transducer	Range	Resolution	Level of Importance
1	Longitudinal acceleration,	Accelerometer	±10g	±0.02g	Secondary
2	Lateral acceleration	Accelerometer	±5g	±0.02g	Primary
3	Vertical acceleration	Accelerometer	±10g	±0.02g	Primary
4	Pitching velocity	Rate gyro	±250°/s	±10°/s	Primary
5	Yawing velocity	Rate gyro	±250°/s	±10°/s	Primary
6	Rolling velocity	Rate gyro	±450°/s	±10°/s	Primary
7	Euler angles	Attitude gyros			Secondary
8	Angle of attack	Flow direction, velocity sensor	±25°	$\pm 0.25^0$	Primary
9	Angle of sideslip	Flow direction, velocity sensor	±30°	$\pm 0.25^0$	Primary
10	Control deflections	Control position transducer	+40° to -10°	±0.2°	Primary
11	Airspeed	Pressure transducer	0 to 5psi or 0 to 60 knt		Primary
12	Altitude	Pressure transducer	0 to 15 psi		Secondary
13	Air temperature	Thermometer			Secondary
14	Engine rotational speed	Tachometer			Secondary
15	Time	Digital clock			Primary

The type of sensor needed depends upon the purpose of the flight test, and the capability of the instrumentation systems. Coleman (1981) with his STABILEYE RPV conducted flight tests with only body rates and control deflection measurements. With this limited number of sensors, he failed to get several dominant lateral derivatives. He then proposed to add a lateral accelerometer to the aircraft.

Due to the limitation in the number of sensors in their first flight test, Howard (1991) at the US-NAVY, measured only engine rpm and angle of attack onboard the vehicle. The airspeed was

measured by observation on the ground. Only lift and drag plots were obtained from this experiment, and a significant scatter in the drag measurement was apparent.

The method of flight data analysis also dictates the type of sensors that need to be installed. When regression analysis is used, each term involved in the regression equation has to be measured. This means that, for example, to extract longitudinal derivatives 5 variables (α, q, a_z , $\dot{q}$, and $\delta_{elevator}$) need to be measured or derived. However, a fewer number of sensors are needed when an output error technique is used, such as maximum likelihood method (Maine, 1986). The only requirement is the availability of input and output variable measurements.

If redundant measurements are available, then a data compatibility analysis can be performed to the obtained flight data. The analysis can reveal any bias, scale factor and other errors, thus enabling correction to the flight data prior to estimation of the control and stability derivatives. This is known as flight reconstruction (Klein 1977 and Wingrove 1973).

Generally among all the inertia sensors, accelerometers produce the *noisiest* signals. The structural and the engine vibration noises are the two major contributors to the accelerometer signal noise (Maine, 1986). Therefore, a low-pass filter should filter the signal) before analysis. The accelerometers should also be mounted on a rigid attachment to reduce noise from any structural vibrations.

2.1.2 (Data acquisition system)

The most common problems with the data acquisition systems are (Maine, 1986):

1. Time tags.

Time tagging ensures that all the measurements are taken at the same time reference. Error in the time tagging degrades the estimation process. This error should be less than 10 msec. Hodge (1975) in his paper pointed out that the worst inaccuracy in the estimated parameters is found when there is a time shift in the control surface measurements.

2. Aliasing and prefiltering

The antialising and prefiltering should be performed before sampling, for example by using a 40% Nyquist frequency filter.

3. Sample rate.

Normally the data are sampled at 100 - 200Hz. Then the data is filtered out and thinned to 25-50Hz for post-flight data analysis. However, in a radio controlled model flight test, a sampling rate of 25-60 Hz is commonly used (Coleman 1981, Wong 1989 and Yip 1992).

4. Resolution.

Butter (1976) pointed out that the dominant factor effecting the errors in the estimated derivatives is the control surface deflection errors. Hence the resolution of the control surfaces should be as good as possible, typically 1/100 - 1/200 of the full scale.

2.1.3 (Telemetry system)

There are a number of telemetry systems available, such as FM, AM, PCW, PCM, etc. However the pulse coded modulation (PCM) is the most frequently used in the flight test program. Iliff (1976), Colemann (1981), and Wong (1989) used PCM telemetry system). Remtron RTS-1 system is one of the commercially available PCM typed telemetry systems. This system is the one that the Computer System Department at the Royal Melbourne Institute of Technology is developing (Howel, 1994).

2.2 Flight data analysis

2.2.1 Model dynamics

The linear mathematical model is adequate for small perturbation analysis of a conventional configuration UAV. The linear model has also been extensively used for the extraction of stability and control derivatives from flight test data of general aviation aircraft (Iliff 1976, Colemann 1981, and Budd 1993).

The model should be selected so as to give the simplest meaningful model of the vehicle's dynamic for a particular manoeuvre. Validation of the assumed model is then carried out, by utilising a statistical analysis (e.g. residual analysis).

A non-linear model becomes important in critical flight regimes where consideration of non-attached flow is assumed. Examples of such conditions are post stall regimes, high angle of attack flights, unconventional configuration and rapid manoeuvres. Eulrich (1974) and Raisinghani (1993) discuss such non-linear modelling. However, the non-linear analysis was not considered necessary for the Telemaster T-240 project.

2.2.2 Parameter estimation methods

Many papers have been written which discuss the parameter estimation methods such as Klein (1973), Ross (1979), Maine (1986), and Iliff (1989). Klein (1973) and Ross (1979) discussed in particular, the estimation of stability and control derivatives from flight data. In principle, the parameter estimation method is divided into 2 main approaches in respect to model structures; equation error approach and output error approach.

Equation error techniques (such as linear regression) solve simultaneous linear algebraic equations. The equation of the form Ax=y is solved to find the unknown matrix A. Here x is the state matrix and y is the output matrix. This technique is quite simple. However, it requires a large number of measurements, namely the system's states as well as the input-output. All those measurements ought to be measured with a relatively high-accuracy instrumentation system. The performance of this technique degrades drastically in the presence of bias errors in the instrumentation. Examples of this technique can be found in Laban (1994) and Mulder (1994). The Delft University of Technology has also developed 'Two Step Method' which is a combination of 'Flight Path Reconstruction' and 'Data Compatibility Check' with regression analysis.

The output error approach is more popular in the field of parameter estimation than the equation error. The output error approach requires fewer numbers of sensors. Generalised least square (or weighted least square), Maximum Likelihood method and Bayes method are based on this output error approach. The difference among the three methods described above lies in the selection of the cost function. The Generalised Least Square allows only a near zero level of noise, or known noise level of the various instrumentation used. The Maximum Likelihood Method (MLM) assumes a White-Gaussian noise in the instrumentation. However, if a process or input noise is present, the

method fails to converge into a solution. A Kalman filter should then be incorporated to the MLM to enable the estimation of the system's states (Milne, 1992).

The MLM is the most widely used method on the extraction of stability and control derivatives from flight test data. NASA has developed a computer code (MMLE3) to perform this algorithm (Maine, 1981).

The Bayes method is not widely used in the estimation of stability and control derivatives. The reason for this is that the method assumes a known a-priori statistical noise. In practice this a-priori statistical noise is not always available.

In this project, the Maximum Likelihood Method is selected as the main algorithm to extract stability and control derivatives of a small UAV from the flight test data. This method has several beneficial features such as the following:

- It gives asymptotically unbiased and consistent estimates.
- Only input and output data is required, and hence less number of sensors needed.
- Good performance, even in the presence of output noise. If input or process noise is present, then a MLM+Kalman filter is used.
- A Cramer-Rao bound, which is by-product of the algorithm, can be used as a measure of accuracy of the individual estimated parameters (Maine and Iliff, 1981)
- A-priori information can be incorporated, e.g. from wind tunnel results.
- MLM is widely used in the extraction of stability and control derivatives of either small or large UAV, and other types of aircraft.

- A routine to perform MLM algorithm is available in either MATLAB MMLE3 toolbox (Milne, 1992) or Xmath (Matrix-X) identification module. Both Matlab and Xmath software are accessible at the Aerospace Engineering Department, RMIT.

Some problems commonly encountered in using the maximum likelihood analysis occur if;

- There is a linear dependency between the unknown parameters.
- There is aeroelastic coupling between flight mechanics and structural modes, e.g. structural vibration.
- Drifts in the states e.g. caused by variation in flight conditions.
- Improper specification of instrumentation and inaccurate modelling.

2.3 Input forms

The most widely used inputs for dynamic flight testing are single pulse and doublet (Iliff 1976, Colemann 1981, Howard 1991 and Yip 1992). Both inputs are relatively easy to execute while at the same time producing responses with a relatively rich information about the dynamics of the vehicle. Other commonly used inputs are PRBS, sine-sweep and 3211 type (see Figure 2-1). Several papers have also been written in formulating a *mathematically optimal* input (Chen, 1975). However this type of input is rather complex and difficult to execute during flights. Other constraints that dictate the input form selection are safety, envelope coverage, hardware constraints, and control systems influence.

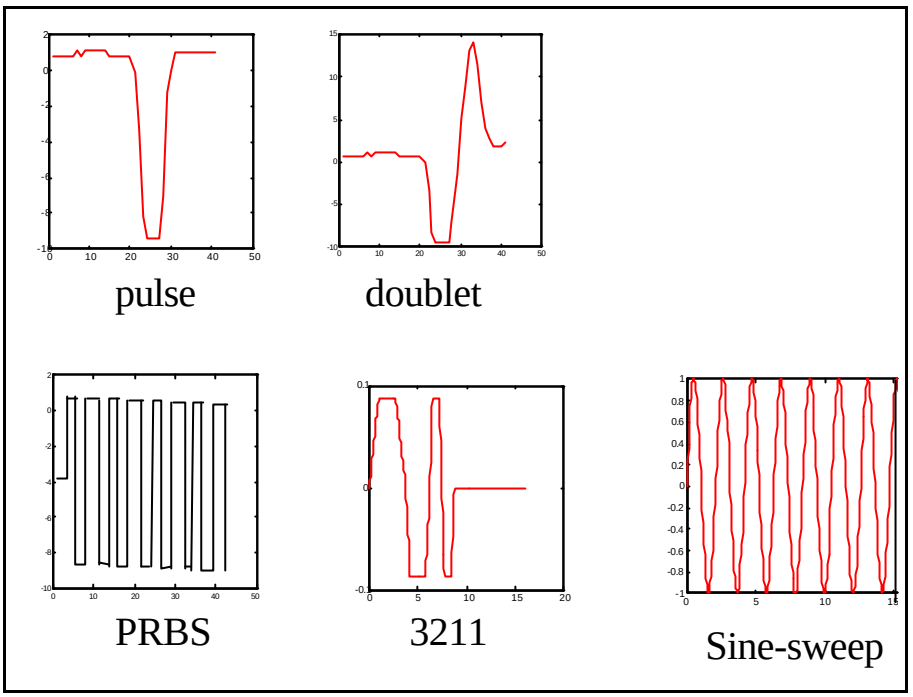

Figure 2-1: Type of control inputs for dynamic flight testing

3. Overview of the method

Selection of a particular method in flight testing a model aircraft depends on the objective of the test, number of measurements taken and their type of accuracy, and means of computational available. In this project, the stability and control derivatives of the Telemaster T240 model are estimated from flight test data using an output error method.

The output error method is used in extracting the stability and control derivative of the aircraft (Figure 3-1). The method minimises a defined error cost function (J) to produce the best fit between the flight data and its simulated responses of the assumed mathematical model. Since the assumed mathematical model consists of several unknown parameters that have to be identified, the method is also commonly known as the parameter identification.

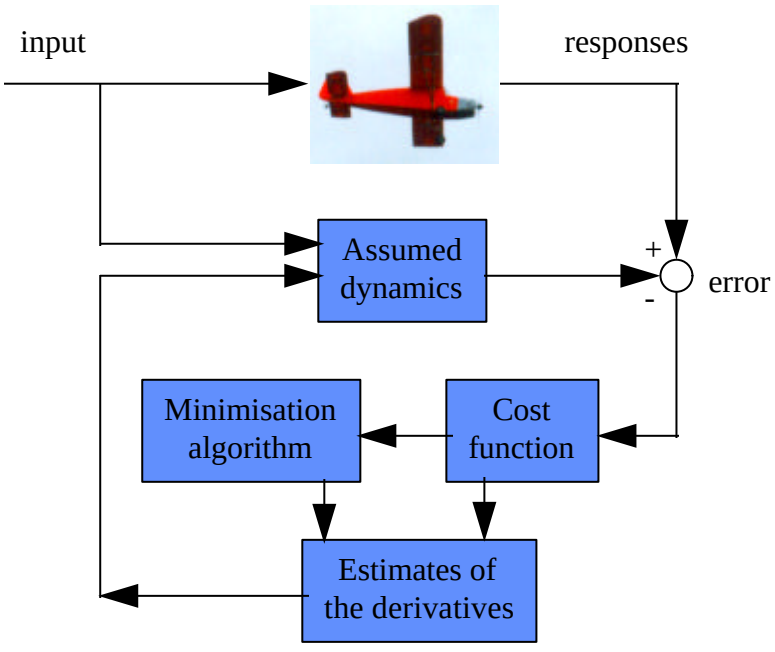

Figure 3-1: Output error algorithm

The whole activity in flight testing the UAV model is depicted in Figure 3-2. Test planning, mass characteristics' determination and calibration of instrumentation are categorised as pre-flight activities, whereas data processing & analysis, data compatibility check and parameter identification as post-flight activities.

A-priori information about the derivatives is used to either complement or assist in the process of extracting derivatives from flight data. This a-priori information may be derived from several sources such as hand calculation (pure theory or semi-empirical), wind tunnel testing, computational fluid dynamic or other independent flight tests. In this project only the hand calculation (performed using Advance Aircraft Analysis AAA-V.1.7 software program) and results from previous flight tests are used as a-priori information for the subsequent analysis.

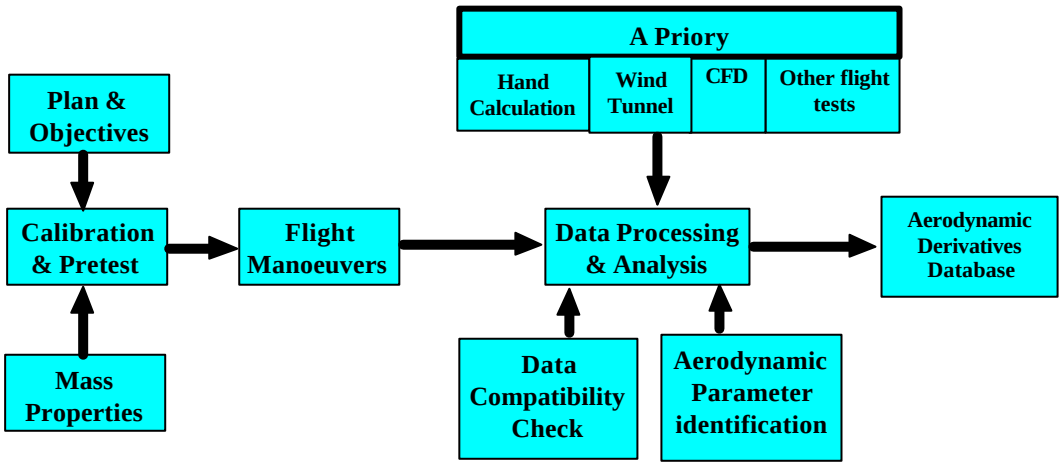

Figure 3-2: Flight dynamic test activities

As for comparison to the parameter identification techniques, several existing conventional techniques have also been automated. Chapter 3.1 describes briefly the theory behind these selected conventional techniques.

3.1 Conventional Methods

There are several existing conventional methods to analyse dynamic flight data, such as TPR (Transient Peak Ratio), MTPR (Modified Transient Peak Ratio), TR (Transient ratio), MS (Maximum Slopes) and SRR (Separated Real Roots). All of these methods are based on extracting dynamic characteristics (such as damping ratio and natural frequency) from the recorded system responses. For example, one can extract the natural frequency and damping ratio of a short period mode from a recorded pitch rate. Similarly, the Spiral and Dutch characteristics can be estimated from the recorded yaw rate. One main difficulty when using these methods is that it is sometimes difficult to analyse data from a well damped recorded response that shows little oscillatory behaviour. References such as Ward (1993) and Eshelby (1991) deal with the practical application of these conventional method of dynamic flight testing.

The following two conventional methods are selected for this project since they are simple, practical and easy to program in Matlab script language.

1. TPR (Transient Peak Ratio) method.

The process involved in the TPR method is depicted in Figure 3-1 below:

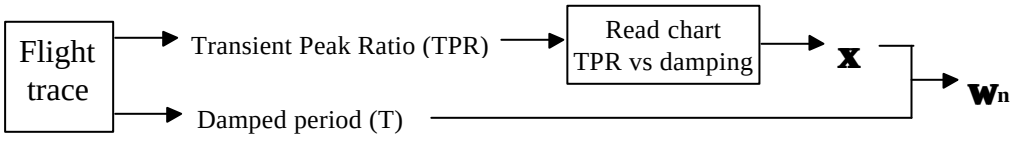

Figure 3-1: Transient Peak Ratio method diagram

Where: $TPR = \frac{x_2}{x_1} = \frac{x_3}{x_2}$ **.....(3-1)**

And $w_n = \frac{2p}{T\sqrt{1-x^2}}$ **.....(3-2)**

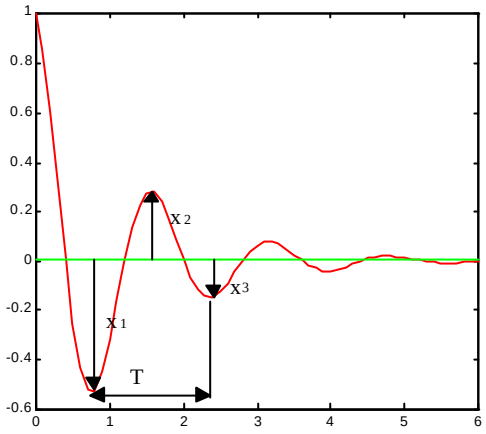

Figure 3-2: Transient Peak Ratio Measurements

A complete detail theory can be found in Ward (1993) from page 211 to 225.

The method has been automated by the author using Matlab. To execute the program, simply type *TPR* at the Matlab prompt.

2. Curve Fitting

This method is based on fitting a first or second order curve to the flight response. Newton minimisation algorithm is used to minimise the error between the fitted curve and the flight response.

The first order system is given as: $y = K_1 + K_2 e^{-t/t}$ **.....(3-3)**

The second order system is given as: $y = Ke^{-xw_n t}\cos\left(w_n t\sqrt{(1-x^2)} + f\right)$ **.....(3-4)**

The Matlab programs needed to perform these methods are contained in files; orde11.m, orde12.m, orde21.m and orde22.m. Type orde12 to perform a first order curve fitting or orde22 to perform a second order curve fitting.

3.2 Parameter identification techniques

Three different parameter identification methods, The Linear Regression (LR), Maximum Likelihood (ML), and Interactive Curve Matching (ICM) are selected for identifying the aerodynamic stability and control parameters from flight data. The ML method is the main algorithm in this project, whereas the LR and ICM are complements. The parameters obtained from the LR and ICM analyses are used as initial estimates for the Maximum Likelihood.

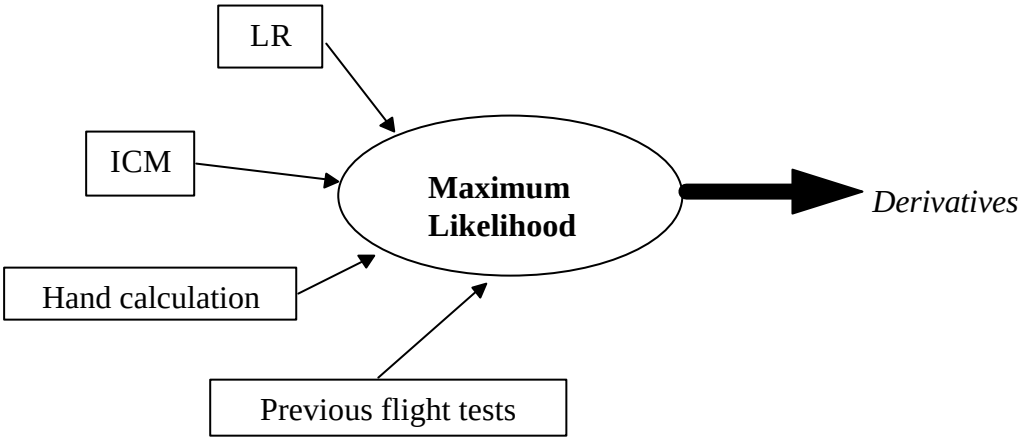

Figure 3-1: Relationship among the different techniques used in this project

Linear regression analysis treats the aircraft equation of motion separately (see equation 3-19 and 3-20). The parameter estimates are obtained by minimising the error cost function for that particular equation. However, when the regressors (independent variables) are contaminated with measurement noise, the method produces a biased estimate of parameters.

In contrast to LR, the ML method minimises a combined cost function of several equations. The method produces an asymptotically unbiased, efficient and consistent estimate of parameters. The method is more complex than the regression. Also a good initial estimate of parameters is required when extracting parameters from poorly excited responses in the flight data (Iliff, 1989).

In contrast to the previous two numerical approaches (LR and ML), the ICM is entirely a graphical technique. The Interactive Curve Matching, as the name suggests, is a method of trying to fit the measured aircraft flight test responses with computed responses by interactively adjusting the values of the derivatives. This method is very simple, and allows a graphical observation during the identification process. It is the basic principle of all the output error methods. The only different is that the criterion of fit is decided by the operator by observing the goodness of fit on the computer monitor, and hence is a subjective matter.

Figure 3-2 illustrates the inputs and outputs of the three different methods described above. The MLM and ICM methods require fewer measurements in both longitudinal and lateral variables than the LR.

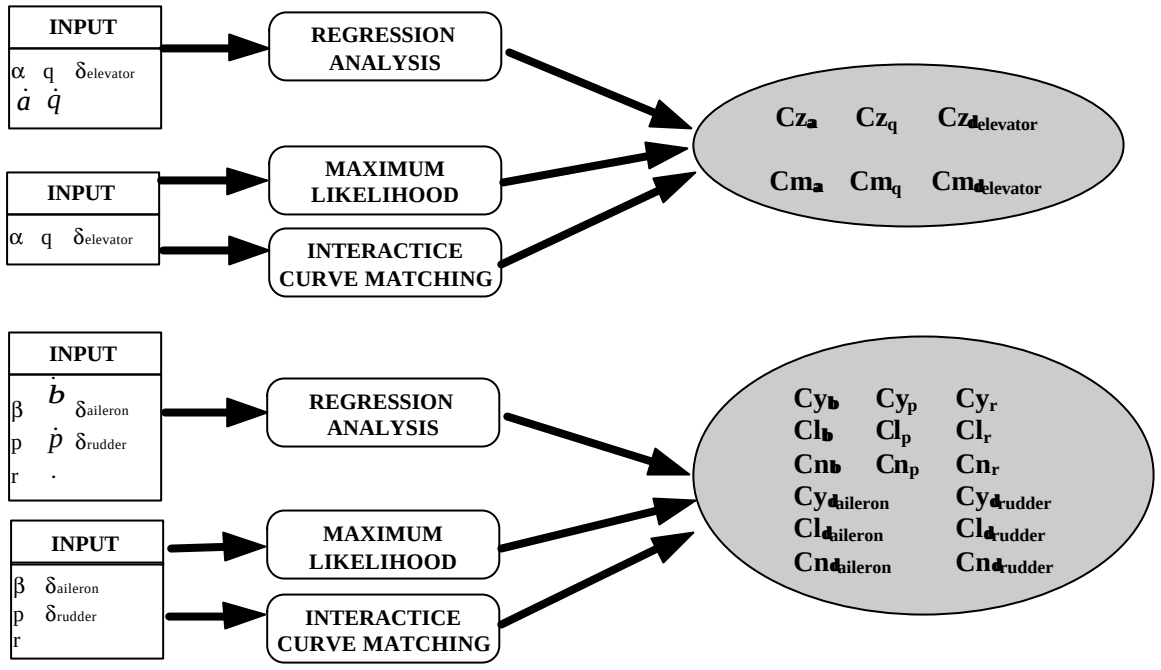

Figure 3-2: Input - Output for the three different identification methods

3.2.1 Linear regression

This section describes briefly the linear regression technique, the solution and its statistical accuracy.

Draper and Smith (1981) give a more detailed explanation of the technique.

For a linear system, the model can be represented in a polynomial form as:

$$y(t) = \theta_0 + \theta_1 x_1 + \theta_2 x_2 + \ldots\ldots\ldots\ldots + \theta_{n-1} x_{n-1} + \varepsilon \qquad \text{.....(3-5)}$$

or as a regression equation; $Y = X\theta + \varepsilon$ **.....(3-6)**

where; $X = \begin{bmatrix} 1 & x_1 & x_2 & x_3 & \ldots\ldots & x_{n-1} \end{bmatrix}$ *and* $\theta = \begin{bmatrix} \theta_0 & \theta_1 & \theta_2 & \theta_3 & \ldots\ldots & \theta_{n-1} \end{bmatrix}^T$ **.....(3-7)**

X	= regressor matrix (N x n)	N	= number of parameter
Y	= measured Y matrix (N x 1)	N	= number of data points
ε	= equation error	θ	= estimated parameters

The parameter estimate θ is obtained by minimising the error cost function J, given as;

$J = \sum_{1}^{N} [e_i]^2$, Which produces the parameter estimate $\hat{q}$ as;

$$\hat{q} = (X^T X)^{-1} X^T Y \qquad \text{.....(3-8)}$$

The spread of parameter estimate (covariance) is calculated as;

$$\text{covariance}(\hat{q}) = s^2 (X^T X)^{-1} \qquad \text{.....(3-9)}$$

Where $s^2 \approx \frac{e^T e}{N - n}$ **.....(3-10)**

The quantity of information in the data that can be explained by the model is given in the coefficient of determination R^2, where;

$$R^2 = \frac{\text{sum of square}_{\text{regression}}}{\text{sum of square}_{\text{total}}} = \frac{\sum (\hat{y}_i - \bar{y})^2}{\sum (y_i - \bar{y})^2} \qquad 0 \le R^2 \le 1 \qquad \text{.....(3-11)}$$

$\bar{y} = \text{mean of } y_i$ and $\hat{y} = \text{estimate of } y_i$

The correlation between the regressor is given as R;

Where $R = \frac{X^T X}{\sqrt{w w^T}}$ $w = \text{diagonal elements of } (X^T X) \text{ matrix}$ **.....(3-12)**

and X is the centred data $X_j - \bar{X}_j \quad j = 1,2,....$

The adequacy of the model can be assessed by looking at the R^2, F and PRESS values.

$$R^2 = \frac{\hat{q}^T X^T Y - N \bar{y}^2}{(n-1)s^2} \qquad \text{.....(3-13)}$$

$$PRESS = \sum_{1}^{N} \frac{[y(i) - \hat{y}(i)]^2}{\left[1 - \frac{\text{variance}(y(i))}{s^2}\right]} \qquad \text{.....(3-14)}$$

$$F = \frac{N-n}{n-1} \frac{R^2}{1-R^2} \qquad \text{.....(3-15)}$$

A better model is indicated by high values of the above variables.

The following assumptions are used when using the linear regression method:

(i) X is deterministic (no noise)

(ii) ε is uncorrelated with X

(iii) ε is identically distributed and uncorrelated with zero mean and variance σ^2 (i.e. white noise).

3.2.2 Maximum likelihood method

A linear dynamic model of an aircraft can be given in a state-space form as;

$$\dot{x}(t) = Ax(t) + Bu(t) + F\boldsymbol{h}(t)$$
$$z(t) = Cx(t) + Du(t) + Gn(t) \qquad \text{.....(3-16)}$$

Where;

$x(t)$	= *State at time t*	A	= *Dynamic matrix*
$z(t)$	= *Measurement at time t*	B	= *Control distribution matrix*
$u(t)$	= *Input at time t*	C	= *State measurement matrix*
$n(t)$, $\boldsymbol{h}(t)$	= *Gaussian noise*	D	= *Transmission matrix*
		F	= *Square root of the state noise spectral density,* FF^T
		G	= *Square root of measurement noise covariance matrix*

The maximum likelihood estimator maximises the conditional probability density function of the output, given the set of parameter θ., i.e. maximising $P(y_i / \theta)$.

$P(y_i / \theta)$ is normally given in logarithmic form and known as the logarithmic likelihood function LLF(θ).

$$LLF(\boldsymbol{q}) = \frac{1}{2}\sum_{i=1}^{N} \tilde{z}_i^T (RR)^T \tilde{z}_i + \frac{N}{2}\log\left|RR^T\right| + \frac{Nm}{2}\log 2\boldsymbol{p} \qquad \text{.....(3-17)}$$

Where $RR^T = E[\tilde{z}_i \tilde{z}_i^T]$

To minimise the likelihood function above, a Quadratic, Marquart, Constrained Newton or other minimisation technique can then be used to predict the successive estimate of the unknown parameters. The detail computational technique used in this project is described in chapter 4.

Suppose the parameter set to be estimated is ξ, then the estimate of ξ at iteration L+1 is given as:

$$\tilde{x}_{L+1} = \tilde{x}_L - \left[\nabla_x^2 LLF(\tilde{x}_L)\right]^{-1}\left[\nabla_x LLF(\tilde{x}_L)\right] \qquad \text{.....(3-18)}$$

For a fixed RR^{-1}, the first and second gradient are given as:

$$\nabla_x LLF(x) = GRAD = -\sum_{i=1}^{N} (\nabla_x \tilde{z}_i)^T (RR^T)^{-1} \tilde{z}_i \qquad \textbf{.....(3-19)}$$

$$\begin{aligned} \nabla_x^2 LLF(x) &= \sum_{i=1}^{N} (\nabla_x \tilde{z}_i)^T (RR^T)^{-1} (\nabla_x \tilde{z}_i) + \sum_{i=1}^{N} (\nabla_x^2 \tilde{z}_i)(RR^T)^{-1} \tilde{z}_i \\ &= HES + \sum_{i=1}^{N} (\nabla_x^2 \tilde{z}_i)(RR^T)^{-1} \tilde{z}_i \end{aligned} \qquad \textbf{.....(3-20)}$$

Where $HES = \sum_{i=1}^{N} (\nabla_x \tilde{z}_i)^T (RR^T)^{-1} (\nabla_x \tilde{z}_i)$ **.....(3-21)**

The accuracy of the parameter estimates can be assessed by determining their Cramer Rao Bounds $(CR)_{bound}$, which gives an estimate of the standard deviation of each parameter. The CR bound is calculated via the information matrix H as follows;

$$\left(CR_{bound}\right)^2 = H^{-1} = \frac{2\, LLF(x)_{minimum}}{(N-1)}\, HES \qquad \textbf{.....(3-22)}$$

A more detail explanation of the method can be found in Iliff and Maine (1979) and Iliff (1989).

3.2.3 Interactive Curve Matching

The basic idea of this method is to interactively change the value of stability and control derivatives of the assumed mathematical model, to obtain a good fit between the calculated responses and those of flight data. The algorithm for this method is given in Figure 3-7.

The application of this technique is possible due to a facility known as GUI (Graphical User Interface) offered in MATLAB software. Figure 3-2 shows a longitudinal ICM with 8 different sliders representing 8 different derivative values. Also shown is the corresponding error between the flight data and the fitted curve.

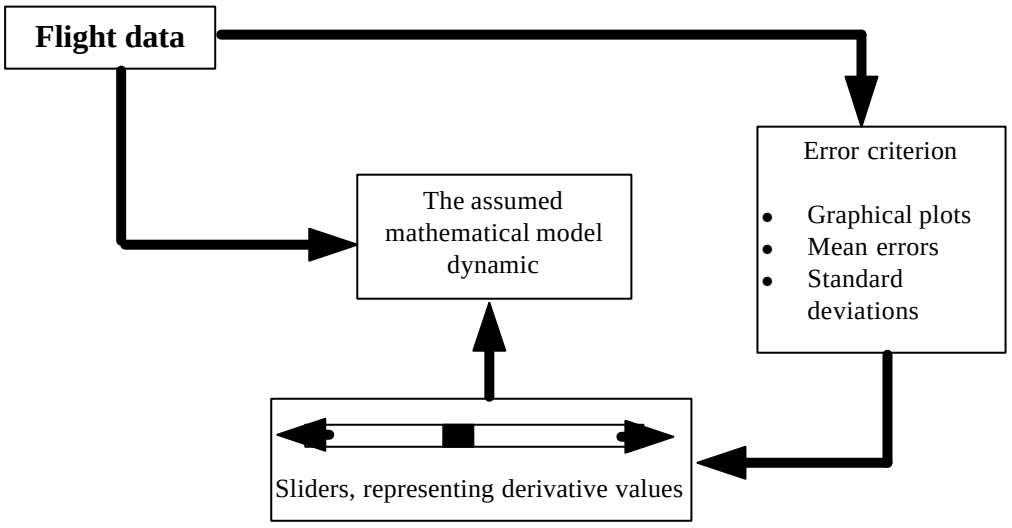

Figure 3-1: The Interactive Curve Matching algorithm

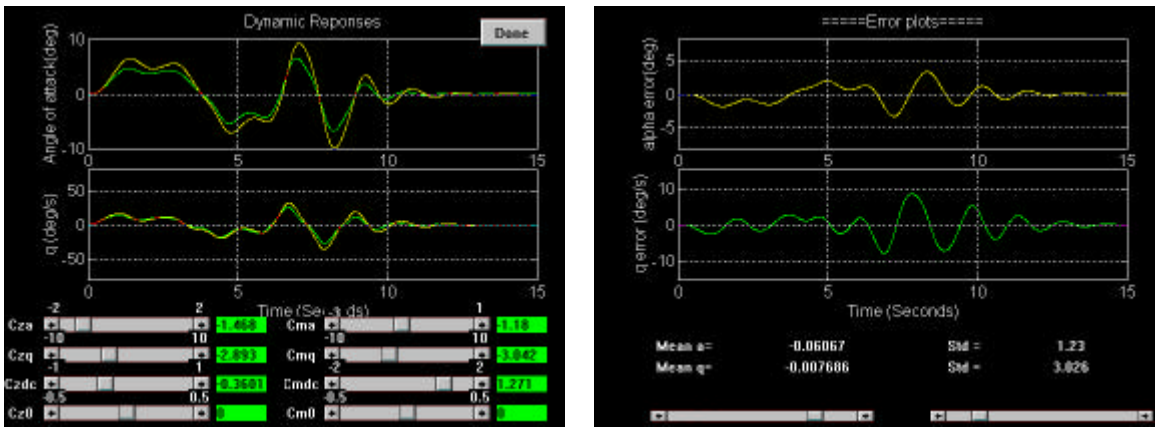

Figure 3-2: Longitudinal Curve Matching Menu programmed in Matlab, and it's corresponding error layout.

3.3 Model dynamics

Selection of an 'adequate model' in the analysis of flight test data is critical to the success of the identification process. The criteria for the adequate model are however, difficult to quantify. The model is said to be adequate if it is simple and yet has a physical meaningful interpretation. A-priori information such as that from wind tunnel testing is normally used to assist in the selection of the right model.

For a rigid aircraft, its dynamics can be represented by a six degree of freedom, non-linear mathematical model. This model consists of 6 equations, which couple the longitudinal and lateral motion of the aircraft. Due to the complexity of the equations, this model is not normally used in the extraction of stability and control derivatives from flight data. Instead, reduced linear, uncoupled equations of motions are frequently used.

Similarly in this project, the linearised uncoupled longitudinal and lateral equations of motion are selected for the analysis of the flight data. These equations have been used extensively and successfully to analyse flight data (Iliff, Maine and Montgomery 1979, Coleman 1981, Budd 1993). Since the aircraft is of a conventional configuration and the manoeuvres conducted are of small perturbation, these reduced equations should prove to be adequate. Theoretically from these equations, 6 longitudinal and 15 lateral derivatives can be extracted. However in practice, it is not always possible to get all the 21 derivatives from a single manoeuvre. A low information content of the flight data is a typical cause of the problem.

(a) The longitudinal motion, expressing perturbation from a horizontal steady flight is written as (Klein, 1994):

$$\begin{aligned} a_z / V_0 &= \dot{\alpha} - q = \frac{\rho V_0 S}{2m}\left(Cz_\alpha \alpha + Cz_q \frac{qc}{2V_0} + Cz_{delevator}\delta_{elevator} + Cz_0 \right) \\ \ddot{q} = \dot{q} &= \frac{\rho V_0^2 Sc}{2I_y}\left(Cm_\alpha \alpha + Cm_q \frac{qc}{2V_0} + Cm_{delevator}\delta_{elevator} + Cm_0 \right) \end{aligned} \qquad \text{.....(3-23)}$$

Or in a state-space form as;

$$\begin{bmatrix} \dot{\alpha} \\ \dot{q} \end{bmatrix} = \begin{bmatrix} \frac{\rho V_0 S}{2m} Cz_\alpha & 1 + \frac{\rho Sc}{4m} Cz_q \\ \frac{\rho V_0^2 Sc}{2I_y} Cm_\alpha & \frac{\rho V_0 Sc^2}{4I_y} Cm_q \end{bmatrix} \begin{bmatrix} \alpha \\ q \end{bmatrix} + \begin{bmatrix} \frac{\rho V_0 S}{2m} Cz_{\delta_{elevator}} & \frac{\rho V_0 S}{2m} Cz_0 \\ \frac{\rho V_0^2 Sc}{2I_y} Cm_{\delta_{elevator}} & \frac{\rho V_0^2 Sc}{2I_y} Cm_0 \end{bmatrix} \begin{bmatrix} \delta_{elevator} \\ 1 \end{bmatrix} \text{...(3-24)}$$

Note that in the moment equation, the Cm derivatives are the compound effect of several variables as follows; $Cm = Cm'(\alpha, \dot{\alpha}, q, \delta_{canard})$

$$Cm_a = \mathrm{C}m'_a + \frac{r\,\mathrm{Sc}}{4\,\mathrm{m}}\mathrm{C}m'_{\dot{a}}\,\mathrm{Cz}_a$$

i.e.; $$\mathrm{C}m_q = Cm'_q + \mathrm{C}m_{\dot{a}}\left(1 + \frac{r\,\mathrm{Sc}}{4m}\mathrm{Cz}_q\right) \qquad \textbf{.....(3-25)}$$

$$\mathrm{C}m_{d_{elevator}} = \mathrm{C}m'_{delevator} + \frac{r\,\mathrm{Sc}}{4m}\mathrm{C}m'_{\dot{a}}\,\mathrm{Cz}_{delevator}$$

(b) The lateral motion, expressing perturbation from a steady flight condition;

$$\begin{aligned}
a_y/V_0 &= \dot{\beta} + r - \frac{g}{V_0}\cos\theta_0\,\phi = \frac{rV_0S}{2m}\left(Cy_\beta\beta + Cy_p\frac{pb}{2V_0} + Cy_r\frac{rb}{2V_0} + Cy_{d_{aileron}}\delta_{aileron} + Cy_{drudder}\delta_{rudder} + C_{y0}\right)\\
\dot{p} - \frac{I_{xz}}{I_x}\dot{r} &= \frac{rV_0^2Sb}{2I_x}\left(Cl_\beta\beta + Cl_p\frac{pb}{2V_0} + Cl_r\frac{rb}{2V_0} + Cl_{d_{aileron}}\delta_{aileron} + Cl_{d_{rudder}}\delta_{rudder} + Cl_0\right)\\
\dot{r} - \frac{I_{xz}}{I_z}\dot{p} &= \frac{rV_0^2Sb}{2I_z}\left(Cn_\beta\beta + Cn_p\frac{pb}{2V_0} + Cn_r\frac{rb}{2V_0} + Cn_{d_{aileron}}\delta_{aileron} + Cn_{d_{rudder}}\delta_{rudder} + Cn_0\right) \qquad \textbf{.(3-26)}\\
\dot{\phi} &= p + r\tan\theta_0\\
a_y &= V_0(\dot{\beta} + r) - (g\cos\dot{\theta}_0)\Phi
\end{aligned}$$

Or in the state-space form as;

$$\begin{bmatrix} 1 & 0 & 0\\ 0 & 1 & -\frac{I_{xz}}{I_x}\\ 0 & -\frac{I_{xz}}{I_z} & 1 \end{bmatrix}\begin{bmatrix}\dot{\beta}\\ \dot{p}\\ \dot{r}\end{bmatrix} = \begin{bmatrix} \frac{rV_0S}{2m}Cy_\beta & \frac{rSb}{4m}Cy_p & \frac{rSb}{4m}Cy_r - 1\\ \frac{rV_0^2Sb}{2I_x}Cl_\beta & \frac{rV_0Sb^2}{4I_x}Cl_p & \frac{rV_0Sb^2}{4I_x}Cl_r\\ \frac{rV_0^2Sb}{2I_z}Cn_\beta & \frac{rV_0Sb^2}{4I_z}Cn_p & \frac{rV_0Sb^2}{4I_z}Cn_r \end{bmatrix}\begin{bmatrix}\beta\\ p\\ r\end{bmatrix} +$$

$$\begin{bmatrix} \frac{rV_0S}{2m}Cy_{d_{aileron}} & \frac{rSb}{2m}Cy_{d_{rudder}} & \frac{rSb}{2m}Cy_0 + \frac{g}{V_0}\cos\theta_0\phi\\ \frac{rV_0^2Sb}{2I_x}Cl_{d_{aileron}} & \frac{rV_0^2Sb}{2I_x}Cl_{rudder} & \frac{rV_0^2Sb}{2I_x}Cl_0\\ \frac{rV_0^2Sb}{2I_z}Cn_{d_{aileron}} & \frac{rV_0^2Sb}{2I_z}Cn_{rudder} & \frac{rV_0^2Sb}{2I_z}Cn_0 \end{bmatrix}\begin{bmatrix}\delta_{aileron}\\ \delta_{rudder}\\ 1\end{bmatrix} \qquad \textbf{.....(3-27)}$$

For preliminary analysis, the model can be further simplified into three simple single plane models (equations. 3-28 to 3-30). These mathematical models are valid if we assume that small perturbations are made about one axis only, and that the motion is confined to that plane only.

Pitch only model:

$$\begin{aligned} \dot{a} &= q + \frac{rV_0 S}{2m}\left(Cz_a\, a + Cz_q \frac{qc}{2V_0} + Cz_{delevator}\, d_{elevator} \right) \\ \dot{q} &= \frac{rV_0^2 Sc}{2I_y}\left(Cm_a\, a + Cm_q \frac{qc}{2V_0} + Cm_{delevator}\, d_{elevator} \right) \end{aligned} \qquad \textbf{.....(3-28)}$$

Roll only model:

$$\dot{p} = \frac{rV_0^2 Sb}{2I_x}\left(Cl_p \frac{pb}{2V_0} + Cl_{d_{aileron}}\, d_{aileron} \right) \qquad \textbf{.....(3-29)}$$

2D Yaw-roll model:

$$\begin{aligned} \dot{b} &= \frac{rV_0 S}{2m}\left(Cy_b\, b + Cy_{drudder} d_{rudder} \right) - r \\ \dot{p} &= \frac{rV_0^2 Sb}{2I_x}\left(Cl_b\, b + Cl_p \frac{pb}{2V_0} + Cl_{d_{aileron}}\, d_{aileron} \right) \\ \dot{r} &= \frac{rV_0^2 Sb}{2I_z}\left(Cn_b\, b + Cn_p \frac{pb}{2V_0} + Cn_{d_{rudder}}\, d_{rudder} \right) \end{aligned} \qquad \textbf{.....(3-30)}$$

To model any non-linear effect, Eulrich and Rynasky (1974), and Raisinghani (1993) discuss some of the non-linear modelling. However, this non-linear modelling is outside the scope of this project.

Table 3-2: Stability and control parameters used in the linear dynamic model.

	Longitudinal (6 parameters)			**Lateral (15 parameters)**		
Level of importance	*Static*	*Dynamic*	*Control*	*Static*	*Dynamic*	*Control*
Primary	Cz_α Cm_α	Cm_q	$Cm_{\delta elevator}$	Cl_β Cn_β	Cl_p Cn_r	$Cl_{\delta aileron}$ $Cn_{\delta rudder}$
Secondary		Cz_q	$Cz_{\delta elevator}$	Cy_β	Cn_p Cl_r	$Cn_{\delta aileron}$ $Cl_{\delta rudder}$
Tertiary					Cy_p Cy_r	$Cy_{\delta aileron}$ $Cy_{\delta rudder}$

3.4 Flight Test Manoeuvres

The following criteria were taken into account when choosing the type of control inputs and manoeuvres to be performed by the pilot:

- Most dynamic derivatives can be extracted successfully from manoeuvre with only a doublet input, with the input frequency near the vehicle's natural frequency, which is approximately 5 rad/s for the T240 model. This form of input is the most practical (Maine, 1986).
- Alternatively, the 3211 form input should be performed since this input has a wider frequency content and thus produces a better estimate of parameters. The wider the frequency spectrum the more likely the aircraft is to be excited. However, this type of input is rather difficult to realise in practice than the pulse or doublet forms.
- Minimise any cross coupling between the longitudinal and lateral motions.
- The manoeuvre should be performed in the linearity range (i.e. α and β excursions should not exceed ± 5 degrees) and of constant speed, so that the validity of the linear equation of motions are preserved.
- The manoeuvre should be performed on smooth air, i.e. no turbulence present. Turbulence can introduce modelling errors, since no turbulence model is incorporated in the flight data processing software.
- The manoeuvres are best performed at engine idle, thus minimising any effect of the engine loads and vibrations.
- To increase the statistical confidence of the parameter estimates, every manoeuvre should be repeated at least twice.

4. Flight Test Software Development

To process and analyse data from the flight tests, a computer program has been developed specifically for this project. The program must perform the following tasks:

- Dynamic simulation of the model aircraft
- Signal processing of the flight data
- Graphical representation of set of data.
- Identification of stability and control derivatives.
- State estimation of unmeasured variables (Flight reconstruction).

The MATLAB software has been selected since it has several beneficial features, such as:

- A powerful computing capability.
- A good graphic capabilities.
- Graphical User Interface (GUI) capabilities.
- Many built-in functions.
- Relatively easy to program (in the form of script M files).
- A Personal Computer version is available.
- Simulation program is supported (SIMULINK).
- It has a special *toolbox* for Maximum Likelihood Algorithm The Fortran version of this program (MMLE3) is normally used in aircraft industry to perform their parameter identification process.

The structure of the program is given in Figure 4-1. It has 5 main categories; dynamic simulation, flight data, stability & control derivative estimation, data compatibility analysis, and a-priori. Each category consists of several functions, which perform the necessary calculations for that particular category.

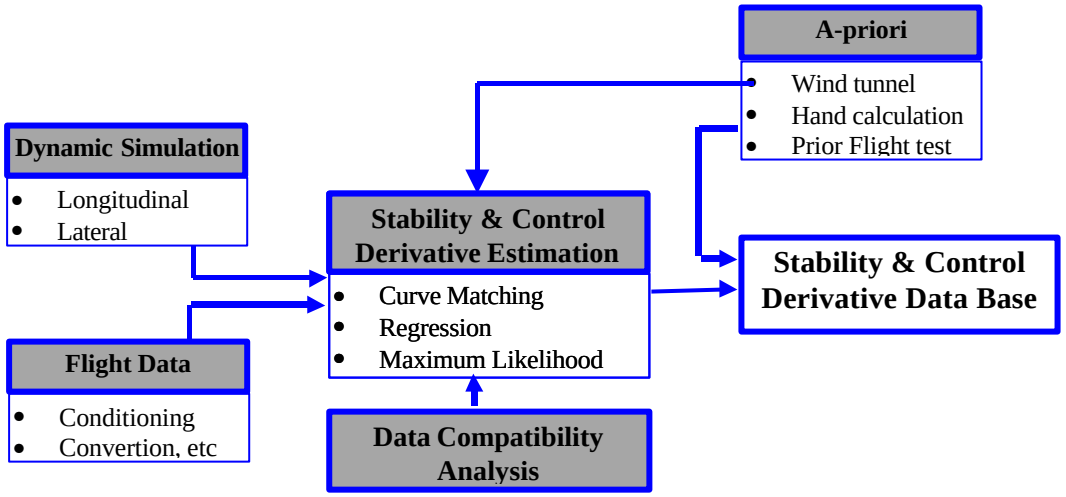

Figure 4-1: The structure of the flight test computer program developed for the project

The whole program contains several sub-programs in the form of M script files. These M files perform just as subroutines in programming languages such as C or Fortran. The result of the calculation from each M file is saved in a binary form with extension .mat (therefore named as mat files). The interconnection between M files and mat files in the program is described in Figure 4-2.

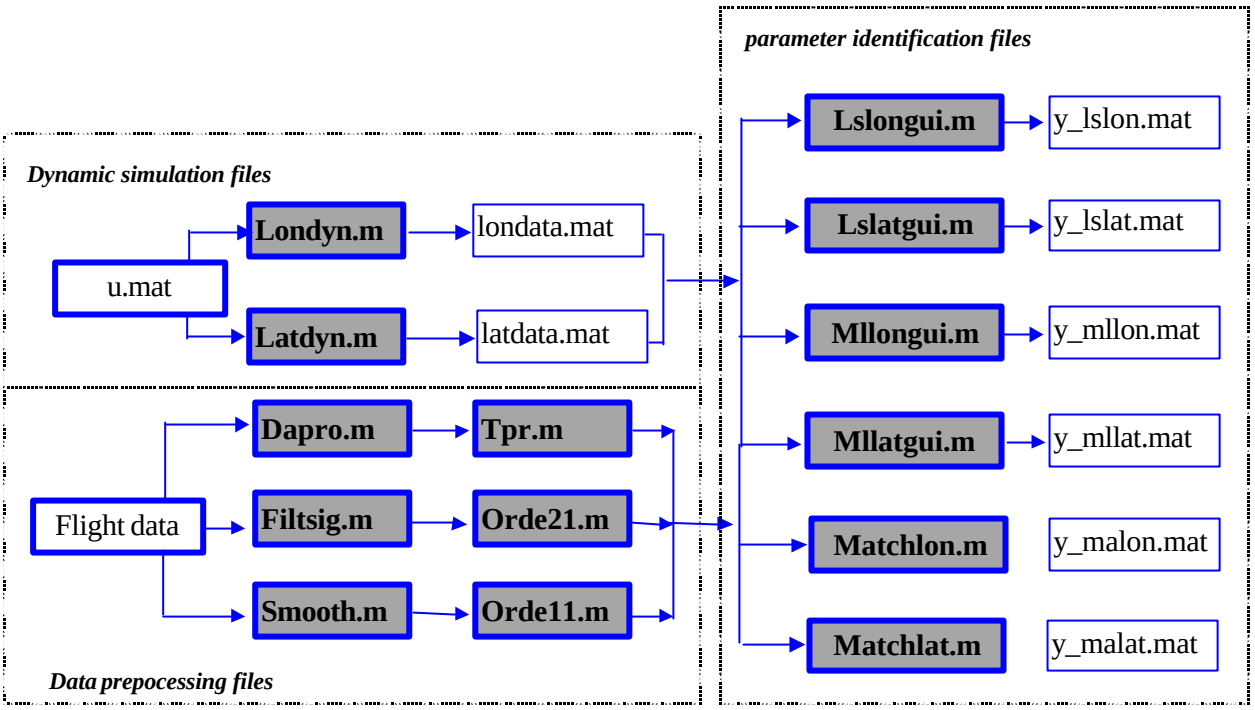

Figure 4-2: Interconnection between M and mat files in the program

Interaction between the program and the users is made as friendly as possible. Thanks to the facility known as GUI in MATLAB that makes it possible. The user can change any values and click any buttons to perform any required functions. The complete window menus available in the program are given in appendix 5.

4.1 The MMLE3 State-Space Identification Tool-box on Matlab.

The tool-box contains functions for the parameter estimation of continuous linear time-invariant, multi-input multi-output, state-space models from observed input-output data, using either the maximum likelihood or output error method. The tool-box is an enhanced Matlab implementation of the widely used parameter identification program in processing flight data (Maine 1981). It runs on a personal computer, under the environment of Matlab software. The tool-box is very user friendly, accessible, and easy to modify or incorporated with other data processing functions in Matlab. The steps needed for the estimation is given in Figure 4-1.

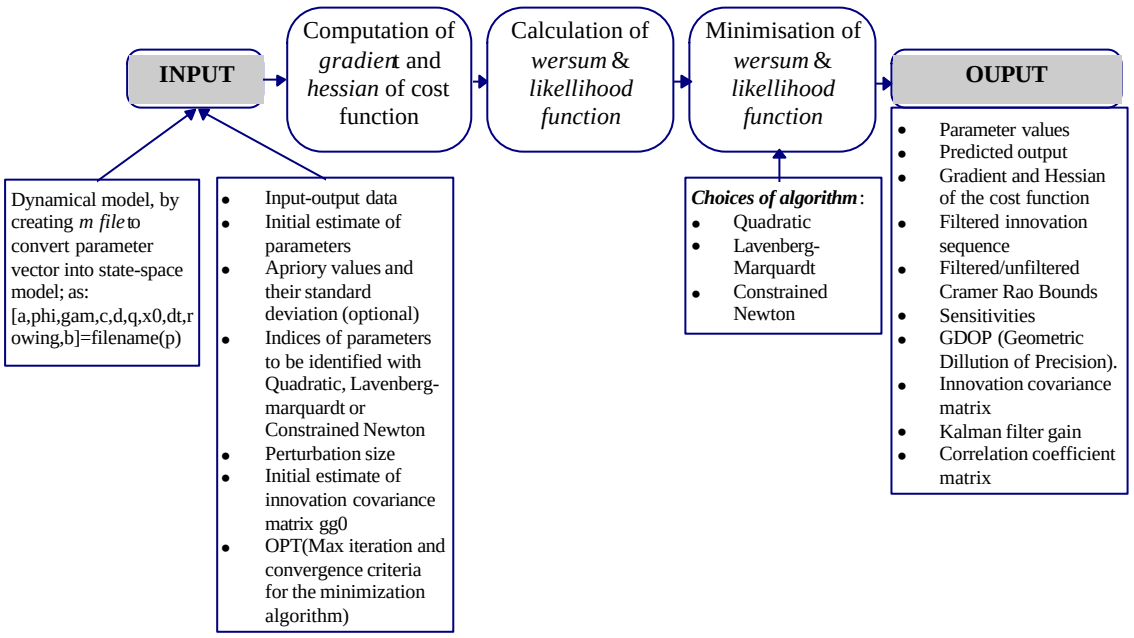

Note :
wersum is defined as $\frac{1}{Nm}\sum_{1}^{N}\tilde{z}_i^T (RR^T)^{-1}\tilde{z}_u$, and it converges to 1 at the minimum. The logarithmic likelihood function is then calculated as: $LLF = \frac{N}{2}(m\ wersum + \log|gg|)$

Figure 4-1: Summary on the use of MMLE3 toolbox in MATLAB

The parameters being identified are given in variable name p(pid). To ensure that the algorithm has reached the global minimum point, and therefore the p(pid) is the maximum likelihood parameters, then the following properties are worth investigating:

- The value of LLF has reached the minimum value.
- The value of wersum $\rightarrow$ 1 (i.e. residual = Gaussian), as the cost function $\rightarrow$ minimum.
- The gradient approaches zero, i.e. variable MaxGrad $\rightarrow$ 0.
- No further change in parameter, i.e. max(dP) $\rightarrow$ 0.
- The plot of output data and response estimate (yest) are matched.
- The plot of innovation (inovt) should show an uncorrelated Gaussian noise.
- The RRnsum (sum of residual covariance) $\rightarrow$ a fixed value as the cost function $\rightarrow$ minimum.
- Small value of Cramer Rao Bounds (2fcramer) and insensitivities. Large values of these variables indicate a poor information content in the data to identify a particular parameter (i.e. insensitive to parameter). These parameters should then be fixed or supplied with a-priori information from wind tunnel or previous flight test data.
- The scatter of parameter estimates from repeated experiments is approximately 1-2 times the filtered Cramer-Rao Bound, where $CR_{filtered} = CR\frac{\sqrt{f_{filter}}}{\sqrt{f_{-3dB}}}\frac{\sqrt{f_{Nyquist}}}{\sqrt{Nm}}$

4.2 Data Compatibility Analysis (Flight Data Reconstruction)

Data compatibility analysis to the measured outputs is becoming an important procedure prior to processing flight dynamic test data. The analysis gives estimates to any unmeasured variables (acts as a state estimator), and also estimates any biased errors in the measured response data. Papers written by Wingrove (1973) and Klein (1977) present several methods in conducting the compatibility analysis.

The proposed compatibility checking in this project is described in the Figure 4-1 below:

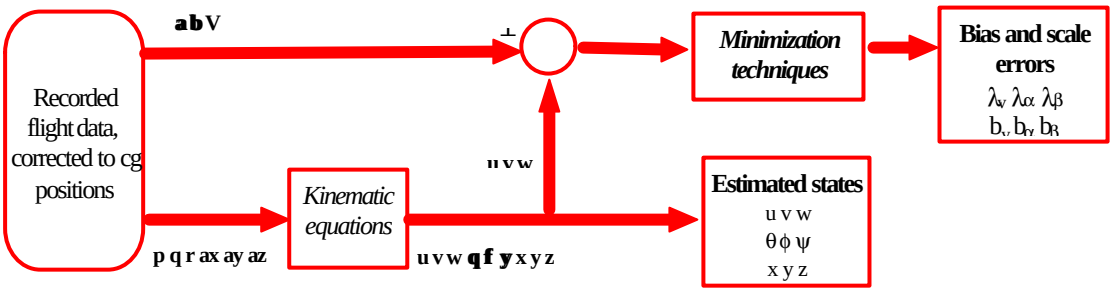

Figure 4-1: Compatibility checking algorithm used in this project

The complete kinematics equation is given as;

$$\begin{aligned} \dot{u} &= a_x - qw + rv - g\sin q \\ \dot{v} &= a_y - ru + pw + g\sin f\cos q \\ \dot{w} &= a_z - pv + qu + z_0 + g\cos f\sin q \end{aligned} \qquad \text{.....(4-1)}$$

$$\begin{aligned} \dot{q} &= q\cos f - r\sin f \\ \dot{f} &= p + q\sin f\tan q + r\cos f\tan q \\ \dot{y} &= r\cos f/\cos q + q\sin f/\cos q \end{aligned} \qquad \text{.....(4-2)}$$

$$\dot{h} = u\sin q - v\cos q\sin f - w\cos q\cos f$$
$$\dot{x} = u\cos q\cos y + v(\sin f\sin q\cos y - \cos f\sin y) + w(\cos f\sin q\cos y + \sin f\sin y) \quad \textbf{..(4-3)}$$
$$\dot{y} = u\cos q\sin y + v(\sin f\sin q\sin y + \cos f\cos y) + w(\cos f\sin q\sin y - \sin f\cos y)$$

And the output equation as:

$$V = (1 + l_v)\sqrt{(u^2 + v^2 + w^2)} + b_v$$
$$b = (1 + l_b)\tan^{-1}\left[\frac{v}{u}\right] + b_b \qquad \textbf{.....(4-4)}$$
$$a = (1 + l_a)\tan^{-1}\left[\frac{w}{u}\right] + b_a$$

If p,q,r,a_x, a_y, and a_z are measured without error, i.e. deterministic systems, then the unknown bias (b_v , b_α,, b_β) and scalar errors (λ_v , λ_α,, λ_β) can be obtained using a linear regression to the above equations.

To simplify the analysis, the complete non-linear kinematics equations above are reduces to uncoupled longitudinal and lateral equations as:

(Assuming constant velocity V), then

$$\dot{a} = \frac{a_z}{V} + q \quad \Rightarrow \quad \hat{a} = \int\left(\frac{a_z}{V} + q\right)dt$$
$$\dot{b} = \frac{a_y}{V} - r \quad \Rightarrow \quad \hat{b} = \int\left(\frac{a_y}{V} - r\right)dt \qquad \textbf{.....(4-5)}$$

Assuming a_z, a_y, q and r are measured without error, then

$$a_m = (1 + l_a)\hat{a} + b_a + \text{measurement noise}$$
$$b_m = (1 + l_b)\hat{b} + b_b + \text{measurement noise} \qquad \text{.....(4-6)}$$

The scale and bias errors are then estimated by minimising $\Sigma_i (a_i - \hat{a}_i)^2$ and $\Sigma_i (b_i - \hat{b}_i)^2$.

5. Model Description & Testing

5.1 Model Description

The aircraft model to be flight tested is the Telemaster T240 (Figure 5-1). It is a conventional wing-tail configuration with elevator, flap, aileron and rudder as the aerodynamic control surfaces. The model has 2.26m wingspan and 1.55m fuselage length. More detailed characteristics of the model are given in appendix 3.

Figure 5-1: The Telemaster T240 aircraft model to be flight tested.

The model weighs about 10Kg, of which 60% constitutes the structural weight. Table 5-1 shows the complete weight breakdown of the model.

Table 5-1: Weight breakdown of the T240 aircraft model

Components	Mass (gram)	% of total weight
Body and engine	5192	50.1
Undercarriage	547	5.3
Left wing	1238.3	12.0
Right wing	1169.6	11.3
DAS + IMU	1480.9	14.3
DAS power supply	335.7	3.2
Pressure sensor	106.3	1.0
Flow vanes boom	122.3	1.2
Pitot static boom	167.4	1.6
Total	**10359.5**	**100**

The whole vehicle is constructed from commercial home-built components. The structure of the T240 is balsa wood, covered with composite skin. The main wing structure consists of a single plywood spar strengthened by several balsa wood ribs along the wing span.

The vehicle is powered by a small 22cc aeromodelling glow-plug engine Irvine-150. A two bladed fixed pitch propeller (16" diameter and 8" pitch) is used. With this engine and propeller combination, approximately 15N thrust can be produced for cruise at engine speed of 7500rpm. This was measured in the wind tunnel, as can be seen in Figure 5-4.

Three main control surfaces (elevator, rudder and aileron) are used to control the aircraft. A flap is also added as to generate more lift if needed. The control surfaces are driven by electrically servo actuators. All these servos are controlled by Futaba RC Max-7 system, which uses PCM encoding at frequency of 36 MHz. However, at a later stage in flight testing, the PCM transmitter was replaced by a TF-FM at 29.725 MHz due to interference. The control systems, including the on-board receivers are powered by a 7.2 Ni-Cad battery with capacity of 1.2 ampere hour.

5.2 Engine testing

The following section describes the thrust measurement in the wind tunnel. This is needed to make correction when the flight test is conducted with engine on. However, when the test is conducted at engine idle, the correction will not be necessary.

Various thrust measurement techniques are available such as direct force measurement, propeller slipstream measurement, propeller models, and combined propeller and engine models (Laban, 1990, page 57). The propeller model technique was selected in this project due to its simplicity. Also, the technique requires only measurement of propeller operating conditions.

The propeller model technique relates wind tunnel measurements of airspeed (v) and propeller rotational speed (n) to the thrust generated by the propeller. For a fixed pitch propeller, the blade element theory shows that the thrust produced is directly proportional to the advance ratio J (where J=v/nD), see Laban (1990) page 71.

The set up of the experiment is given in Figure 5-1. The engine was supported on the thrust balance. This balance measured the change in thrust as the engine rpm and wind tunnel speeds were varied.

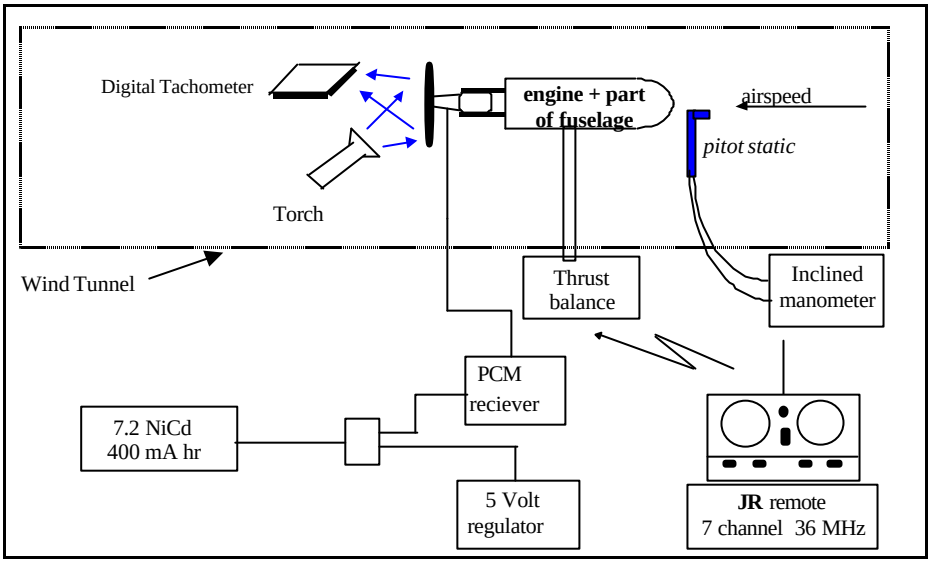

Figure 5-1: Experiment set-up for the engine test

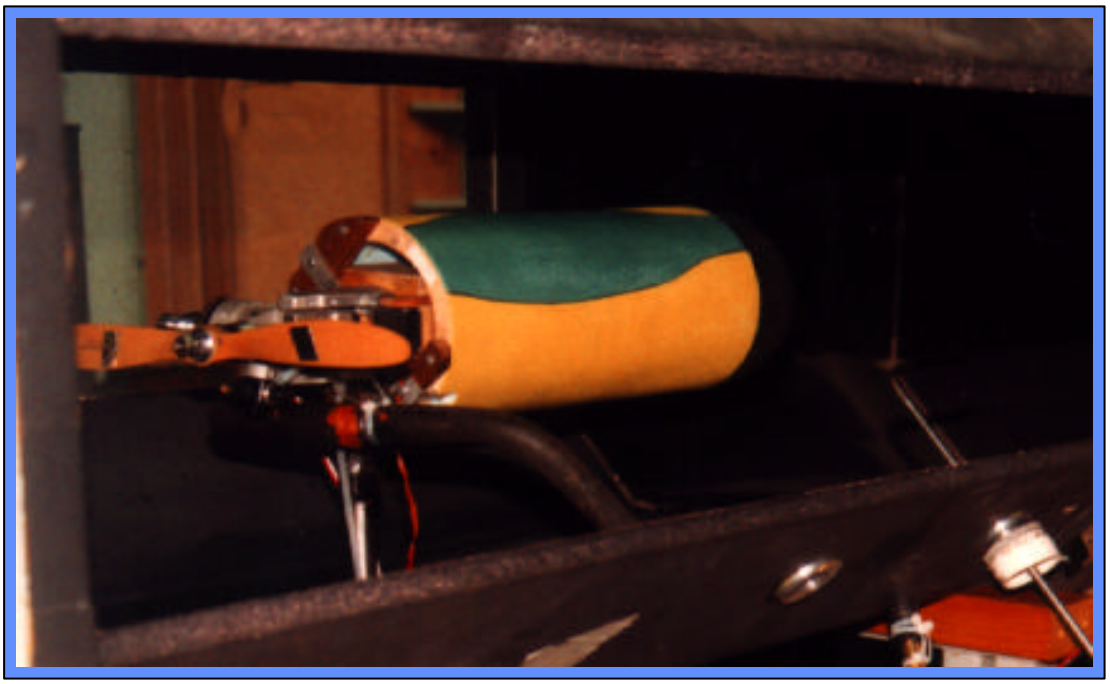

Figure 5-2: Thrust measurement in the 50x50cm Aerospace Engineering wind tunnel, RMIT.

Figure 5-2 shows the testing of the RC-80 engine in the wind tunnel. However, since we encountered many problems with the RC-80 in time of T240's first flight testing, we just had to change the engine to Irvine-150. Though, the engine test result could still be used since we utilised the same type of propeller.

The result of the engine test is given in Figure 5-3 and Figure 5-4. Figure 5-3 shows that the thrust coefficient is linearly related to the advance ratio J. The graph covers most of the advance ratio operating range for the actual flight. From this graph, a good linear model can be extracted. Figure 5-4 shows a good agreement between the experimental results and those predicted by the model.

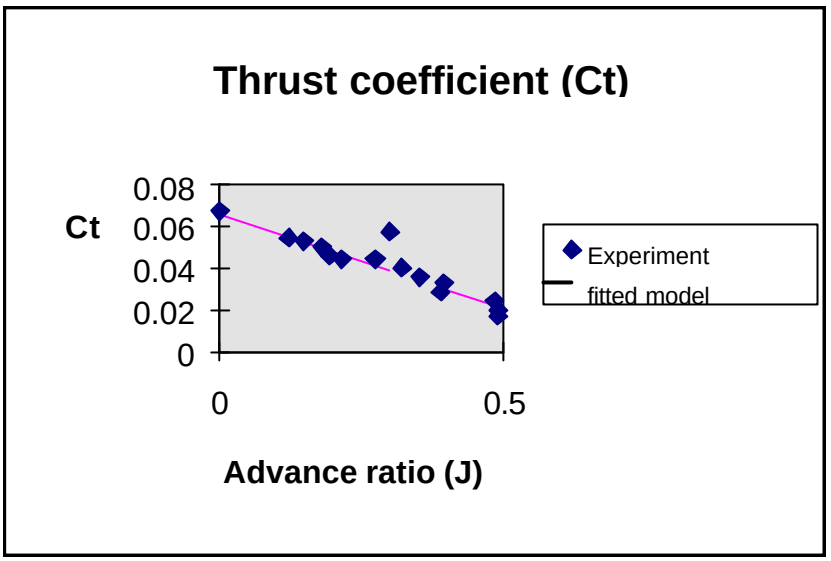

Figure 5-3: Thrust coefficient to advance ratio relationship for the propeller model

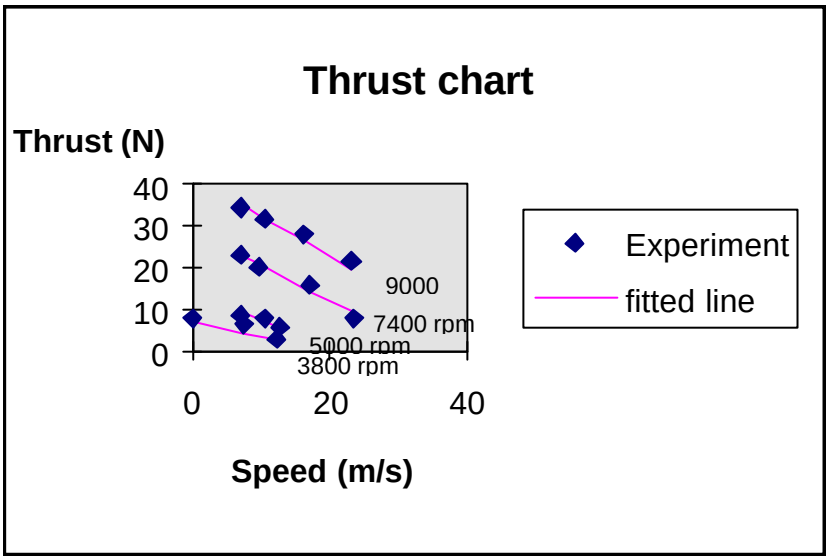

Figure 5-4: Comparison of the thrust chart from the experiment and the derived thrust model.

Comments on the result:

An adequate thrust model has been derived from the experiment, i.e. Ct=0.065-0.089J, with the standard deviation of the fitted line to the experiment data of 1 Newton (error of 3%).

Some of the possible sources of errors during the experiment were;

- The unsteady thrust reading due to the engine vibration.

- The presence of the wall in the working section (blockage effect). This error was calculated using a formula taken from Pope (1947, page 256) as follows;

$$\frac{V'}{V} = 1 - \frac{t - \frac{A}{C}}{2\sqrt{1+2t}}, \text{ where } \tau = \text{thrust} / (\rho A V^2)$$

A = propeller disc area, and C = tunnel cross sectional area.

A typical blockage effect of 4% was obtained from the calculation at the thrust value of 8.3N and tunnel speed of 10.4m/s. This value was small enough to be neglected in the analysis.

- Extraneous drag produced by the engine support and the exhaust hose.

- Thrust misalignment between the engine body and the airflow (a 2.4^0 misalignment results in approximately 0.8N error in thrust measurement).

- Limited accuracy of the instrumentation. The accuracy of the tachometer and the manometer are equivalent to 0.2N and 0.3N error in the thrust measurement respectively.

Centre of Gravity (CG) and Moment Of Inertia Determination

The centre of gravity (CG) locations and the moment of inertias were determined experimentally (see appendix 6 for the results).

Horizontal and vertical CG locations were determined by placing the T240 model on weighing scales at two different points, and measuring the reaction forces at these points. The model was then tilted and the scale readings were noted. The experiment was repeated for a number of tilt angles.

The equation for determining the CG is given in Wolowicz (1974) as:

$$\frac{R_N d}{W\cos q} = \bar{x} - \bar{z}\tan q \qquad \text{where } W = R_N + R_M \qquad \textbf{.....(5-7)}$$

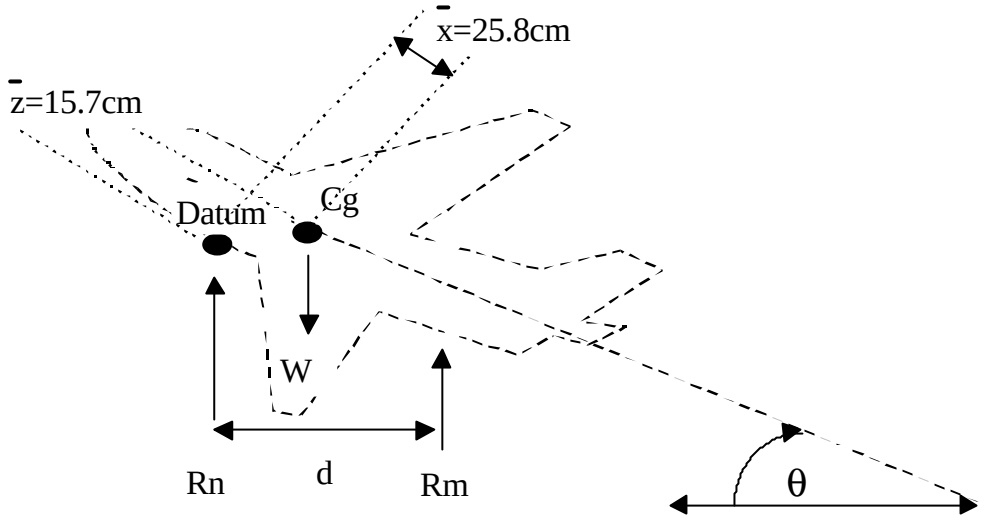

Figure 5-1: Experimental technique for determining weight and CG positions

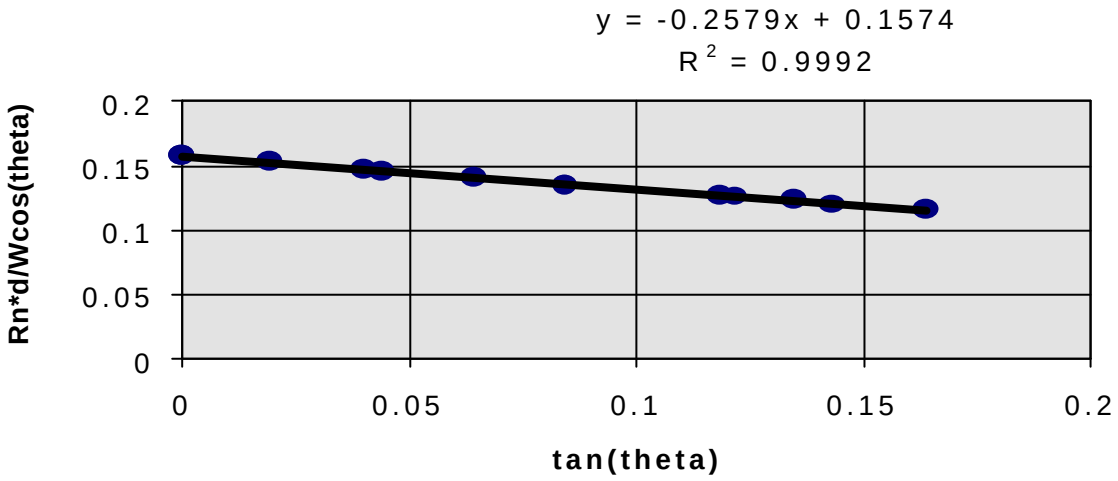

Figure 5-2: Results from the cg experiment

The result of the CG test indicated that the centre of gravity was located at 25.8 cm aft of the datum and 15.7 cm above the datum point (see Figure 5-1).

The pitching moment of inertia was determined by using a knife edge method. The model was supported on two knife-edges along the y-axis and allowed to oscillate (Figure 5.8). The time taken

for several oscillations were noted and averaged. The pitching moment of inertia was then calculated as (De Jong, 1987):

$$I_{yy} = \frac{T^2 Mgl_y}{4p^2} \qquad \textbf{.....(5-8)}$$

Where ly is the vertical distance between the cg and pivot point (in metre).

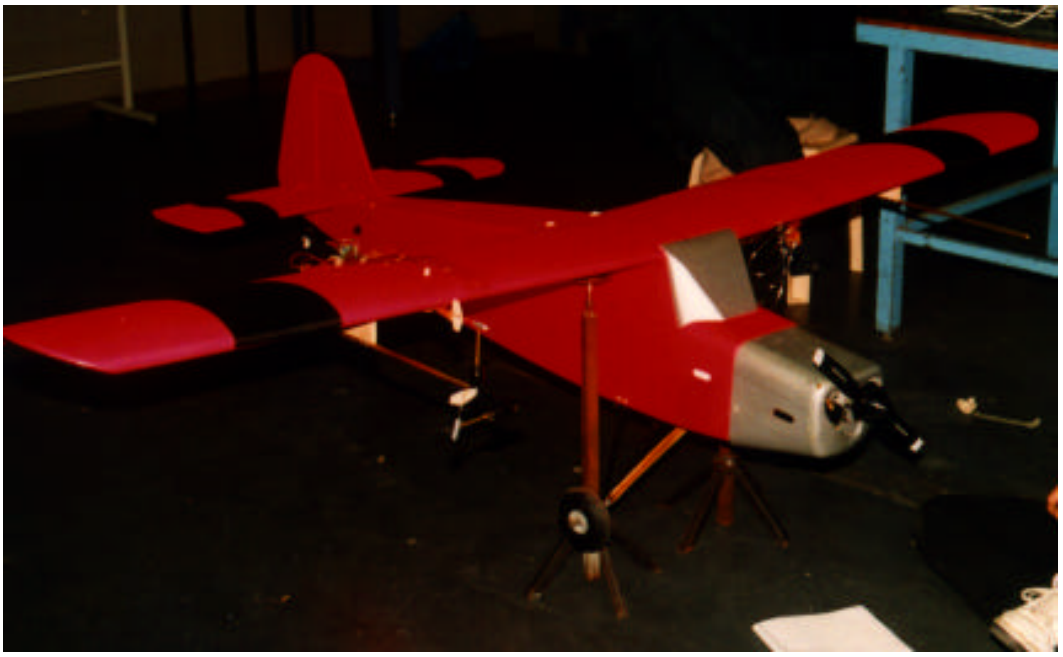

Figure 5-3: Pitching moment of inertia determination using a knife edge method

The yaw and roll inertias were determined experimentally using bifilar suspension method. In this method, the model was suspended by two thin strings equidistant from the centre of gravity and allowed to oscillate freely about the vertical axis passing through the centre of gravity. During the experiment, several samples were taken, and an average reading is used in the calculation. The equation to calculate the moment of inertia is given as (wolowicz, 1974):

For the yaw mode**:** $$I_{zz} = \frac{T^2 MgR^2}{4p^2 l} \qquad \textbf{.....(5-9)}$$

and for the roll mode : $I_{xx} = \frac{Mgl_x T^2}{4p^2}$ **.....(5-10)**

Figure 5-9: Experimental set-up to determine yaw and roll inertias

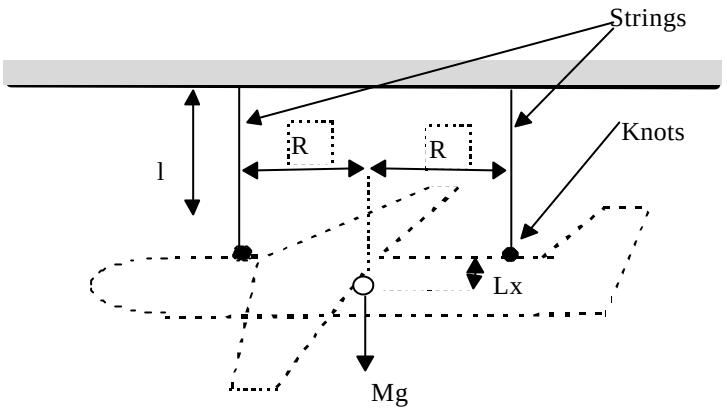

R (m)	=	0.25
l (m)	=	0.44
Lx	=	0.10
M (kg)	=	10.3

Figure 5-10: Yaw and Roll moment of inertias determination using bifilar suspension method

Table 5-2 shows the results of the inertia experiments.

Mode	Period (sec)	Calculated inertia (Kgm2)	Radius of gyration R (m)	Non-dimensional R
Yaw (I_{zz})	1.95	1.28	0.35	0.37
Roll (I_{xx})	2.12	1.15	0.33	0.30
Pitch (I_{yy})	1.90	1.30	0.36	0.46

Table 5-2: Results of moment inertia experiments

5.4 Theoretical Stability and Control Derivative Estimation

Theoretical stability and control derivatives estimation was conducted for the following purposes:

- To construct simulated flight test data and analyse the effectiveness of the various parameter identification methods prepared in this project.
- To provide a priori information for the Maximum Likelihood and Interactive Curve Matching methods.
- To compare with the derivatives estimated from flight test data.

Two different theoretical methods were used to estimate the stability and control derivatives of the T240 model.

(1) The AAA (Advanced Aircraft Analysis, version 1.7) software program (DARcorporation, 1996). This program is based on the theory given in the book written by Roskam (1985). The software provides a user friendly, iterative calculations of stability and control derivative of any aircraft. In addition, a data base approach of the software allows the user to use common sets of aircraft parameters when the parameters of the calculated aircraft are not yet available.
The estimation of the T240 stability and control derivatives was partly undertaken by an undergraduate student working on his final year project (Chow, 1996).
(2) A computer program written by the author based on the theory given in Smetana (1984). The theory has been proved successful in estimating the derivatives of several conventional-subsonic light aircraft.

6. Data Acquisition and Instrumentation Systems

6.1 Description And Specification

The data acquisition and instrumentation systems required to collect flight data, depend on several factors such as test objectives, method of analysis and hardware limitations. The system for extracting aircraft stability and control parameters may have different requirements than those for performance testing. In the former testing, for example, thrust and longitudinal acceleration measurements can be of secondary important when a Maximum Likelihood method is used. In contrast, the thrust and longitudinal acceleration measurements are critical in performance testing.

In this project, the data acquisition and instrumentation requirement is established by looking at other similar research in model flight testing (Coleman 1981, Wong 1989, Hamory 1994, and Budd 1993). Also NASA RP1168 (Maine 1986) provides essential guidance in establishing these requirements.

6.1.1 The data acquisition system

The data acquisition system (DAS) in this project is divided into that on-board (Figure 6-1) and on-ground (Figure 6-2). The system was developed separately by the Department of Computer Systems Engineering at the RMIT (Kneen 1994).

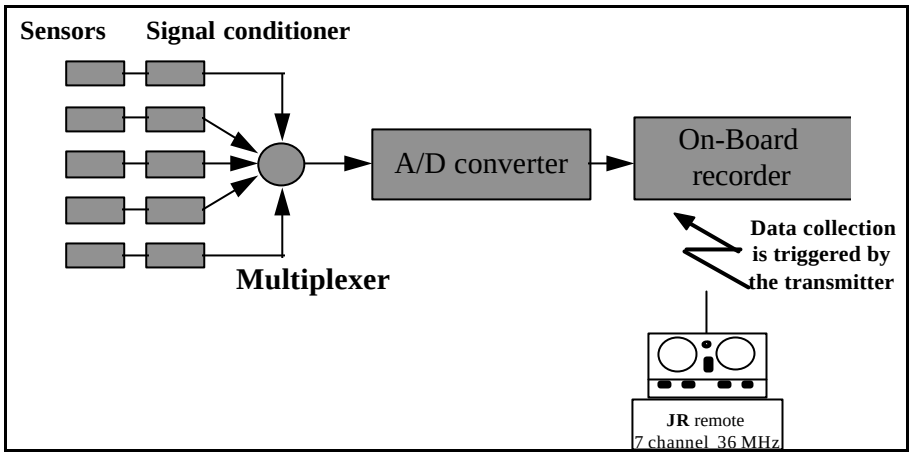

Figure 6-1: On-Board data acquisition systems

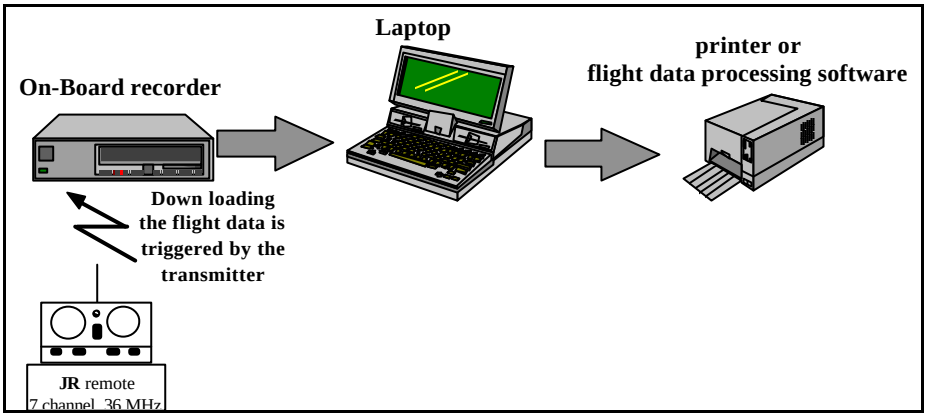

Figure 6-2: On-ground data system

Figure 6-3 shows the block diagram for the on-board DAS. The system is based on an Intel 8031 microprocessor operating at 3.6864 MHz. There are two 8 channel, analog to digital converters plus one timer input (channel 17 & 18). The DAS samples every 4 mill seconds (25 Hz) with 8-bit data resolution i.e. 256 counts for a full range data calibration. A total of 256 Kbytes onboard memory allows up to 10 minutes of data acquisition for each flight.

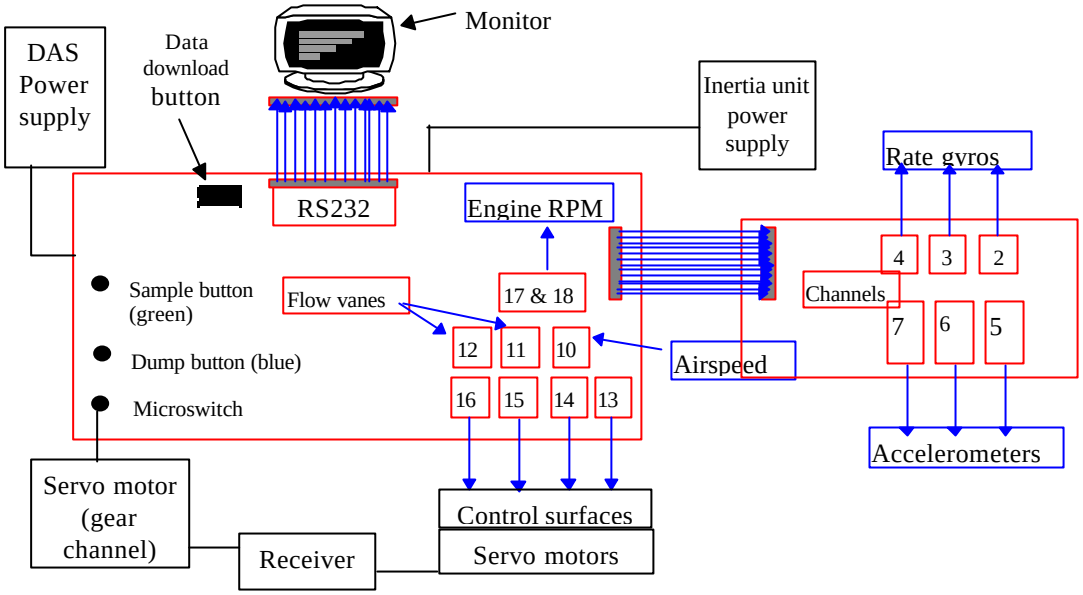

Figure 6-3: The on-board data acquisition block diagram for the T240 flight test program

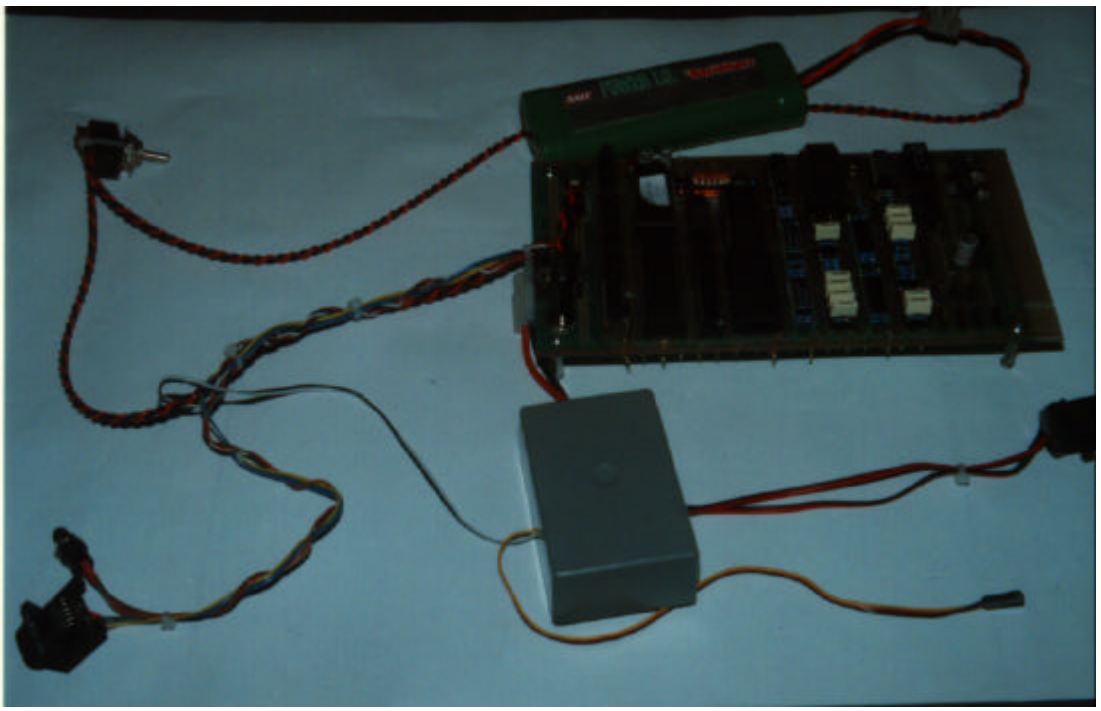

Figure 6-4: The DAS card used in the flight test

During flight, the onboard memory records flight data for intervals of 16 seconds. The recording is initiated by means of a microswitch operated from the radio transmitter, and terminated automatically after 16 seconds of data acquisition. At the end of every flight, the data is

downloaded into a personal computer via RS232 for further processing using Telemate communication software.

The system is equipped with 2 control-input buttons (see Figure 6-3), sample (green button) and dump (blue button). When the sample button is activated, the DAS will record one set of sample for 16 seconds. When the dump button is activated, the DAS will transmit the contents of its memory over the RS232 channel. This dump button has a secondary function, i.e. for a calibration mode. If the button is pressed during reset, the microprocessor is reset by removing and applying power, the DAS will then go into calibration mode. In this mode the input channels are continuously monitored and the results are transmitted via the RS232 line to a monitor. The Telemate communication software is used to display and save the results for further analysis.

The DAS collects 3 different type of input data, potentiometer inputs, voltage inputs and timer. The potentiometer inputs can deviate positive or negative. For maximum sensitivity, the potentiometers should be mounted so that to give reading close to 000 at minimum negative potentiometer deflection, and close to 255 at maximum positive deflection. If the required range can not be achieved, the resistors in the DAS circuit can be changed to alter the sensitivity.

One channel is organized to handle voltage input. This channel will indicate 000 with no input applied and 255 with the maximum. As for the potentiometer input, the sensitivity of this input can also be altered by changing the resistor in the DAS circuit.

The timer input is used to measure the time between input pulses. In practice, these pulses will be obtained from a hall effect switch, which measures the rotational speed of the aircraft's propeller. The timer provides two sets of outputs. The full result is obtained by combining 256 x first reading + second reading. These readings will indicate the propeller rotational speed and is obtained from the

calibration. In contrast to potentiometer and voltage inputs, the sensitivity of the timer can not be easily changed.

6.1.2 Instrumentation systems

There are 14 sensors used to measure inertia and air data during flight maneuvers. The characteristics of these sensors are listed in appendix 1. Most of the sensors are sufficiently accurate and commercially available at a relatively low cost. The rate piezo gyro for example, is the hobby type normally used in helicopter models, and has an acceptable linearity range (up to 720 deg/s).

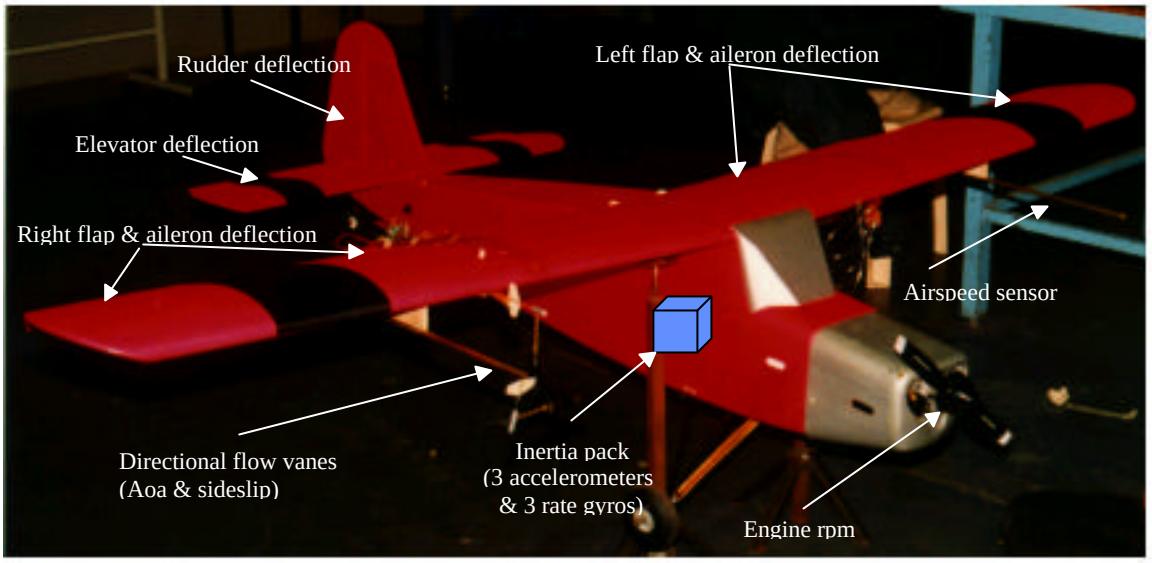

Figure 6-1: Sensor location on the T240 model

Figure 6-1 shows the location of each sensor on the aircraft. The individual sensors used in this project are described as follows:

Acceleration measurement

Linear accelerometers are used to measure longitudinal, lateral and vertical accelerations of the vehicle. The accelerometers are of the SETRA systems type, model 104, with 0.7 critical damping and 350 Hz natural frequency. They have an excellent static and dynamic response, with unlimited resolution (limited only by output noise level), low transverse sensitivity (0.005 g/g), compact and light-weight. In ± 6g nominal range, they have ±1% linearity, and produce a flat response from static up to 22 Hz. The accelerometers are normally used in vibrations, shock and impact measurements.

Angular rate measurement

Pitch, roll and yaw rate measurements are obtained using 3 piezo-rate gyros (type NE-1000). These gyros use flexural vibration of a piezo-electric triangular bar (see. Howell & William 1994). These rate gyros have a linearity range up to 720^0/sec.

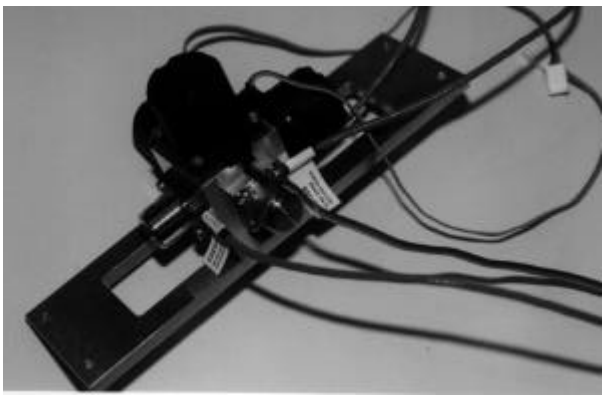

Figure 6-2: Inertia unit consists of 3 linear accelerometers (silver) and 3 rate gyros (black)

Since the accelerometers and rate gyros are not located exactly on the center of gravity of the aircraft, then corrections should be carried out to their readings. These corrections are dealt with in appendix 2. The accelerometer readings are required to perform this correction.

Airflow direction measurement

The airflow directions (angle of attack α, and sideslip β) are obtained using noseboom mounted flow vanes. A low rotational friction potentiometers are used to measure the vane angular deflections. The Murata MP06M3R1HA potentiometers have a very low minimum torque of 5 gr.cm, which is an essential feature in measuring the airflow direction. The potentiometers are also shielded

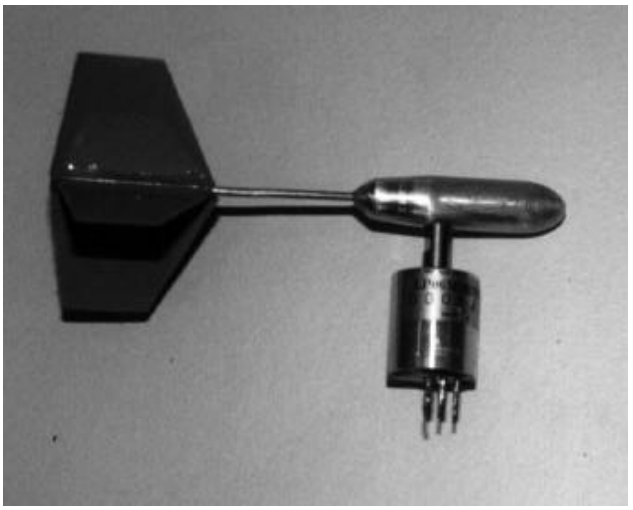

Figure 6-3: The angle of attack flow vane mounted on a low friction potentiometer

against any electromagnetic interference. From calculation of the vane dynamics, the vane has a natural frequency of 108 rad/s and damping of 0.2. The vane's natural frequency is well above the vehicles dynamic, and hence should not pose any problem.

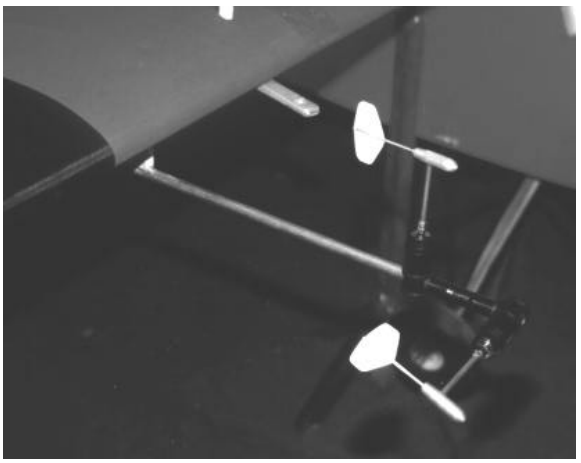

Figure 6-8: Flow vanes boom mounted on the wing of the aircraft

Air speed measurement

A pressure transducer and a pitot static tube were used in the airspeed measurement. The pressure transducer senses the different between total and static pressures from the pitot-static tube, and converts this into an equivalent airspeed. The pressure transducer (Sensym SCX01DNC) operates at 0-1 psi differential pressure range with a static sensitivity of 18 mV/psi. An amplifying circuit has been built to provide a 2-5Volt output for a 0-10 inches of water pressure measurement (equivalent to 0-65 m/s of airspeed)

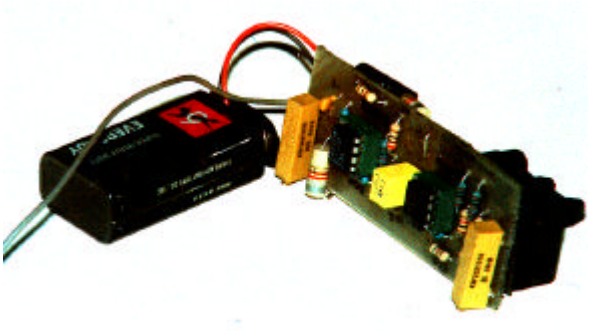

Figure 6-9: Differential pressure sensor used as speed indicator

Engine rotational speed measurement

A hall effect IC switch is used as a sensor to measure the engine rotational speed. The IC produces a "bounce-free" switching when influenced by a magnetic field. Hence by mounting a magnet on a disc, which rotates with the engine, the IC will produce a pulse train, which corresponds to the rotational speed of the engine.

The hall effect IC switch was selected since it was reliable, small in size, inexpensive, robust to environmental contamination such as heat and light, and can operate up to a high repetition rate (100 KHertz).

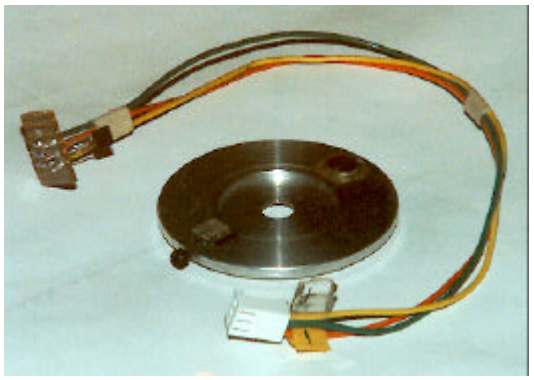

Figure 6-4: Engine rpm sensor and the rotating disc

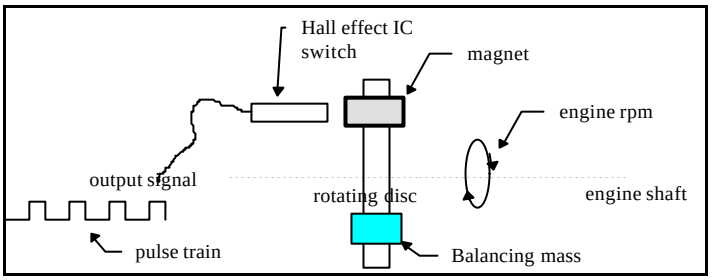

Figure 6-5: Propeller rotational speed measurement using a hall effect IC switch device

Holcomb and Tumlison from NASA (1977) used a hall effect device to measure their engine rotational speed successfully. A light sensor device can also be used, however a direct light from the sun may introduce an error, as experienced by Sydney University RPV (Wong 1989).

Control surface deflection measurement

Servo potentiometers RS173-574 are used to measure the angular deflections of the control surfaces. The deflections to be measured are those of elevator, rudder, left and right ailerons. The left and right ailerons are measured separately, since they are driven by a separate servomotor. On the other hand, the elevator deflection is obtained by measuring only one side of the control surface deflection since the left and right elevators are mechanically connected.

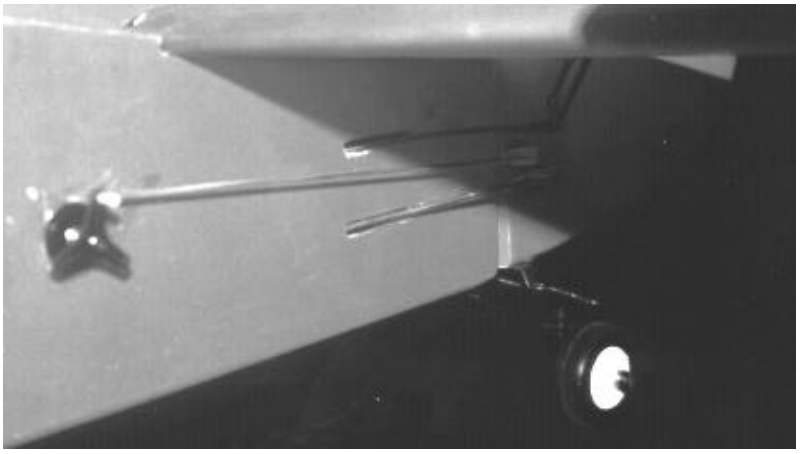

Figure 6-6: Rudder deflection sensor

The analysis of the sensor errors, deterministic and random, is described in appendix 2.

6.2 Calibration

Follow this procedure to carry out sensor calibrations:

- Connect the sensor to the allocated channel number on the DAS (refer to Figure 6-3).
- Run the Telemate Communication software and connect the DAS output port to the RS232 on the computer.
- Apply power to the DAS and at the same time press the dump button (blue).
- You should then be able to monitor all the sensor readings continuously on the monitor.

The results of the sensor calibration are given in appendix 4, including the fitted and the associated error curves.

Rate gyros

A rate table was used to calibrate the pitch, yaw and roll rate gyros (Figure 6-1). Since there was no rotational speed measurement available on the rate table, a switch potentiometer was used to measure the time taken for every revolution. Figure 6-2 shows a typical sample of rate gyro calibration result.

Figure 6-1: Rate gyro calibration using a rate table

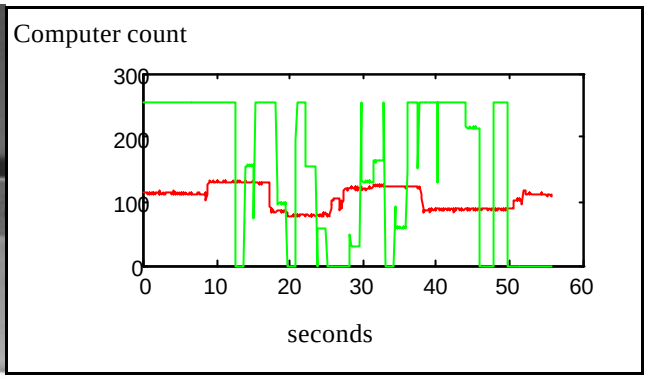

Figure 6-2: Rate gyro calibration trace

Airflow direction indicator

The calibrations for angle of attack and yaw vanes were conducted at the 3x2m Mechanical Engineering, RMIT. The whole model was mounted on a sting, with an adjustable pivot for changing the angle of attack. For one particular angle of attack setting, the model was yawed from -25 deg to +25 deg by rotating the table on which the model was supported. The procedure was repeated for several angle of attack settings.

The speed correction due to blockage effect in the wind tunnel was carried out using a formula taken from Pope (1947, page 220) as follows;

$$\frac{V'}{V} = 0.65\frac{Vol}{h^2 b}$$

where Vol = model volume

b = length of side of tunnel parallel to wingspan

h = height of tunnel

The calculated blocking correction for this experiment turned out to be 0.0054.

Control surfaces

The control surface calibrations were conducted by deflecting the appropriate control surfaces while noting the output from the corresponding channels. The control deflections were measured by a digital inclinometer, which has an accuracy of 0.2 deg.

Pressure sensor (Airspeed indicator)

Calibration of the airspeed indicator (pitot-static boom) was conducted in the 50x50cm Aerospace Engineering wind tunnel, RMIT. The pitot-static boom was removed from the aircraft and placed inside the wind tunnel for calibration. An inclined manometer was used to measure the tunnel speeds. Voltage outputs from the airspeed sensor were noted for several tunnel speeds and plotted to obtain the sensor calibration.

To minimize pressure errors caused by the boom installation on the wing, the boom length was designed to be at least four times the wing thickness (Gracey, 1981). Hence no pressure error was considered in this project, except the *kinematics position error* due to offsets from the aircraft's center of gravity (see appendix 2).

From the calibration, the obtained sensor characteristics are summarized in Figure 6-3 below:

Figure 6-3:Results of the sensor calibrations

Sensors	Calibration	Error		Range	Resolution
		Standard deviation (% full scale)	Mean		
Accelerometers					
Rate gyro 1 (chn 2)	1.4283X-216.88	1.0005 deg/s (0.27)	1.345×10^{-14}	-170 to +170 deg/s	1.4 deg/s
Rate gyro 2 (chn 3)	1.5342X-234.38	1.1977 deg/s (0.30)	-3.527×10^{-14}	-170 to +170 deg/s	1.5 deg/s
Rate gyro 3 (chn 4)	-1.3555X+170.84	3.9375 deg/s (1.14)	3.4639×10^{-14}	-170 to +170 deg/s	1.3 deg/s
Angle of attack vane (chn 12)	-0.43511X+63.768	0.6745 deg (0.66)	1.228×10^{-14}	-30 to +30 deg	0.4 deg
Yaw vane (chn 11)	0.41327X-57.99	0.7515 deg (0.74)	-0.962×10^{-14}	-20 to +20 deg	0.4 deg
Elevator (chn 15)	$-1.0155x10^{-5}X3+3.1717x10^{-3}X^2+5.9756x10^{-2}X-33.208$	0.2096 deg (0.5)	-0.7905×10^{-15}	-30 to +11 deg	0.25 deg
Rudder (chn 16)	$-6.1266x10^{-6}X^3+2.4028x10^{-3}X^2+9.3398x10^{-2}X-45.87$	0.3346 deg (0.6)	1.5258×10^{-15}	-30 to +30 deg	0.25 deg
Right aileron (chn 14)	$2.2612x10^{-6}X^3-9.3349x10^{-4}X^2-7.5499x10^{-2}X-21.917$	0.5094 deg (1.2)	5.9164×10^{-15}	-20 to +21 deg	0.25 deg
Left aileron (chn 13)	$-2.767x10^{-6}X^3+1.3356x10^{-3}X^2-4.477x10^{-3}X-18.115$	0.1747 deg (0.58)	-1.790×10^{-15}	-13 to +17 deg	0.25 deg
Flap (Channel 14)	$-2.5549x10^{-6}X^3+5.9816x10^{-4}X^2+1.9118x10^{-1}X-5.4749$	0.4075 deg (1.02)	2.6412×10^{-15}	0 - +40 deg	0.17 deg
Airspeed (chn 10)	$(1890.3X-3544.6)^{0.5}$	1.7 m/s (2.6)	9.2667×10^{-13}	0-65m/s (0-10 inc H_2O	0.12 inc H_2O
Engine rotational speed (chn 17 and 18)	256*channel 17 + channel 18	-	-	100-25000	100 rpm

Note: X is the corresponding channel reading.
Pressure (inc water) = $2.40867x10^{-3}$ Speed^2 (m/s)
Channels 8 and 9 are spares.

7. Practice and implementation problems

7.1 Problems encountered during the development of the instrumentation systems

- We originally planned to use a Remtron RTS-1 Telemetry System for collecting the flight data. The system was developed by the Computer System Engineering Department, RMIT (Howell and Wiliams, 1994). However, since we were anticipating more problems in trying to make the system works (e.g. signal interference with the receiver), then we decided to develop an onboard DAS instead. The onboard DAS would also produce a better flight data reading than the telemetry system.

- Due to memory devices' problems in the DAS, we could not have the 256 Kbytes (corresponds to a 10 minutes of data acquisition) onboard memory originally planned. Instead we have a 16-second of flight data recording.

- The rate gyros consume a lot of current. In the calibration, all the three gyros gave an inconsistent result. A large drift was noticed, especially on roll gyro. Eventually, an extra power supply was added using a 7.2 NiCad battery.

- We had problems in getting the accelerometers working. There was no provision made in the DAS for the accelerometer offset voltage, and hence the accelerometer drove the amplifiers into saturation.

- Sensor and DAS adjustments, such as reading range and resolution, were an elaborate process. The process had to be carried out in two different places. The sensor calibration was conducted at the Aerospace Engineering Department; and the adjustment of the sensor sensitivity in the DAS was carried out at The Computer System Engineering Department.

7.2 Transmitter and DAS (Data Acquisition System) interference.

We experienced an interference problem between the transmitter signal and the DAS. During preliminary flight tests, the transmitter signal has momentarily lost twice. The existent of the interference was also noticed during the ground range test. The transmitter signal terminated immediately when the DAS was switched on.

Two immediate actions were taken before continuing the flight test. First, the whole DAS was placed in an enclosed metal box and grounded to the battery. Second, the receiver and antenna were moved to the bottom of the fuselage so that their positions are as far away from the DAS as possible. However, no significant improvement was noticed from these two actions.

The interference problem was solved after many trials and errors. There was substantial assistance and suggestions from John Kneen[1], Mal Wilson[2] and Mitchell Lennard[3]. The steps taken to reduce the interference are described below. They are listed chronologically.

1. Enclosing the whole DAS in an aluminium box to prevent any radiation from the DAS.
2. Moving the receiver and antenna to the bottom of the aircraft's fuselage, as far away as possible from the DAS.
3. Collecting all the sensor ports into a single port, and hence reducing the complexity of the sensor wiring going into the DAS.
4. Replacing all the cables parallel to the antenna (those of rudder, elevator and engine rpm) by shielded computer data cables. Then all these sensors had to be recalibrated.

[1] Associate Professor John Kneen is a senior lecturer at the Computer System Engineering Department, RMIT. He has built the DAS for this project, and currently supervising 2 Phd's in flight control systems.

[2] Mal Wilson is a technical staff at the Aerospace Engineering, RMIT, formerly electrical technician with RAAF. He has flown model aircrafts for more than 15 years, and has a lot of experience in electrical and communication.

[3] Mitchell Lennard is an avionic design consultant with Mikley system integration.

5. Moving all the power supplies into the aluminium box together with the DAS. This was done since the power supplies might radiate signals which interfered with that of the transmitter.

6. Moving all the switches (that for data retrieval, power supplies and rate gyro) into the aluminium box. By this time, all the cables were contained inside the box, except that from the sensors located around the aircraft.

7. Installing a digital low pass filter ('D' connector) to all the cables carrying currents. The attenuation of the filter was approximately 20dB at 40 MHz.

8. Elimination of all intermittent ground loops.

9. Replacing the on/off relay switch by a microswitch to trigger the DAS. The microswitch was operated by a servomotor through the gear channel on the radio transmitter. The idea was to eliminate any direct cable connection between the receiver and the DAS. Also by using a separate motor, we would have an option to use a separate transmitter to trigger the DAS. By this time, the ground range was considerable improved to approximately 150 meter. However, this was still not yet considered adequate for the aircraft to fly safely.

10 Changing the radio transmitter frequency from a PCM 36 MHz to TF-FM 29.725 MHz. This was done since we suspected that the DAS clock (operating at 3.6864 MHz) somehow interferes with the transmitter signal at 36 Mho (1/10 harmonic). Another option was to change the internal clock of the DAS. However, this would create problems in retrieving the data from the DAS since the 3.6864 divides down to give the standard serial baud rates of 9600.

By this point, significant increase in the transmitter range satisfied us to resume our flight testing.

7.3 Problems on the aircraft model to be tested.

- The first aircraft model to be flight-tested was the half scale MAFV (Figure 7-1). A pitot-static and flow vane's boom was mounted on the nose of the model. The model was tested in the wind tunnel. The lift, drag and pitching moment were measured using strain gages. However, the result was not satisfactory. Except for the lift, significant scatters on the drag and pitching moment were apparent.

- Unfortunately, the half scale MAFV model crashed on the first flight trial. The propeller hit the ground on take off. After a few seconds of flight the pilot felt that the canard control was too sensitive and decided to cut off the engine. However, the aircraft became nose heavy and crashed to the ground. To proceed with the project, we purchased and assembled a Telemaster Precedent T240 aircraft model (Figure 7-2). In approximately 2 ½ Months the aircraft was ready to undergo its first flight testing.

Figure 7-1: The half scale MAFV

Figure 7-2: The Telemaster Precedent T240

- We also had a problem with engine to power the Telemaster T240. We originally used the RC-80 engine. However, getting this engine to work was a difficult task. Eventually, we decided to

purchase another engine (Irvine-150, 22cc). This was a very good engine and proved easy to start.

- The Telemaster T240 crashed at the 13th flight due to an undetected flat battery. The model suffered a major damage to its engine mounting & cowling, its right fuselage, low directional vanes, engine rpm, rudder and elevator sensors. We spent 3 weeks to rebuilt the model and recalibrate most of the sensors.

7.4 Problems in flying the aircraft.

The following lists some of the problems encountered in the actual flying and conducting the required manoeuvres.

- Weather dependent. The model should be flown in a calm air (free of turbulence), preferable early in the morning. However since we conducted most of the flying in the winter, we would be fortunate to have one perfect day to fly out of one week.
- Limited visual range and lack of information on the model's flying condition.
- Difficulty in getting an exact trim condition.
- Inability of the model to perform a required manoeuvre to *produce a rich information* response.
- Structural vibration due to engine rpm degrades the angular rate readings. Figure 7-1 shows a contaminated roll rate reading during a flight manoeuvre with engine on. Figure 7-2 shows the roll rate response with engine idle.

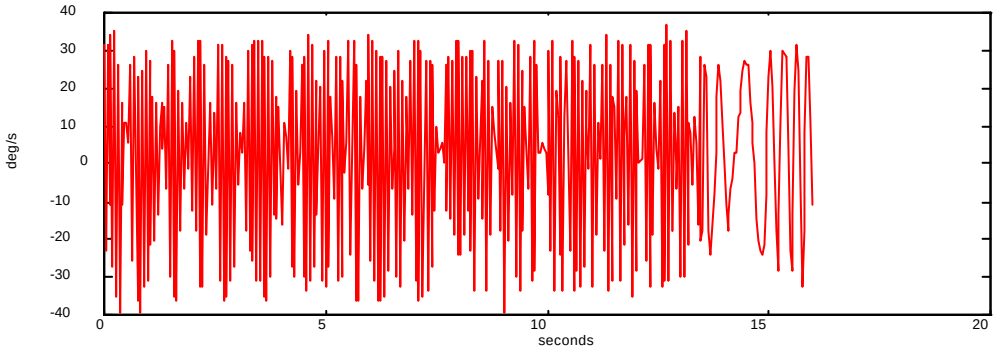

Figure 7-1: Roll rate reading buried in engine noise during a flight manoeuvre

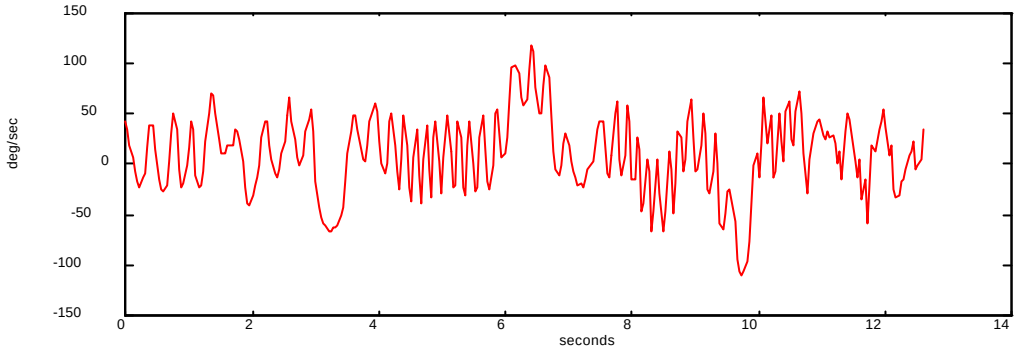

Figure 7-2: Roll rate reading with engine idle

- The presence of air turbulence during the test manoeuvre. Figure 7-3 and Figure 7-4 show the difference in the recorded angle of attack in a turbulence and calm air.

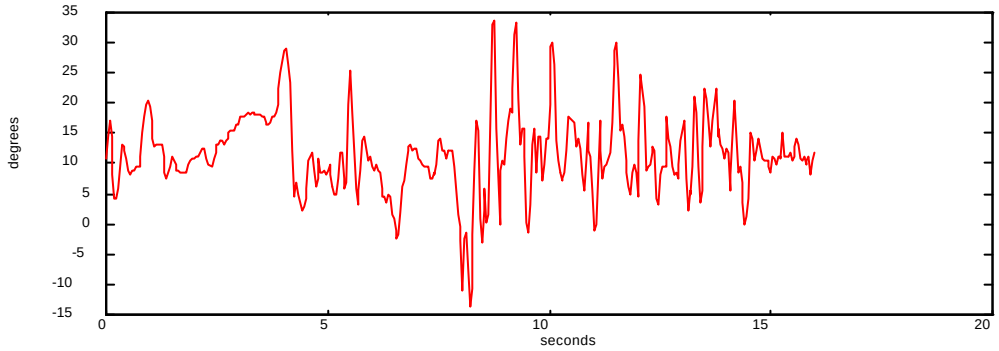

Figure 7-3: Angle of attack reading buried in turbulence during an elevator doublet manoeuvre.

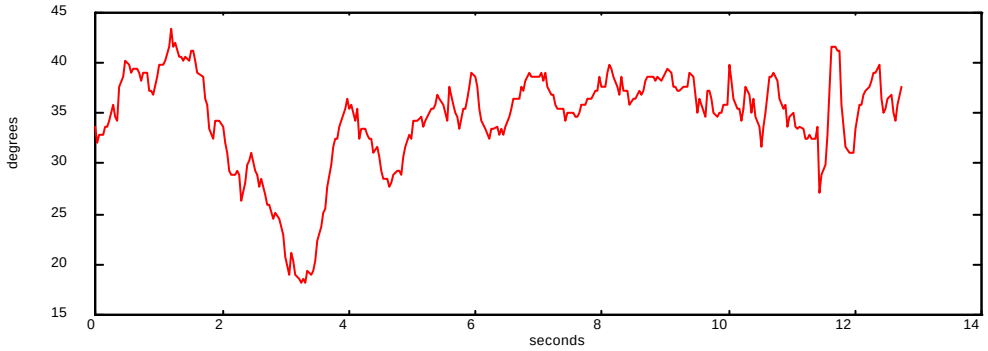

Figure 7-4: Angle of attack response in a reasonable calm air

- Coupled longitudinal and lateral motions during the test.
- Very short dynamic response of the model due to a high inherent stability of the model.

8. Identification from simulated data.

A simulated data has been generated using equations (3-24) and (3-27) to study the effectiveness of the various parameter identification techniques. We divided the work into separate longitudinal and lateral derivatives identification. In order to resemble the actual flight manoeuvre, the control inputs used for the simulation are taken from the real flight test data. The resulted responses were then analysed using several parameter identification techniques.

The work was also extended to study the effect of measurement noise and different input forms to the estimated parameters.

8.1 Longitudinal identification

The aircraft was excited by an elevator doublet as shown in Figure 8-1. The response of the model lasted about 6 seconds.

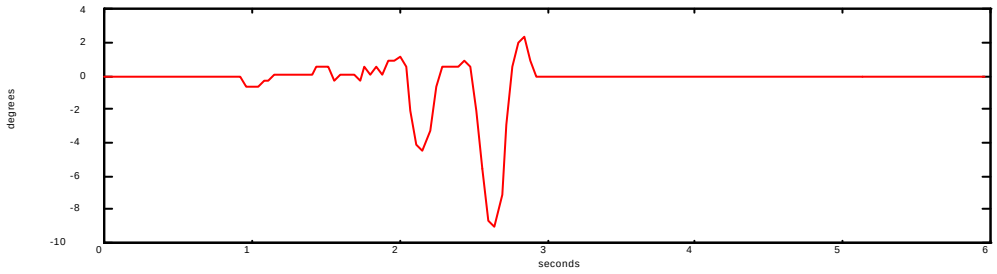

Figure 8-1: Elevator deflection

The results of the longitudinal identification using various identification techniques are summarised in Table 8-1. Also shown in the table are the characteristics of the Short Period Oscillation mode. Note that the ICM does not give a measure of uncertainty for each estimated parameter.

The LR, MLM and ICM have successfully identified the six longitudinal derivatives and the SPO characteristics of the model. The frequency of the SPO was even estimated quite accurately. In the analysis, the results from the LR are used as a-priori values for the MLM and ICM. Among the three

techniques, the MLM produces the best estimate of the derivatives. Table 8-2 shows that the MLM produces the smallest error criterion.

		Algorithms				
		LR		MLM		ICM
Derivatives	**True parameter**	Estimated parameter	Standard deviation	Estimated parameter	Cramer Rao Bound	Estimated parameter
Cz_{α}	-4.399	-3.549	0.004	-4.371	0.084	-1.840
Cz_{q}	-5.851	9.097	0.068	-17.750	1.274	-0.010
$Cz_{elevator}$	-0.364	0.446	0.002	-1.146	0.009	-0.400
Cm_{α}	-1.178	-1.317	0.023	-1.311	0.017	-1.324
Cm_{q}	-11.03	-1.680	0.354	-11.090	0.162	-16.400
$Cm_{elevator}$	-0.941	-0.803	0.010	-0.946	0.010	-0.884
ω_{nSPO} (rad./s)	6.83	6.71		6.85		6.95
ξ_{SPO}	0.51	0.23		0.51		0.52

Table 8-1: Results from various estimation algorithms

	LR	MLM	ICM
mean (α)	0.0066	0.0026	0.0039
standard deviation (α)	0.2924	0.0154	0.0179
mean (q)	0.0148	0.1226	0.3013
standard deviation (q)	1.8822	0.7197	1.1549

Table 8-2: Mean and standard deviation of the fitted error response for the various identification algorithms

Since the acceleration measurements were not available, when performing LS algorithm the α and q records were differentiated to produce Cz and Cm respectively. This explains the reason why significant errors are observed from the LS result. The differentiation of α and q have introduced significant noise. The LR estimated Cz_{α} , Cm_{α} and Cm_{q} quite well. However Cz_{q}, $Cz_{elevator}$ and Cm_{q} were poorly estimated. The resulting fits to α and q are shown in Figure 8-2 and Figure 8-3 respectively. The estimated responses show a significant error after the elevator input was removed (after 3 seconds). The damping was underestimated (50% down), but the frequency was closely estimated (1.5% down).

The MLM algorithm on the other hand, estimated most of the longitudinal derivatives satisfactorily, except for the Cz_q. The large Cramer Rao value for the Cz_q indicates that this derivative is weakly identified. The α (Figure 8-4) and pitch rate (Figure 8-5) show a good fit between the actual and estimated responses. The SPO characteristics were also well identified.

The ICM algorithm estimated Cm_α , $Cm_{elevator}$ and SPO characteristics quite well. Those parameters which do not change the α and q responses significantly such as Cz_α, Czq and Cmq are poorly estimated. Figure 8-6 and Figure 8-7 show the result of the fit.

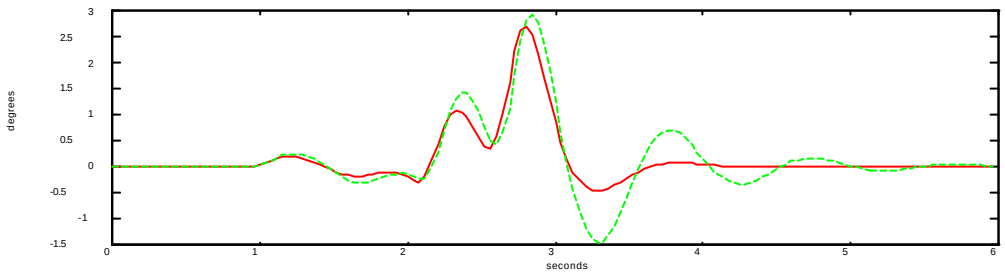

Figure 8-2: Angle of attack response using regression analysis. (--- = estimated))

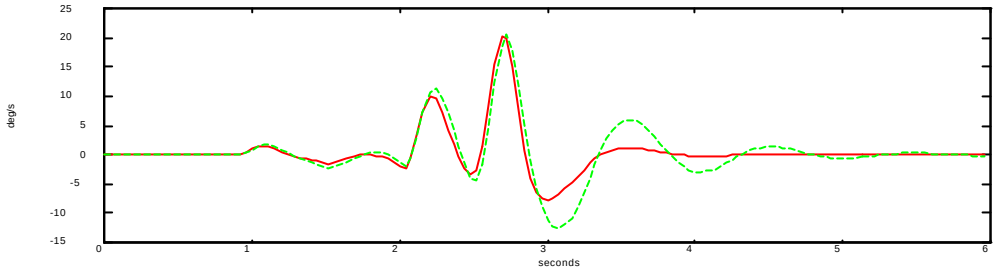

Figure 8-3: Pitch rate response using regression analysis. (--- = estimated)

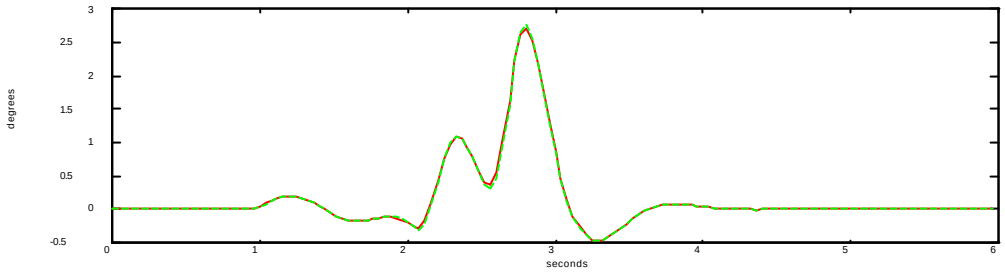

Figure 8-4: Angle of attack response using MLM analysis. (--- = estimated)

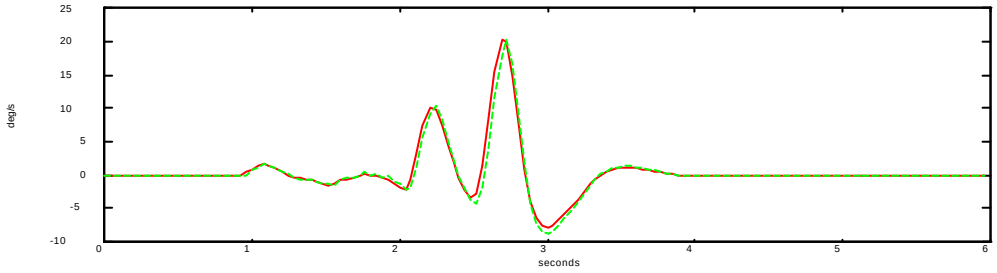

Figure 8-5: Pitch rate response using MLM analysis. (--- = estimated)

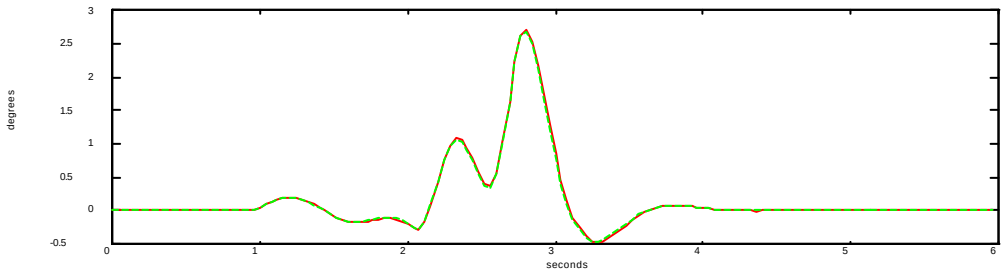

Figure 8-6: Angle of attack response using ICM analysis. (--- = estimated)

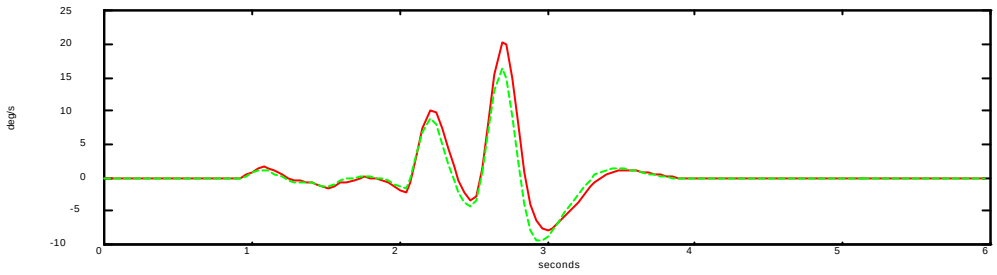

Figure 8-7: Pitch rate response using ICM analysis. (--- = estimated)

8.2 Lateral identification

The aircraft was excited by a rudder doublet (Figure 8-1) followed immediately by an aileron pulse (Figure 8-2). The responses of the model lasted about 8 seconds.

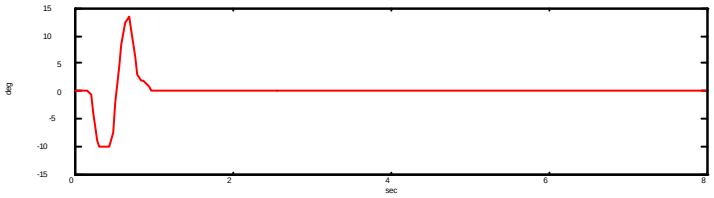

Figure 8-1: Rudder deflection

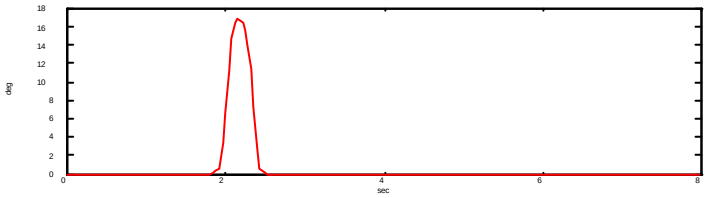

The results of the identification using various identification techniques are summarised in Table 8-3. Also shown in the table are the characteristics of the Dutch and spiral modes.

The LR, MLM and ICM have successfully identified the fifteen lateral derivatives, Dutch and Spiral mode characteristics of the model. In the analysis, the results from the LR are used as a-priori values for the MLM and ICM. Among the three techniques, the MLM produces the best estimate of the

derivatives. Table 8-4 shows that the MLM produces the smallest error criterion. Ideally, the estimated parameters from LR should give exactly similar values as the true parameters. However, the differentiation process of angular rate in the simulation has introduced errors in the LR estimation.

		Algorithms				
		LR		MLM		ICM
Derivatives	**True parameter**	Estimated parameter	Standard deviation	Estimated parameter	Cramer Rao Bound	Estimated parameter
Cy_{β}	-0.354	-0.347	0.0007	-0.349	0.0080	-0.347
Cy_{p}	-0.043	-0.606	0.0069	-0.126	0.0529	-0.606
Cy_{r}	0.153	-0.442	0.0059	0.27	0.0902	-0.442
$Cy_{\delta r}$	0.089	-0.172	0.0015	0.343	0.0013	-0.172
$Cy_{\delta a}$	0	0.034	0.0025	0.041	0.0049	0.034
Cl_{β}	-0.043	-0.038	0.0009	-0.045	0.0012	-0.038
Cl_{p}	-0.733	-0.646	0.0091	-0.751	0.0017	-0.648
Cl_{r}	0.221	0.257	0.0077	0.291	0.0131	0.256
$Cl_{\delta r}$	-0.001	0.001	0.0015	-0.006	0.0007	0.001
$Cl_{\delta a}$	0.321	0.302	0.0033	0.330	0.0027	0.281
Cn_{β}	0.002	0.002	0.0004	0.003	0.0001	0.002
Cn_{p}	-0.084	-0.095	0.0036	-0.065	0.0019	-0.096
Cn_{r}	-0.096	-0.073	0.0031	-0.095	0.0014	-0.073
$Cn_{\delta r}$	-0.045	-0.044	0.0006	-0.044	0.0002	-0.045
$Cn_{\delta a}$	0	0.006	0.0013	-0.008	0.0008	0.006
ωn_{Dutch} (rad./s)	1.38	1.42		1.38		1.43
ξ_{Dutch}	0.75	0.66		0.75		0.65
T_{spiral} (sec)	0.52	0.60		0.51		0.61

Table 8-3: Results using various estimation algorithms

	LR	MLM	ICM
mean (β)	0.0040	0.0005	0.2445
standard deviation (β)	0.6698	0.0088	0.4815
mean (p)	-0.1755	0.0612	-0.1115
standard deviation (p)	1.2178	1.6374	1.0633
mean (r)	0.0134	-0.0195	-0.0434
standard deviation (r)	1.0177	0.4275	0.7946

Table 8-4: Mean and standard deviation of the fitted error response for the various identification algorithms

From the simulation, the sensitivity of each derivative to the flight responses can be studied. Table 8-5 presents the result from the sensitivity study. This table is very useful in assisting which parameters to be held fixed during the MLM estimation.

	Degree of sensitivity		
Derivatives	High	Moderate	Low
Cz_{α}	+		
Cz_{q}			+
$Cz_{\delta elevator}$		+	
Cm_{α}	+		
Cm_{q}		+	
$Cm_{\delta elevator}$	+		
Cy_{β}		+	
Cy_{p}			+
Cy_{r}			+
$Cy_{\delta aileron}$			+
$Cy_{\delta rudder}$		+ (needs high freq input)	
Cy_{β}		+	
Cl_{p}	+		
Cl_{r}		+	
$Cl_{\delta aileron}$	+		
$Cl_{\delta rudder}$			+
Cn_{β}	+		
Cn_{p}			+
Cn_{r}		+	
$Cn_{\delta aileron}$			+
$Cn_{\delta rudder}$	+		

Table 8-5: Sensitivity of each derivative to the flight responses

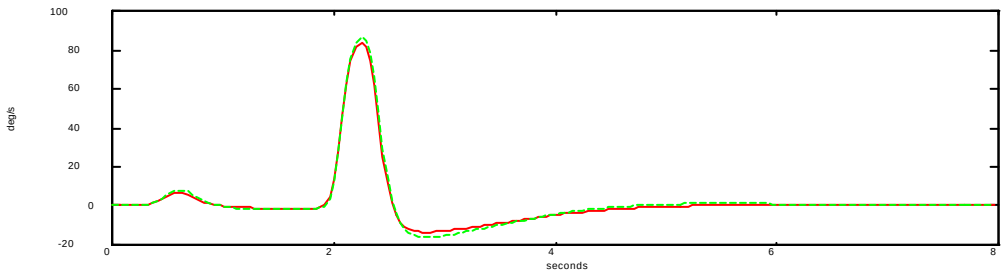

Figure 8-3: Roll rate response using regression analysis. (--- = estimated)

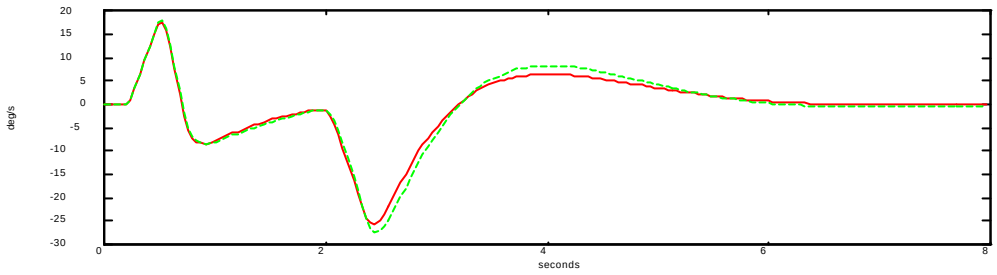

Figure 8-4: Yaw rate response using regression analysis. (--- = estimated)

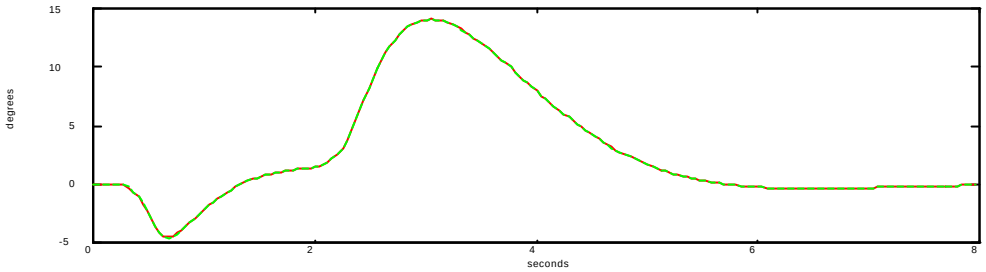

Figure 8-5: Sideslip response using MLM analysis. (--- = estimated)

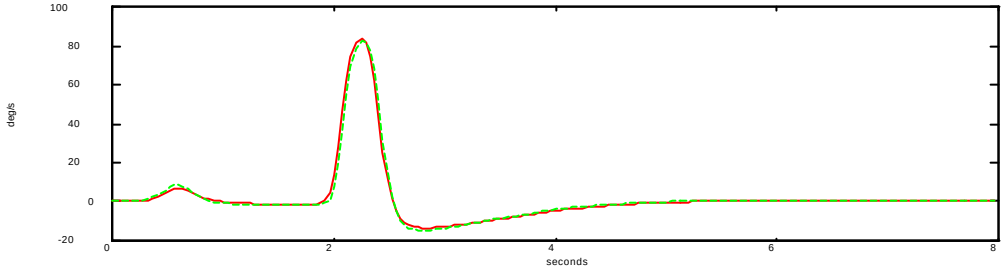

Figure 8-6: Roll rate response using MLM analysis. (--- = estimated)

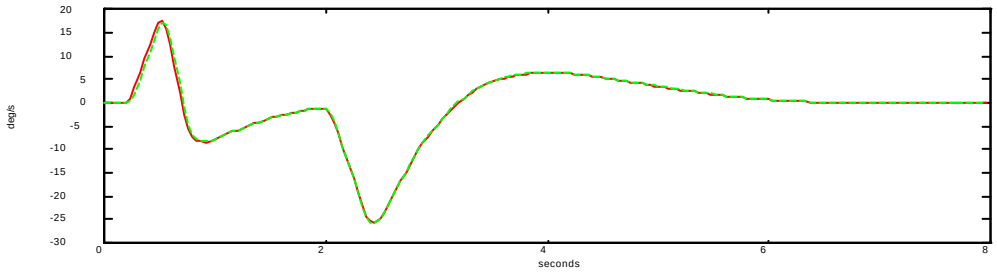

Figure 8-7: Yaw rate response using MLM analysis. (--- = estimated)

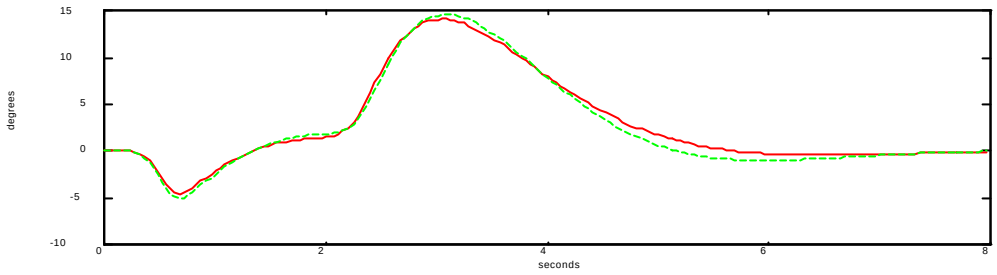

Figure 8-8: Sideslip response using ICM analysis. (--- = estimated)

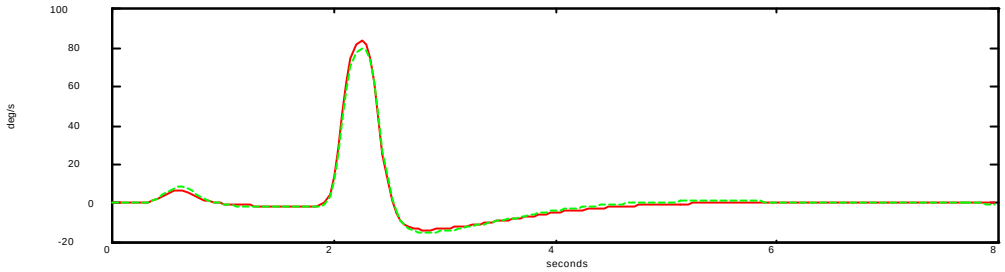

Figure 8-9: Roll rate response using ICM analysis. (--- = estimated)

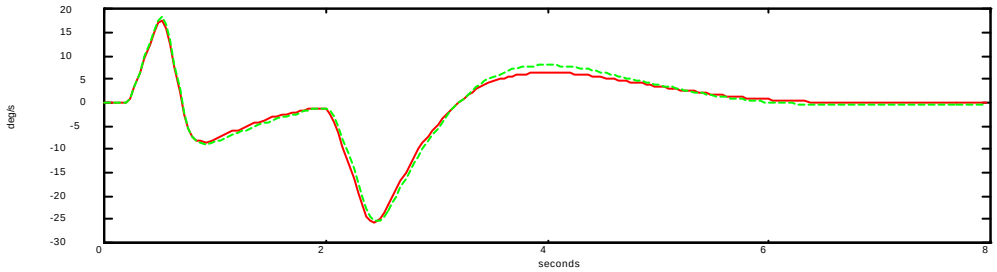

Figure 8-10: Yaw rate response using ICM analysis. (--- = estimated)

8.3 The effect of measurement noise

Measurement noises were added to all the flight records. Then, the MLM was used to estimate the longitudinal and lateral derivatives from the noisy records. We assume a white-Gaussian noise with zero mean and standard deviations as shown in Table 8-6 below. Note that these values were taken as the scatter of the sensor calibrations.

Record	Standard deviation	Maximum signal to noise ratio
Angle of attack	0.7 deg	4
Sideslip angle	0.7 deg	20
Pitch rate	1.2 deg/s	17
Roll rate	1.2 deg/s	69
Yaw rate	1.2 deg/s	15
Elevator deflection	0.2 deg	12
Aileron deflection	0.2 deg	84
Rudder deflection	0.3 deg	45

Table 8-6: Measurement noise level used in the simulation

The results of the MLM algorithm are shown below:

			No noise		With noise	
Derivatives	True values	Airport	Estimated parameter	Cramer Rao Bound	Estimated parameter	Cramer Rao Bound
Cz_{α}	-4.399	-6	-4.371	0.1373	-4.126	0.858
Cz_{q}	-5.851	0	-17.75	2.080	-9.401	25.11
$Cz_{\delta elevator}$	-0.364	0	-1.146	0.015	-1.399	0.909
Cm_{α}	-1.178	-1	-1.311	0.027	-0.966	0.112
Cm_{q}	-11.03	-10	-11.09	0.265	-19.60	2.382
$Cm_{\delta elevator}$	-0.941	-1	-0.946	0.015	-1.113	0.054
ωn_{SPO} (rad./s)		6.83	6.85		6.90	
ξ_{SPO}		0.51	0.51		0.72	

Table 8-7: Estimated Longitudinal Derivatives Using MLM algorithm for cases with and without measurement noise

Derivatives	True values	Airport	No noise		With noise	
			Estimated parameter	Cramer Rao Bound	Estimated parameter	Cramer Rao Bound
Cy_{β}	-0.354	-0.347	-0.349	0.0080	-0.456	0.0705
Cy_{p}	-0.043	-0.606	-0.126	0.0529	-1.853	1.2260
Cy_{r}	0.153	-0.442	0.27	0.0902	-0.220	0.4504
$Cy_{\delta r}$	0.089	-0.172	0.343	0.0013	0.320	0.1346
$Cy_{\delta a}$	0	0.034	0.041	0.0049	0.688	0.4511
Cl_{β}	-0.043	-0.038	-0.045	0.0012	-0.059	0.0026
Cl_{p}	-0.733	-0.646	-0.751	0.0017	-1.012	0.0352
Cl_{r}	0.221	0.257	0.291	0.0131	0.227	0.0204
$Cl_{\delta r}$	-0.001	0.001	-0.006	0.0007	-0.010	0.0041
$Cl_{\delta a}$	0.321	0.302	0.330	0.0027	0.422	0.0132
Cn_{β}	0.002	0.002	0.003	0.0001	0	0.0006
Cn_{p}	-0.084	-0.095	-0.065	0.0019	-0.099	0.0101
Cn_{r}	-0.096	-0.073	-0.095	0.0014	-0.101	0.0033
$Cn_{\delta r}$	-0.045	-0.044	-0.044	0.0002	-0.045	0.0011
$Cn_{\delta a}$	0	0.006	-0.008	0.0008	0.004	0.0039
ωn_{Dutch} (rad./s)	1.38		1.38		1.37	
ξ_{Dutch}	0.75		0.75		0.76	
T_{spiral} (sec)	0.52		0.51		0.34	

Table 8-8: Estimated Lateral Derivatives Using MLM algorithm for cases with and without measurement noise

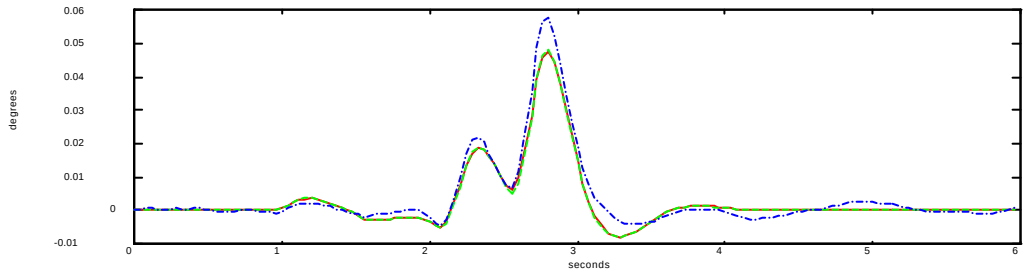

Figure 8-1: The effect of noise on the angle of attack response (solid line = true response, ---- = no noise, -.-. = with noise)

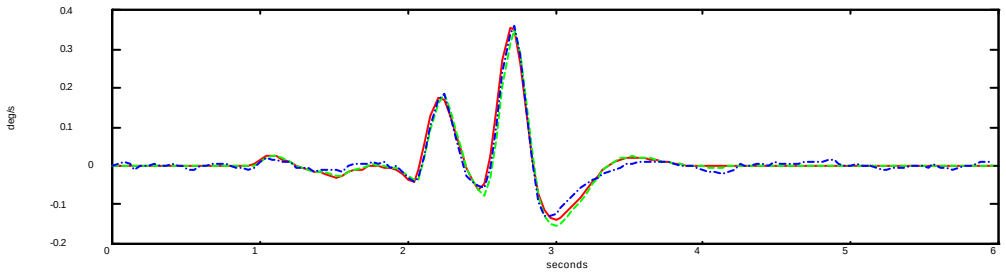

Figure 8-2: The effect of noise on pitch rate response (solid line = true response, ---- = no noise, -.-. = with noise)

The presence of measurement noise increases the uncertainty in the estimated parameters. This increased uncertainty is reflected in the increase of CRB values for both longitudinal and lateral derivatives. However, no significant change was noticed in the predicted responses, as shown in Figure 8-1 and Figure 8-2. The most affected parameters in the presence of noise are pitch rate derivatives (Cz_q and $Cz_{\alpha)}$ in longitudinal mode, and sideforce derivatives (Cy_β, Cy_p, Cy_r, Cy_{dr} and Cy_{da}) in lateral mode.

8.4 The effect of different input forms.

The effect of different input forms (Figure 8-1) to the estimated longitudinal dynamics was studied. The LS and MLM algorithm were then used to extract the derivatives. Table 8-9 and Table 8-10 show the results from the LS and MLM estimation respectively.

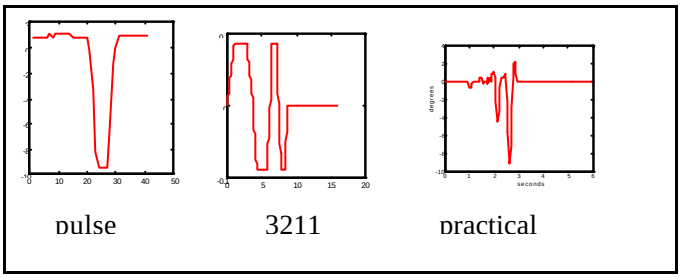

Figure 8-1: The three different input forms used in the simulation

The results from the simulation suggested that there seems to be no significant different in the estimated parameters under this flight condition. However, the CRB values obtained from practical input form were generally higher and hence more uncertainty in the results.

		Input forms					
		Pulse		3211		Practical	
Derivatives	**True parameter**	Estimated parameter	Standard deviation	Estimated parameter	Standard deviation	Estimated parameter	Standard deviation
Cz_{α}	-4.399	-3.573	0.002	-3.572	0.003	-3.549	0.004
Cz_{q}	-5.851	10.09	0.056	10.04	0.068	9.097	0.068
$Cz_{elevator}$	-0.364	0.457	0.002	0.454	0.003	0.446	0.002
Cm_{α}	-1.178	-1.192	0.011	-1.193	0.014	-1.317	0.023
Cm_{q}	-11.03	-6.830	0.290	-6.597	0.353	-1.680	0.354
$Cm_{elevator}$	-0.941	-0.856	0.011	-0.844	0.014	-0.803	0.010
ω_{nSPO} (rad./s)	6.83	6.77		6.75		6.71	
ξ_{SPO}	0.51	0.36		0.36		0.23	

Table 8-9: The effect of different input forms to the estimated longitudinal parameters using linear regression algorithm

		Input forms					
		Pulse		3211		Practical	
Derivatives	**True parameter**	Estimated parameter	Cramer Rao Bound	Estimated parameter	Cramer Rao Bound	Estimated parameter	Cramer Rao Bound
Cz_{α}	-4.399	-4.782	0.056	-4.654	0.056	-4.371	0.137
Cz_{q}	-5.851	-19.820	1.08	-20.39	0.984	-17.750	2.08
$Cz_{elevator}$	-0.364	-1.177	0.008	-1.177	0.008	-1.146	0.015
Cm_{α}	-1.178	-1.330	0.014	-1.339	0.013	-1.311	0.027
Cm_{q}	-11.03	-10.290	0.108	-10.54	0.107	-11.090	0.265
$Cm_{elevator}$	-0.941	-0.980	0.009	-0.980	0.008	-0.946	0.016
ω_{nSPO} (rad./s)	6.83	6.87		6.85		6.85	
ξ_{SPO}	0.51	0.51		0.51		0.51	

Table 8-10: The effect of different input forms to the estimated longitudinal parameters using maximum likelihood algorithm

9. Flight Test Results

9.1 Flight data

The flight test was conducted at the Weribee flying field, Melbourne. Four flight sets of data were gathered. The complete recorded flight data are given in appendix 7.

Table 9-1 lists the description of the flights.

Flight number	Description	Length of data	Filename
1	Aileron manoeuvre	16.00 seconds	flight_1
2	Elevator manoeuvre	16.00 seconds	flight_2
3	Elevator and aileron + rudder manoeuvre	12.64 seconds	flight_3
4	Elevator and aileron + rudder manoeuvre	12.76 seconds	flight_4

Table 9-1: Flight description

From the above four flights, four 'sections' of manoeuvre data were analysed successfully. The manoeuvres are described in Table 9-2. All the filenames for these manoeuvres are saved in the accompanying disc in subdirectory c:/data.

Manoeuvre no.	Taken from flight no.	Description	Length of data analysed	Filename
1	3	Elevator manoeuvre	4 seconds	mano_1.mat
2	3	Elevator manoeuvre	8 seconds	mano_2.mat
3	4	Rudder and aileron manoeuvre	6.04 seconds	mano_3.mat
4	4	Rudder manoeuvre	1.4 seconds	mano_4.mat

Table 9-2: Manoeuvre description

Data from flight number 1 and 2 could not be analysed. This was due to the presence of a significant vibration noise in the angular rate measurements, and turbulence noise in the angle of attack and sideslip. See records of flight 1 and 2 in appendix 7.

The relevant flight test conditions and flight configurations are summarised in the Table 9-3, and all the collected flight data are presented in appendix 7.

	Manoeuvre number			
Flight parameters	**1**	**2**	**3**	**4**
Airspeed (m/s)	15	15	15	15
Approximate reference altitude (m)	30	30	30	30
Flap setting (deg)	5	7	5	7
Trim angle of attack (deg)	5	5	5	5
Elevator trim angle (deg)	4.8	5.96	4.8	5.96
Centre of gravity (cm from wing leading edge)	47.5	47.5	47.5	47.5
Mass (Kg)	11	11	11	11
Ixx (Kgm^2)	1.15	1.15	1.15	1.15
Iyy (Kgm^2)	1.3	1.3	1.3	1.3
Izz (Kgm^2)	1.28	1.28	1.28	1.28

Table 9-3: Flight test conditions for every manoeuvre

9.2 Data pre-processing

Before proceeding with the estimation of stability & control derivatives, the following data pre-processing was carried out:

- Converting raw data into engineering units using the sensor calibration in appendix-4.
- Checking for outliers and missing data, and correcting them as appropriate. The correction of data was carried out manually using a text editor for ASCII. Whereas the plotting of all data were carried out using Matlab.
- Cropping the flight data according to the length of data to be analysed.
- Filtering the flight data by a low pass filter. Note that all data records should be filtered with the same filter to avoid any *time shifts* in data records, which would degrade the parameter identification process. A program called *filtcoba.m* has been prepared to perform this

operation. However, in analysing flight record 3 and 4, no software filtering were necessary since the MLM estimation produced a good convergence even without filtering.

- Smoothing any selected flight data record (use a program called *smooth.m*).
- Correcting incidence angles (α and β) for rates effect (see appendix-2).
- Removing the non-zero steady state values from each record.

9.3 Stability and control derivative estimation

The linear regression analysis has failed to give satisfactory results, since no acceleration measurements were available. Estimating these measurements by differentiating angle of attack and pitch rate did not help. The noise in the data was actually attenuated by the differentiation process. Hence we proceed with the maximum likelihood method (MLM) for analysing of all the flight test data.

For the MLM analysis, the a-priori values for each parameter are obtained either from theoretical method (calculated from AAA software) or earlier flight data analysis.

9.3.1 Longitudinal stability and control derivatives estimation

The estimated longitudinal stability and control derivatives are given in Table 9-4 and Table 9-5, and the matchings of flight data are presented in Figure 9-1 and Figure 9-2.

	Analysis 1-1			Analysis 1-2		
Derivatives	**A-priori**	**Estimated parameter**	**Cramer Rao Bound**	**A-priori**	**Estimated parameter**	**Cramer Rao Bound**
Cz_{α}	-4	fixed	-	-4	fixed	-
Cz_{q}	-5.9	fixed	-	-5.9	fixed	-
Cm_{α}	-1	-1.283	0.1198	-1.427	-1.33	0.1365
Cm_{q}	-10	-7.742	1.894	-9.668	-9.682	2.168
$Cz_{elevator}$	0	1.334	0.2203	1.525	1.427	0.2123
$Cm_{elevator}$	-1	0.805	0.0912	0.966	0.830	0.1025
ω_{nSPO} (rad./s)		6.80			6.64	
ξ_{SPO}		0.43			0.49	

Table 9-4: Estimated longitudinal parameter from recorded data (manoeuvre 1) with two different sets of a-priori values

Table 9-4 shows the estimation results from manoeuvre 1 data using two different sets of a-priori values. In the first set (analysis 1-1), we used the a-priori based on the theoretical work (AAA software). However, the first attempt to estimate all the six longitudinal derivatives simultaneously has failed. The maximum Likelihood Method (MLM) did not converge into solutions. From the simulation study (chapter 8), we found that the Cz_q was weakly identified, and hence should be kept fixed during the identification process. In the second attempt, we fix both Cz_α and Cz_q, to these a-priori values. The value of Cz_α was also available with quite a reliable accuracy. The MLM then converged to solutions in 20 iterations. Further iteration did not change the values of the estimated derivatives. The maximum gradient of 0.0 was achieved with the minimum logarithmic value of -398.33.

In the second set (analysis 1-2), we used a-priori values which were obtained from estimating the derivatives one at a time. We first estimate Cm_α by fixing all other derivatives constant. Then the estimated Cm_α was used as a-priori for the next estimation, and tries to estimate Cm_q while fixing the other derivatives constant. The process was repeated until all the derivatives were estimated. It should be noted here that this approach is very much dependant on the accuracy of those parameters held fixed. It is however one alternative way to get the MLM converge into a solution. Looking at the two sets of result in Table 9-4, the analysis 1-1 produced a smaller CRB (Cramer Rao Bound) for each parameter than those in analysis 1-2. Hence we can place more confidence in the analysis 1-1 results than those of analysis 1-2. However, the two sets produced almost similar α and q responses as shown in Figure 9-1.

Table 9-5 shows the estimation results from the manoeuvre 2. The same process as in manoeuvre 1 was performed to arrive to the shown results. Figure 9-2 shows the estimated responses. The fit was reasonable good, except for the pitch rate matching. The poor pitch rate matching might be caused by an unintentional aileron input during this manoeuvre as shown in Figure 9-2.

Derivatives	Manoeuvre 2-1			Manoeuvre 2-2		
	A-priori	Estimated parameter	Cramer Rao Bound	A-priori	Estimated parameter	Cramer Rao Bound
Cz_{α}	-4	fixed	-	-4.32	fixed	-
Cz_{q}	-5.9	fixed	-	-22	fixed	-
Cm_{α}	-1	-0.933	0.1778	-1.427	-0.840	0.1365
Cm_{q}	-10	-14.18	4.664	-9.668	fixed	-
$Cz_{elevator}$	0	2.261	0.3708	1.525	2.897	0.3405
$Cm_{elevator}$	-1	1.148	0.246	0.966	0.971	0.1123
ω_{nSPO} (rad./s)		2.14			5.63	
ξ_{SPO}		0.56			0.57	

Table 9-5: Estimated longitudinal parameter from recorded data (manoeuvre 2) with two different sets of a-priori values

Matching flight data

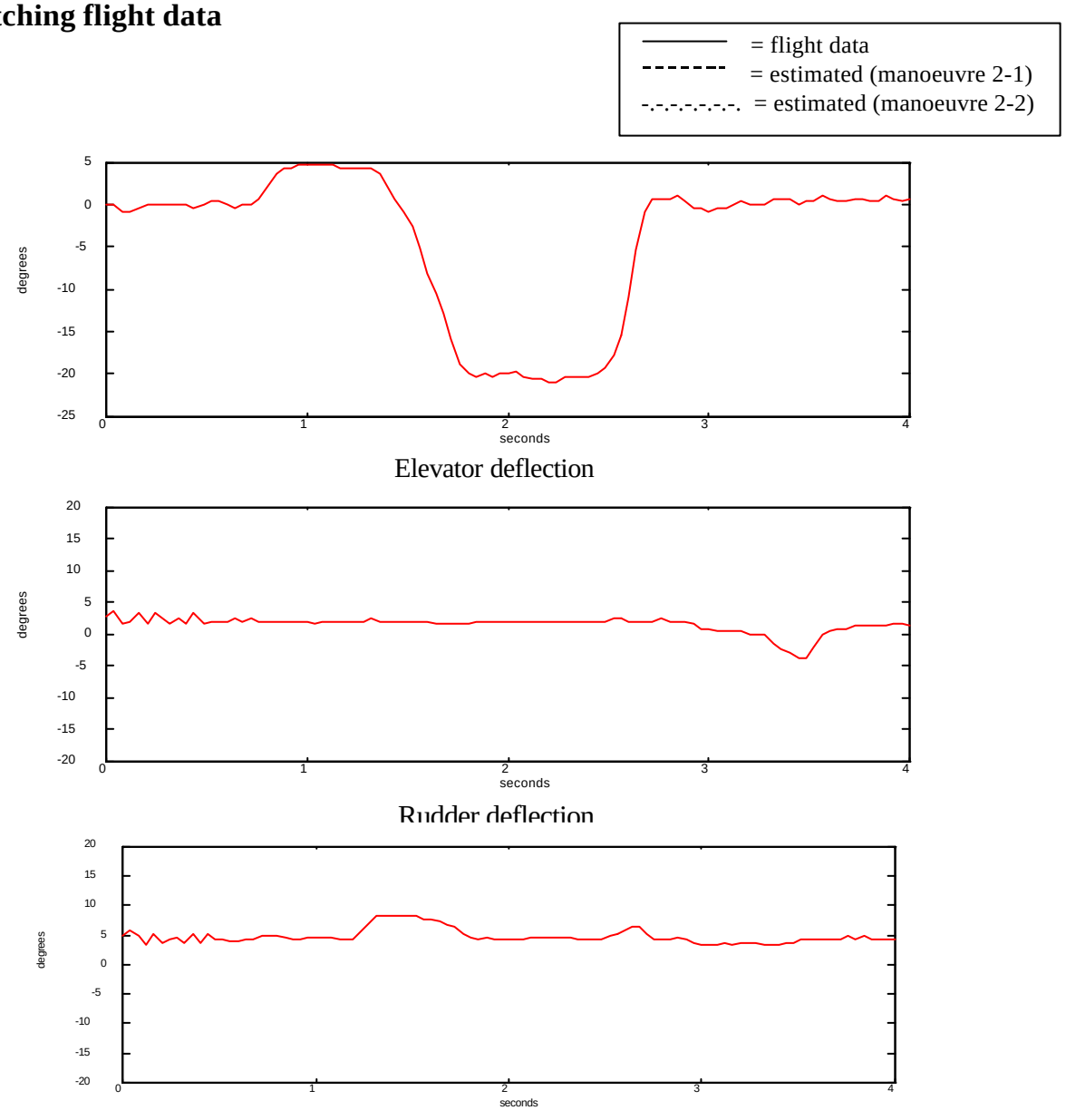

Elevator deflection

Rudder deflection

Right aileron deflection

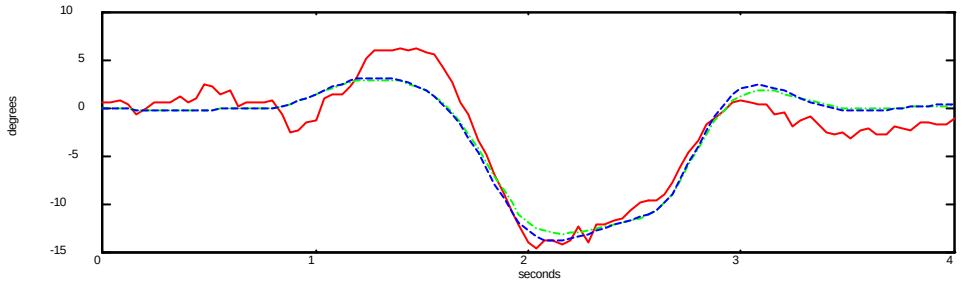

Angle of attack matching

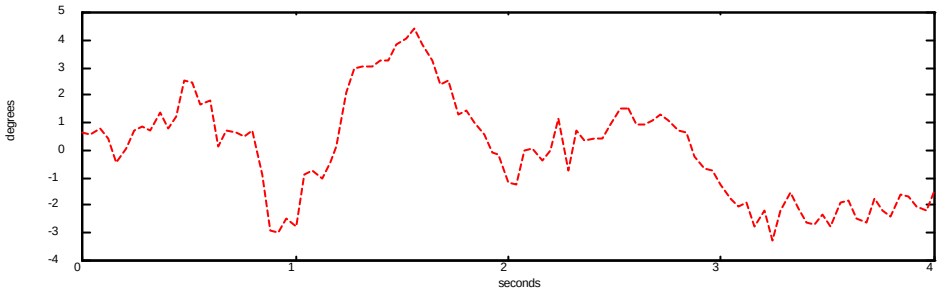

Residual in angle of attack matching

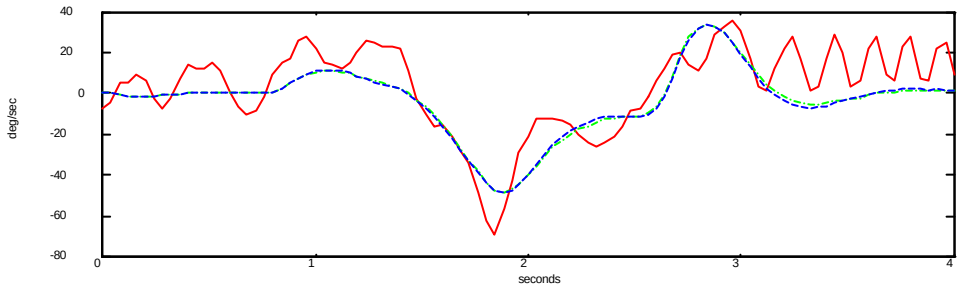

Pitch rate matching

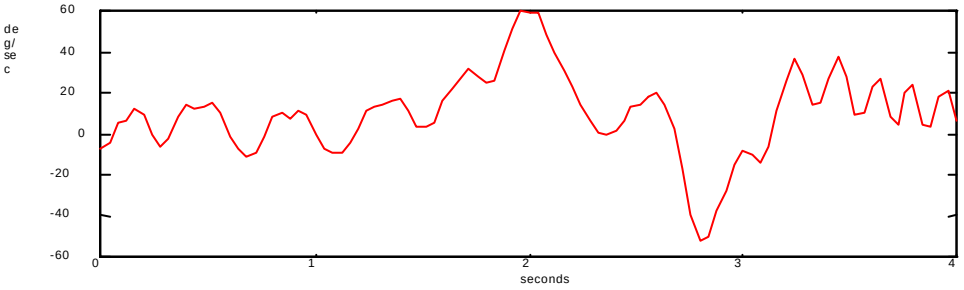

Residual in pitch rate matching

Figure 9-1: Estimated longitudinal responses and their residuals from manoeuvre 1 records

———— = flight data
- - - - - - - = estimated (manoeuvre 2-1)
-.-.-.-.-.-.-. = estimated (manoeuvre 2-2)

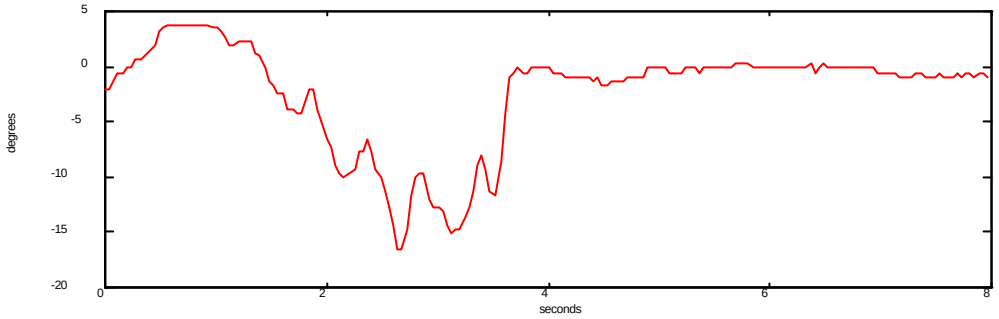

Elevator deflection

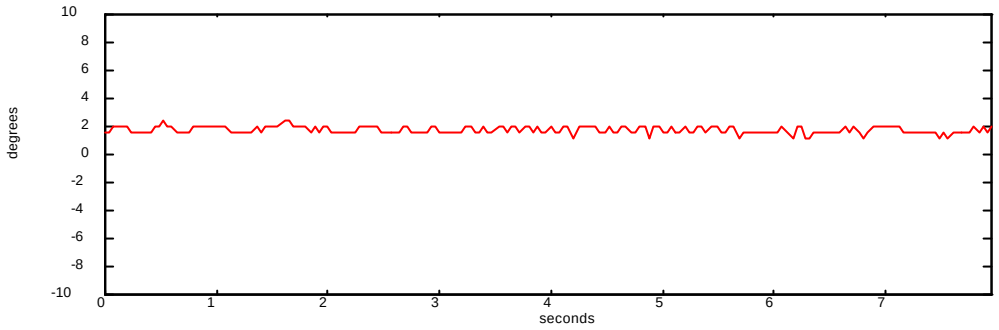

Rudder deflection

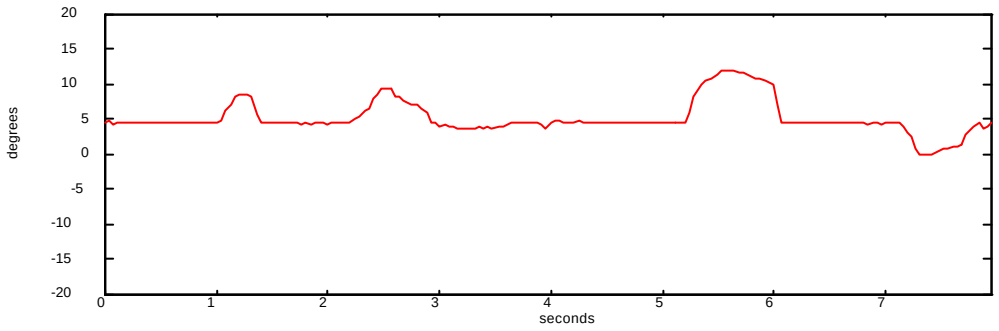

Right aileron deflection

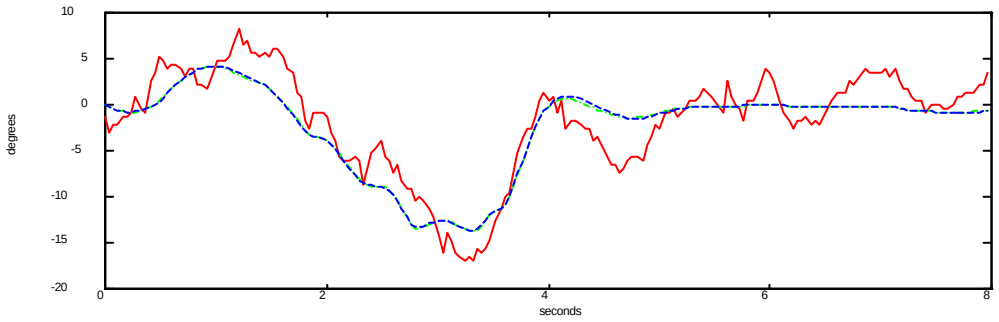

Angle of attack matching

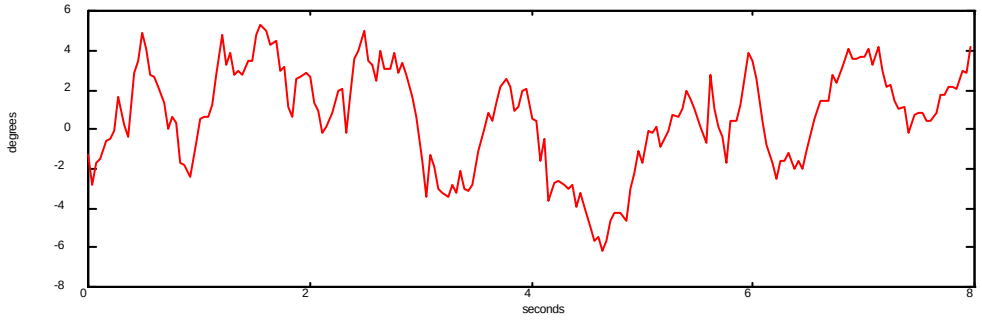

Residual in angle of attack matching

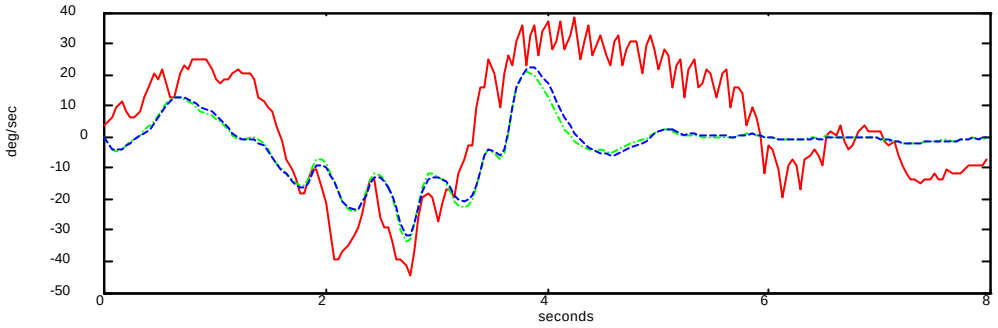

Pitch rate matching

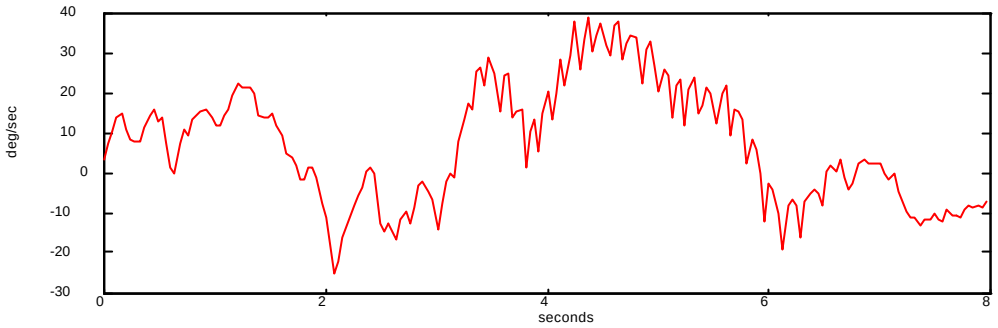

Residual in pitch rate matching

Figure 9-2: Estimated longitudinal responses and their residuals from manoeuvre 2 records

		Mean	Standard deviation
Angle of attack (deg)	Manoeuvre 1	-0.0265	1.888
	Manoeuvre 2	0.6210	2.549
Pitch rate (deg/s)	Manoeuvre 1	6.3934	11.80
	Manoeuvre 2	6.9690	14.64

Table 9-6: Residual characteristics of the estimated longitudinal responses

9.3.2 Lateral stability and control derivative

The estimated lateral stability and control derivatives are given in Table 9-7 and Table 9-8, and the matchings of flight data are presented in Figure 9-1 and Figure 9-2.

	Analysis 3-1			Analysis 3-2		
Derivatives	**A-priori**	**Estimated parameter**	**Cramer Rao Bound**	**A-priori**	**Estimated parameter**	**Cramer Rao Bound**
Cy_{β}	-0.519	fixed	-	-4.184	3.149	2.427
Cy_{p}	-11.29	fixed	-	-11.29	-25.78	9.1
Cy_{r}	-1.609	fixed	-	-1.609	2.794	2.957
Cl_{β}	0.171	fixed	-	-0.0846	-0.115	0.0317
Cl_{p}	-0.733	-1.981	0.1478	0.135	0.120	0.0123
Cl_{r}	0.221	fixed	-	-0.126	-0.012	0.0463
Cn_{β}	0.131	0.125	0.0025	-4.933	-2.895	0.4088
Cn_{p}	-0.072	fixed	-	0.109	0.024	0.0200
Cn_{r}	-0.108	fixed	-	-0.103	-0.103	0.0432
$Cy_{\delta aileron}$	3.012	fixed	-	-0.023	0.037	0.0288
$Cy_{\delta rudder}$	0.107	fixed	-	-0.337	-0.305	0.0958
$Cl_{\delta aileron}$	-0.656	-0.272	0.1247	0.062	-0.120	0.0187
$Cl_{\delta rudder}$	-0.114	fixed	-	4.832	2.788	0.9158
$Cn_{\delta aileron}$	0.121	fixed	-	0.1323	0.166	0.0177
$Cn_{\delta rudder}$	-0.045	0.090	0.0024	0.065	0.099	0.0049
ω_{Dutch} (rad/s)		4.48			4.41	
ξ_{Dutch}		0.18			0.29	
T_{spiral} (sec)		0.19			0.42	

Table 9-7: Estimated lateral parameter from recorded manoeuvre 3 with two different sets of a-priori values

	Analysis 4-1			Analysis 4-2		
Derivatives	**A-priori**	**Estimated parameter**	**Cramer Rao Bound**	**A-priori**	**Estimated parameter**	**Cramer Rao Bound**
Cy_{β}	6.071	9.79	2.75	6.071	19.07	3.787
Cy_{p}	-34.36	-43.42	8.15	-34.36	-79.68	15.82
Cy_{r}	4.567	-2.289	11.52	4.567	52.68	24.09
Cl_{β}	0.355	fixed	-	0.355	fixed	-
Cl_{p}	-0.945	fixed	-	-0.945	fixed	-
Cl_{r}	-0.221	0.034	0.176	-0.221	fixed	-
Cn_{β}	-0.165	fixed	-	-0.165	fixed	-
Cn_{p}	1.236	0.886	0.0745	1.236	1.088	0.0930
Cn_{r}	-1.183	-1.086	0.1989	-1.183	-1.894	0.177
$Cy_{\delta aileron}$	0	fixed	-	0	fixed	-
$Cy_{\delta rudder}$	-2.555	-4.196	1.694	-2.555	-8.123	1.745
$Cl_{\delta aileron}$	0	fixed	-	0	fixed	-
$Cl_{\delta rudder}$	-0.038	fixed	-	-0.038	0.033	0.033
$Cn_{\delta aileron}$	0	fixed	-	0	fixed	-
$Cn_{\delta rudder}$	-0.380	0.256	0.0395	-0.380	fixed	-
ω_{Dutch} (rad/s)		9.20			9.21	
ξ_{Dutch}		0.24			0.22	
T_{spiral} (sec)		0.05			0.04	

Table 9-8: Estimated lateral parameter from recorded manoeuvre 4 with two different sets of a-priori values

A similar procedure as that for the longitudinal estimation was used. Since more parameters were to be estimated in lateral case, the estimation process was slightly more difficult. It involved trying to fix any weakly derivatives and to find a good starting value for the dominant derivatives.

Results from analysis 3-2 was better than the other 3 lateral analysis. Analysis 3-2 produced a better-estimated parameters with smaller CRB, and a better matching of flight data. Analysis 3-2 estimated all the 15 lateral derivatives with a reasonable degree of confidence. The only exceptions are for the sideforce derivatives (Cy_β, Cy_p , Cy_r) and $Cl_{\delta rudder}$. The simulation result had predicted these derivatives would be hard to estimate. No sideforce information can be accurately extracted from a low frequency excitation (Coleman, 1981). A high frequency input with lateral acceleration readings are required to estimate these derivatives.

Two different manoeuvres were conducted for the lateral identification. Manoeuvre 3 had a combined aileron and rudder inputs. Whereas manoeuvre 4 had only rudder input. Estimated parameters from the rudder input only had a significant larger CRB. This was because that the rudder only produced a *less rich* information content. The data analysed in manoeuvre 4 was also shorter (only 1.84 s). The values of residual characteristics in Table 9-9 also support this argument. The mean and standard deviation in manoeuvre 3 was generally less that those in manoeuvre 4.

Another point to notice was that the roll derivatives could not be extracted from a rudder only manoeuvre (as seen from Table 9-8). This suggests that little roll information was contained in the data. Data from an aileron only manoeuvre would certainly be used to extract the roll roll derivatives. Flight 1 was designed to extract the roll derivatives. But since the data was covered by engine vibration noise, the data could not be used.

A reasonably good matching for manoeuvre 3 and 4 were obtained and are shown in Figure 9-1 and Figure 9-2.

Matching flight data

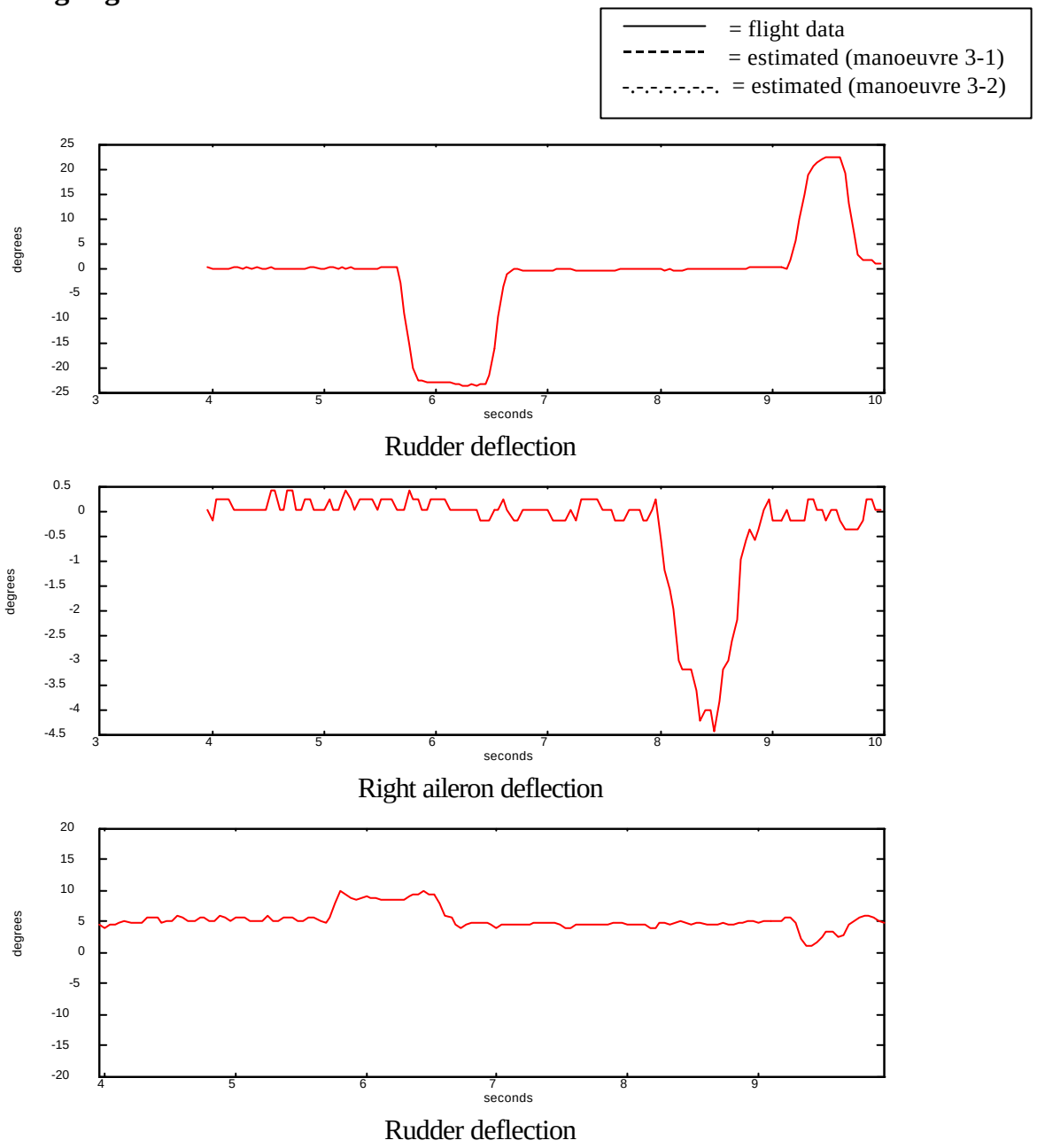

Rudder deflection

Right aileron deflection

Rudder deflection

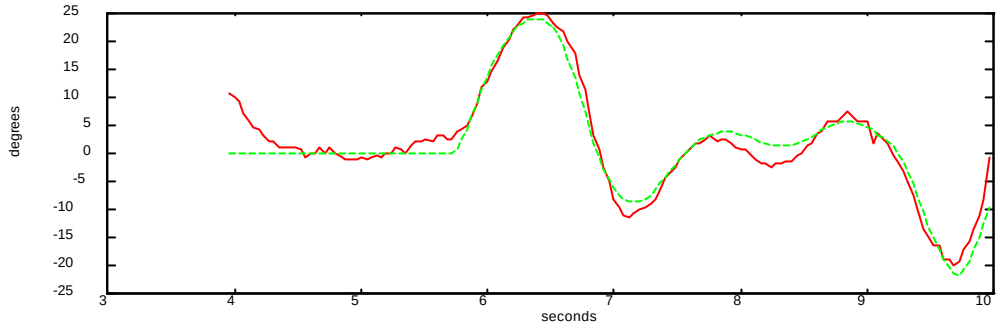

Sideslip matching

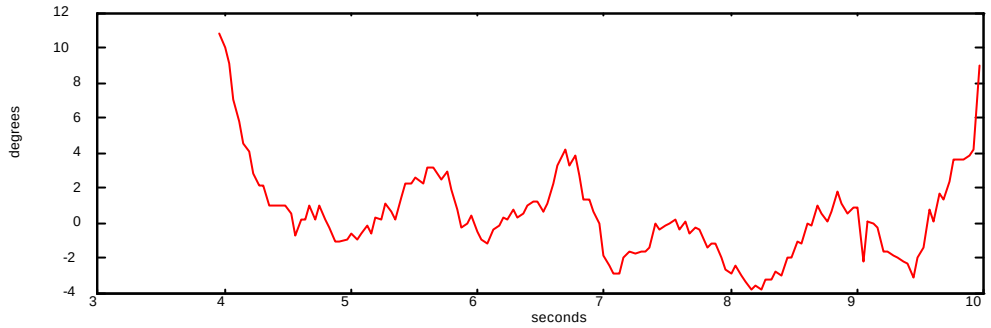

Residual in sideslip matching

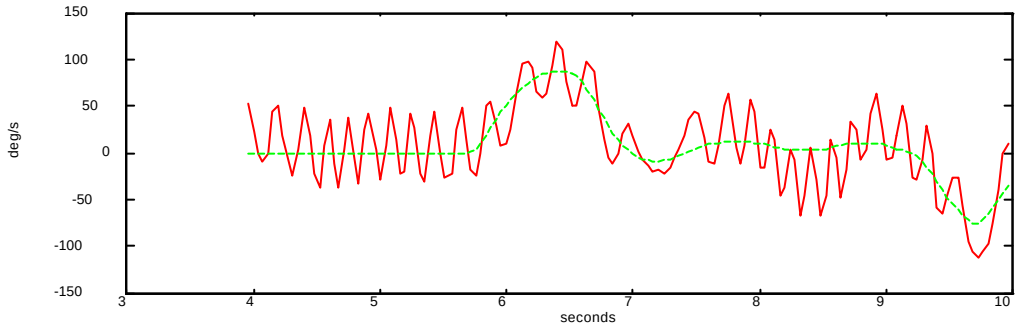

Roll rate matching

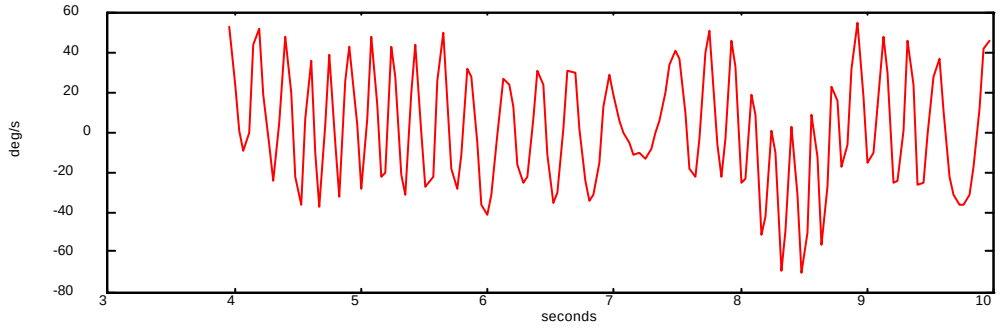

Residual in roll rate matching

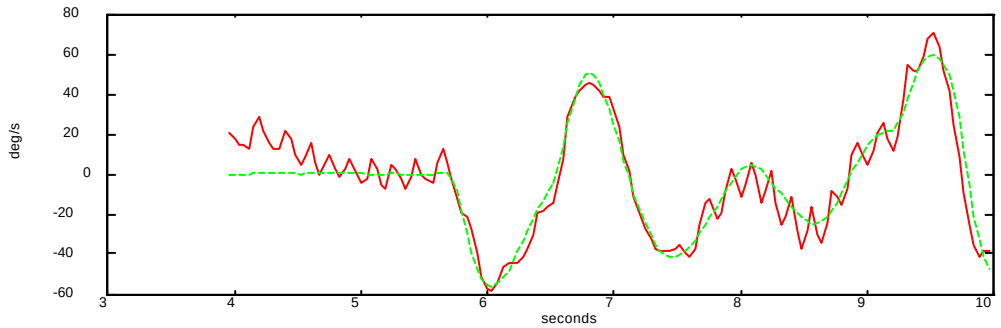

Yaw rate matching

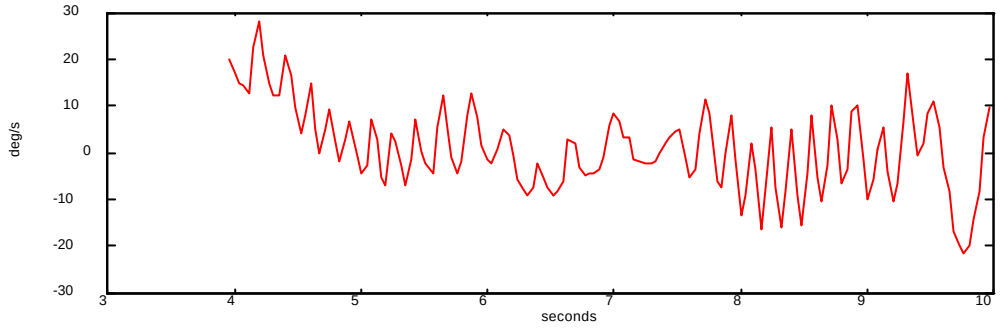

Residual in yaw rate matching

Figure 9-1: Estimated lateral responses and their residuals from manoeuvre 3 records

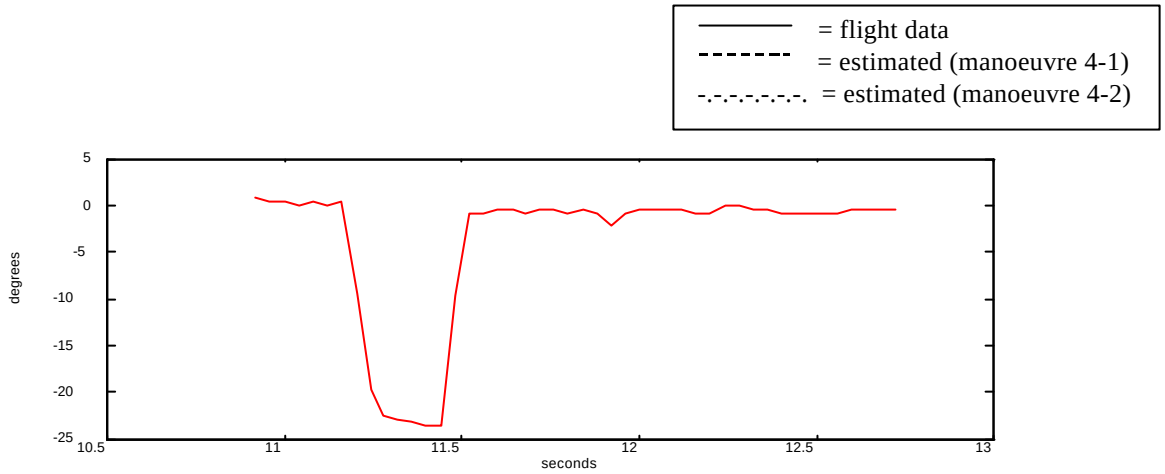

Rudder deflection

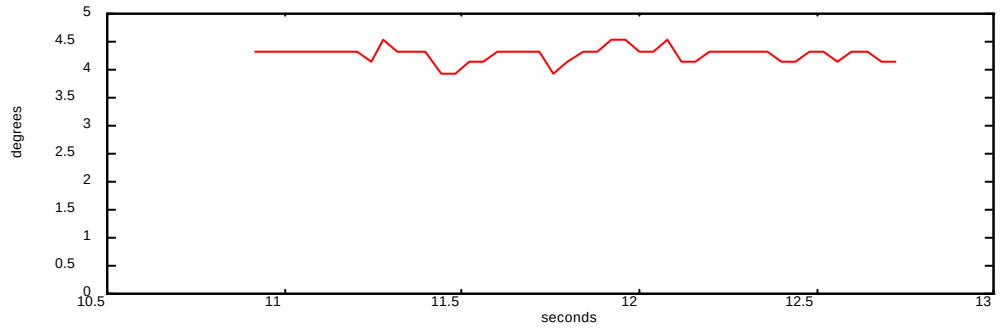

Right aileron deflection

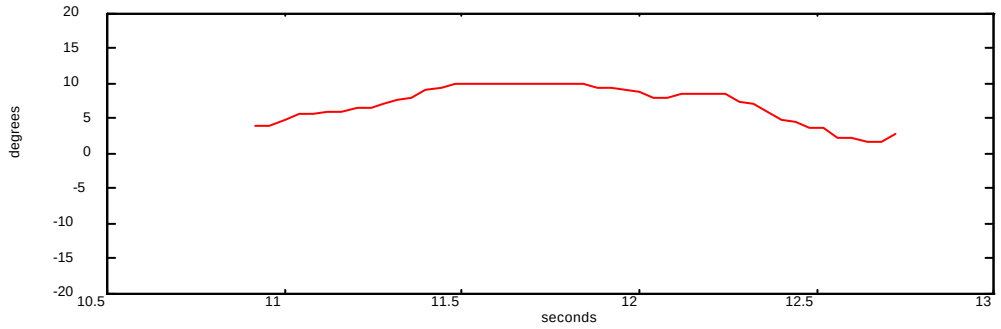

Rudder deflection

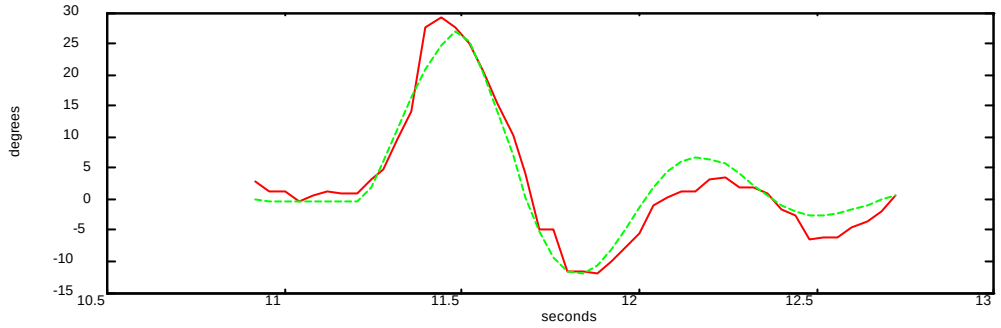

Sideslip matching

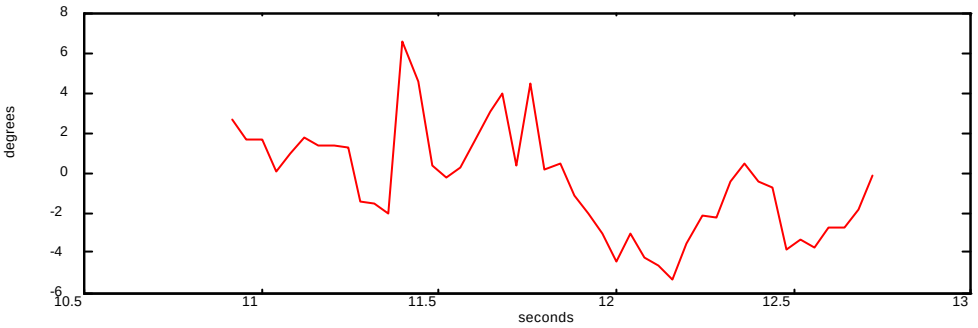

Residual in sideslip matching

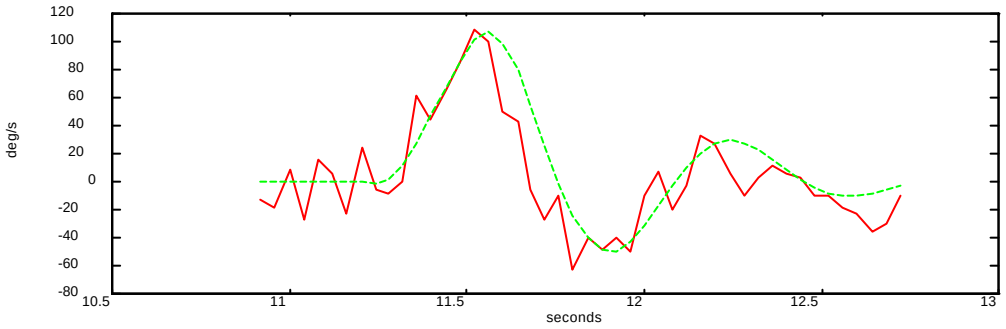

Roll rate matching

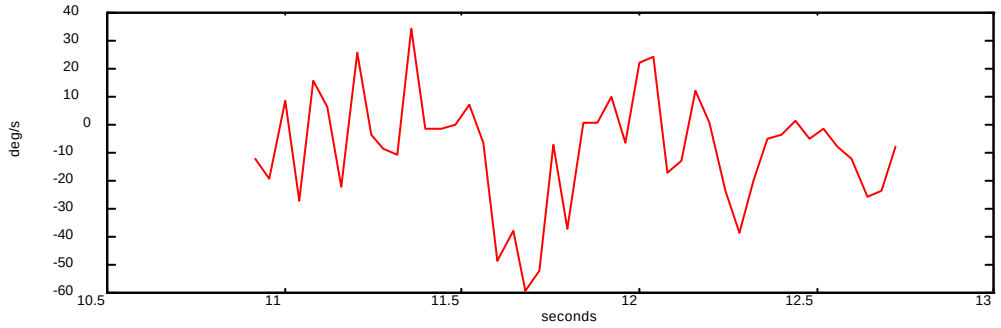

Residual in roll rate matching

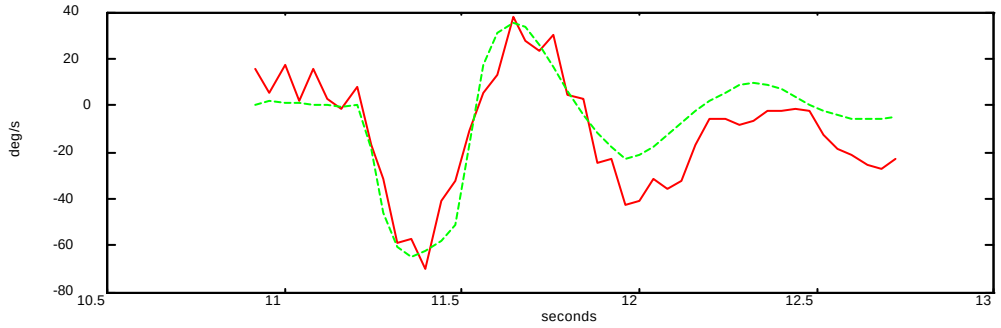

Yaw rate matching

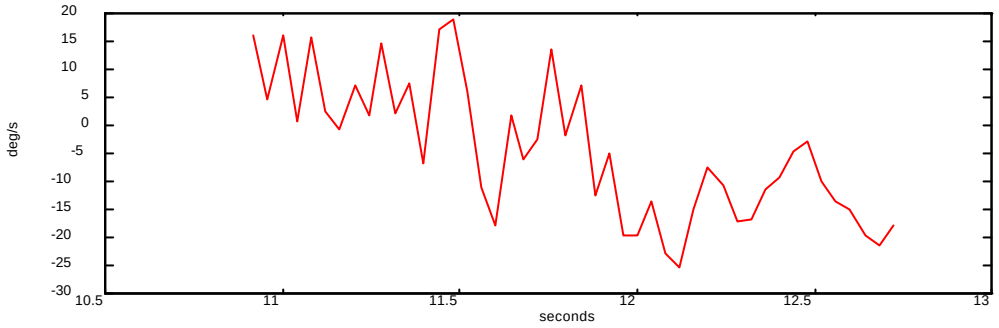

Residual in yaw rate matching

Figure 9-2: Estimated lateral responses and their residuals from manoeuvre 4 records

		Mean	Standard deviation
Sideslip (deg)	Manoeuvre 3	0.423	2.250
	Manoeuvre 4	-0.061	2.952
Roll rate (deg/s)	Manoeuvre 3	0.607	28.50
	Manoeuvre 4	-10.147	23.314
Yaw rate (deg/s)	Manoeuvre 3	0.791	8.880
	Manoeuvre 4	-5.428	14.398

Table 9-9: Residual characteristics of the estimated lateral responses

10. Discussion

10.1 Estimated aircraft dynamics

The project has estimated 6 longitudinal and 15 lateral derivatives from 4 flight manoeuvres data. Only records of control inputs and vehicle's responses were used in the analysis. The results are summarised in Table 10-1 and Table 10-2.

Cm_{α}, $Cm_{\delta elevator}$, Cn_{β}, Cn_{r}, $Cl_{\delta aileron}$ and $Cn_{\delta rudder}$ are strongly identified, whereas Cz_{α}, $Cz_{\delta q}$, Cy_{β}, $Cy_{p,}$ and Cy_{r} are weakly identified. The rest are moderately identified.

	AAA	Analysis 1-1	Analysis 1-2	Analysis 2-1	Analysis 2-2
Cz_{α}	-4.399	-	-	-	-
Cz_{q}	-5.851	-	-	-	-
Cm_{α}	-1.178	-1.283(0.1198)	-1.33(0.1365)	-0.933(0.1778)	-0.840(0.135)
Cm_{q}	-11.03	-7.742(1.894)	-9.682(2.168)	-14.18(4.664)	-
$Cz_{\delta elevator}$	-0.364	1.334(0.2203)	1.427(0.2123)	2.261(0.3708)	2.897(0.3405)
$Cm_{\delta elevator}$	-0.941	0.805(0.0912)	0.830(0.1025)	1.148(0.246)	0.971(0.1123)
ω_{SPO}	6.83	6.80	6.64	2.14	5.63
ξ_{SPO}	0.51	0.43	0.49	0.56	0.57

Table 10-1: Estimated longitudinal derivatives of the Telemaster T240

	AAA	Analysis 3-1	Analysis 3-2	Analysis 4-1	Analysis 4-2
Cy_{β}	-0.354	-0.519(fixed)	3.149(2.427)	9.79(2.75)	19.07(3.787)
Cy_{p}	-0.043	-11.29(fixed)	-25.78(9.1)	-43.42(8.15)	-79.68(15.82)
Cy_{r}	0.153	-1.609(fixed)	2.794(2.957)	-2.289(11.52)	52.68(24.09)
Cl_{β}	0.089	0.171(fixed)	-0.115(0.0317)	0.355(fixed)	0.355(fixed)
Cl_{p}	0	-1.981(0.1478)	0.120(0.0123)	-0.945(fixed)	-0.945(fixed)
Cl_{r}	-0.043	0.121(fixed)	-0.012(0.0463)	0.034(0.176)	-0.221(fixed)
Cn_{β}	-0.733	0.125(0.0025)	-2.895(0.4088)	-0.165(fixed)	-0.165(fixed)
Cn_{p}	0.221	-0.072(fixed)	0.024(0.020)	0.886(0.0745)	1.088(0.0930)
Cn_{r}	-0.001	-0.108(fixed)	-0.103(0.0432)	-1.086(0.1989)	-1.894(0.177)
$Cy_{\delta aileron}$	0.321	3.012(fixed)	0.037(0.0288)	-	-
$Cy_{\delta rudder}$	0.002	0.107(fixed)	-0.305(0.0958)	-4.196(1.694)	-8.123(1.745)
$Cl_{\delta aileron}$	-0.084	-0.272(0.1247)	-0.120(0.0187)	-	-
$Cl_{\delta rudder}$	-0.096	-0.114(fixed)	2.788(0.9158)	-0.038(fixed)	0.033(0.033)
$Cn_{\delta aileron}$	-0.045	0.121(fixed)	0.166(0.0177)	-	-
$Cn_{\delta rudder}$	0	0.090(0.0024)	0.099(0.0049)	0.256(0.0395)	-0.380(fixed)
ω_{SPO}	1.38	4.58	4.41	9.20	9.21
ξ_{SPO}	0.75	0.18	0.24	0.24	0.22
T_{spiral}	0.52	0.29	0.42	0.05	0.04

Table 10-2: Estimated lateral derivatives of the Telemaster T240

The estimated values were not always in a good agreement with those predicted by AAA. The AAA software is normally used for estimating derivatives of a conventional aircraft with minimum mass of 50 Kg, not for a small RPV type aircraft. Here, no direct comparison could actually be made. However, most of the flight test results were in the same order of the AAA. In addition, the AAA predictions have assisted in starting the MLM algorithm.

One interesting point to comment is on the values of $Cz_{\delta elevator}$, and $Cm_{\delta elevator.}$ The AAA predicted the wrong sign of derivatives since it assumed a conventional horizontal tail. In fact, the T240's tailplane is a flat top aerofoil which generates lift when the elevator is deflected upward, hence a positive values of $Cz_{\delta elevator}$ and $Cm_{\delta elevator}$. A pitch up manoeuvre is achieved by a positive (downward) elevator deflection.

The SPO (Short Period Oscillation) mode characteristics were estimated reasonably well. However, the lateral modes showed a little inconsistency. The rudder manoeuvre estimated higher Dutch mode frequency (100% higher) than the combined rudder and aileron manoeuvre. This might be due to the difference in the pulse width of the rudder input. As the Dutch mode is a combination of yawing and rolling oscillations, then the combined rudder and aileron inputs should excite the Dutch mode better, thus resulting in better estimation than the rudder input alone. The Dutch damping on the other hand was quite consistent throughout different estimation process.

The scatter in the obtained longitudinal derivatives was quite low and hence a reasonable confidence in the results. The scatter on the lateral derivatives on the other hand, varied significantly. Those derivatives with high CRB values show high scatter in the results. Dominant derivatives such as Cn_{β}, $Cn_{p,}$ Cn_{r}, $Cl_{\delta aileron}$ and $Cn_{\delta rudder}$ have low CRB values and hence better estimated.

The matching between the prediction and the flight data was generally good. Even in the presence of significant engine vibration noise in the angular rate measurements, the MLM algorithm predicted the

response quite well. When a good match could not be achieved then one of the following reasons might be causing the problem; modelling errors, uncorrected bias errors or a small excitation in the mode of interest.

10.2 Flight data processing

Four recorded manoeuvres (a total of 26 seconds of data) have been processed and analysed to obtain the stability and control derivatives of the Telemaster T240. The software written in Matlab has undoubtedly eased and proved invaluable in the processing of the flight data.

Pre-processing (include converting, filtering, smoothing, cropping, removing outliers, etc) was a lengthy process. Yet it was crucial in the success of the whole identification process.

Some outliers were present in the recorded data. No dropouts of data were apparent. Filtering the angular rate measurements with software has no considerable effect on the estimated derivatives. Hence we allowed all the recorded measurements unfiltered when performing the MLM algorithm.

The MLM was the main algorithm used in estimating the stability and control derivatives of the T240. The LS has failed to give a good match since no acceleration measurements were available. For the longitudinal LS, we need angle of attack rate and pitch acceleration measurements. For the lateral LS, we need sideslip rate, roll and yaw acceleration measurements.

In cases when the MLM could not identify some weak derivatives, such as Cz_{α} and Cz_{q}, the ICM method was used as a *fine-tuning* to estimate these weak derivatives.

The GUI (graphical user interface) facility in Matlab has helped to speed up the MLM estimation process. For example, the a-priori values and the parameter to estimate can be easily changed through the click of the mouse.

Some typical problems encountered during the MLM estimation was that the algorithm sometimes did not converge satisfactorily. A minimum logarithmic value could not be achieved. There main reasons contributed for this unsatisfactory convergence; wrong a priory, wrong parameter to estimate, or wrong mathematical model.

Since the accelerometers were not working, no linear acceleration readings were available. Had these readings were available, we would have been able to perform some corrections to the angle of attack and sideslip (data compatibility checking).

10.3 Flight test manoeuvre.

Most manoeuvres conducted in this project were of pulse or doublet type inputs. These inputs were reasonably easy to perform. Yet the recorded responses contained a sufficient information to enable the MLM algorithm to extract some dominant derivatives.

One major point to consider is a need to compromise between a large magnitude of input and a small magnitude of responses. On one hand, we need a large input to excite the response. On the other hand, the resulted responses should remain within a linear region. So that the validity of the uncoupled linear model can be preserved. This proved to be not an easy task for the pilot. Both manoeuvre 3 and 4 produced quite large sideslip responses. Hence the validity of the linear model used was under question.

Another significant problem was the present of engine vibration noise in the angular rate readings. When the manoeuvre was conducted at a throttle setting, the rate readings were buried in noise. Significant improvements in rate readings were achieved by conducting the manoeuvre with engine idle.

Similarly, a poor quality of flow directional readings (α and β) were found in the presence of air turbulence. Flying the aircraft very early in the morning has a better chance of having no air turbulence during the manoeuvres.

Despite all the problems in conducting the required manoeuvres (summarised in chapter 7.4), the response with the pulse and doublet input produced a reasonably good matching. This indicated that the required manoeuvre for the identification of stability and control derivatives estimation was not very strict. Practically any input that adequately excites the mode of interest is acceptable.

In short, it is recommended that the dynamic manoeuvre for estimating the stability and control derivatives of a model aircraft should be performed at engine idle, at calm air (preferable in the morning), in the form of pulse or doublet inputs. Alternatively, if the thrust model of the engine is available at a very good accuracy, then the test can be conducted at any engine setting (Muhammad, 1995).

10.4 Instrumentation and data acquisition systems

An important objective of the project has been to develop and demonstrate the instrumentation systems needed for the dynamic testing of a model aircraft. The obtained flight result has shown that the whole system can be used to obtain a reasonably good quality of flight data.

All the measurements were recorded on-board the aircraft. Hence no significant signal noises were present. This would certainly not the case, had we used the telemetry system. Coleman (1981) found a significant noise in his flight data obtained from the telemetry system.

The only significant noises contaminating the recorded flight data were from the engine vibration and air turbulence. A soft damper wrapped around the IMU unit would certainly reduce the vibration noise. The turbulence noise can only be reduced by flying the aircraft in a calm air.

Other major problem with the system was that of transmitter signal interference (as described in chapter 7). We spent months trying to reduce this interference. In the end, changing the transmitter frequency from 36 MHz to 29.725 MHz solved the problem.

The sampling rate (25 Hz), resolutions and accuracy of the sensors were adequate for dynamic flight testing. However, for a better result, a resolution of 12 bit could be used in which case the resolution would be increased by 16 times.

A sixteen seconds of data acquisition has proved to be sufficient for recording two different manoeuvres. A memory device's with 256 Kbytes (correspond to 30x16 seconds of data acquisition) would record 60 different manoeuvres in one flight. This would certainly make the dynamic flight testing process quicker and less expensive.

There is a huge potential in using the already developed system for other research in model flight testings. For example, by adding three axes linear accelerometers to the IMU, a performance testing can then be conducted. Consequently, the range and drag polar of the aircraft can then be determined.

10. Conclusion

The potential benefit of using UAV (Unmanned Air Vehicles) has prompted The Sir Lawrence Wackett Center for Aerospace Design and Technology to initiate a project referred to MAFV. The objective of the project is to develop an unmanned autonomous flight vehicle. This thesis is a part of the MAFV project, with the objective of estimating a dynamic characteristic of a model aircraft from flight data using parameter identification techniques.

A Telemaster T240 model has been assembled and equipped with necessary flight test instrumentation. The on-board data acquisition system based on Intel 8030 has been developed in collaboration with The Computer System Engineering Department, RMIT. In addition, the flight data processing software has been written using Matlab.

The whole system has been demonstrated by conducting a dynamic flight test program on the Telemaster T240. During the project, the model has performed 17 number of flights through the whole development of the flight test system. Four sets of maneuver data (a total of 26 seconds of data) have been successfully analyzed to estimate the T240's dynamics. A reasonably good flight data matchings have been achieved and 21 stability and control derivatives (5 longitudinal and 16 lateral) have been estimated.

The project has shown that the dynamic of a model aircraft can be estimated with a reasonable confidence using flight testing.

References

1. Budd, G.D., Gilamn, R.L. (1993), *Operational And Research Aspects Of A Radio Controlled Model Flight Test Program*, AIAA paper 93-0625, January 1993, or NASA TM-104266
2. Butter, R.W., Langhan, T.F. (1976), *Aircraft Motion Sensitivity To Variations In Dynamic Stability Parameters*, Agard Stability & Control Conference, Florence-Italy, October
3. Chen, R.T.N. (1975), *Input Design For Aircraft Parameter Identification: Using Time Optimal Control Formulation. Methods For Aircraft State And Parameter Identification*, AGARD-CP-172, paper 13, May 1st
4. Chow (1996), *Stability and control derivative of the T240 model aircraft,* AV408 undergraduate project, Aerospace Engineering, RMIT.
5. Coleman, R; Robins, A.J., Frary, D.J.; Stephenson, R. (1981), *Mini-RPV Research*, The Aeronautical Journal, Feb.1981, p39-47
6. DARcorporation (1996), *Advanced Aircraft Analysis: User's Manual Version 1.7*, February 1996
7. De Jong, R.C., Mulder, J.A (1987), *Accurate Estimation of Aircraft Inertia Characteristics From a Single Suspension Experiment*, Journal of Aircraft, vol.24, no.6, p.362-370, June 1987
8. Draper, N.R., Smith, H. (1981), *Applied Regression Analysis*, 2nd edition, John Wiley & Sons. Inc, NY
9. Eshelby, M.E. (1991), *Short Course in Experimental Mechanics of Flight*, Cranfield College of Aeronautics
10. Eulrich, B.J., Rynaski, E.G.(1974), *Identification Of Non-Linear Aerodynamic Stability And Control Parameters At High Angle Of Attack*, Agard Conference Proceeding AGARD/FMP Specialist meeting, NASA Langley, Nov. 1974, paper 1-2.
11. Gracey, W. (1948), *The Experimental Determination of the Moments of Inertia of Airplanes by a Simplified Compound-Pendulum Method*, NACA TN-1629
12. Hamory, P.J., Murray, J.E. (1994), *Flight Experience With Light-Weight, Low Power Miniaturised Instrumentation Systems*, Journal of Aircraft Vol.31, No.5, Sept-Oct.1994, p.1016-1021
13. Hodge, W.F., Bryant, W.H., (1975), *Monte Carlo Analysis Of Inaccuracies In Estimated Aircraft Parameters Caused By Unmodelled Flight Instrumentation Errors,* NASA TN D-7712, Feb.1975
14. Holcomb, M.L., Tumlinson, R.R. (1977) , *Evaluation Of A Radio Control Model For Spin Simulation*, Society Of Automotive Engineers, Business Aircraft Meeting Century II, Wichita, March 29- April 1
15. Howard, R.M., Trainer,J.C., Lyons, D.F. (1991), *Flight Test Of A Half Scale Unmanned Air Vehicle*, Journal Of Aircraft, Vol.28, no.12, December
16. Howell, S. and Williams, B. (1994), *Stealmouth Telemetry Systems*, RMIT Engineering Conference Journal, ENGenius'94, p.43-46
17. Iliff, K.W. (1989), *Parameter Estimation For Flight Vehicles*, Journal of Guidance, Control and Dynamics, vol.12, no.5, Sept-Oct 1989
18. Iliff, K.W., Maine, R.E. (1979), *Practical Aspects Of Using A Maximum Likelihood Estimation Methods To Extract Stability And Control Derivatives From Flight Data*, NASA TN-D8209, April 1979

19. Iliff, K.W., Maine, R.E., Montgomery,T.D. (1979), *Important Factors In The Maximum Likelihood Analysis Of Flight Test Manoeuvres*, NASA TP-1459, April 1979
20. Iliff, K.W., Maine, R.E.; Shafer, M. (1976), *Subsonic Stability And Control Derivatives For An Unpowered, Remotely Piloted 3/8 Scale F-15 Airlane Model Obtained From Flight Test*, NASA TN D-8136
21. Klein, V and Williams, D.A. (1973), *On Some Problems Related To The Identification Of Aircraft Parameters*, Identification & System estimation, Proceeding 3rd IFAC Symposium.
22. Klein, V. (1975), *On The Adequate Model For Aircraft Parameter Estimation*, Cranfield Report Aero. No.28, Cranfield Institute of Technology, March 1975
23. Klein, V., Schiess, J.R. (1977), *Compatibility Check Of Measured Aircraft Responses Using Kinematic Equations And Extended Kalman Filter*, NASA TN D-8514
24. Kneen, J. (1994), *Avionics Projects at RMIT*, AOPA (Aircraft Owners and Pilots Association of Australia), Vol.47, No.8, August 1994, p.45-48
25. Laban, M. (1994), *On-Line Aircraft Aerodynamic Model Identification*, ISBN 90-6275-987-4
26. Linse, D.J., Stengel, R.F., (1993*), Identification of Aerodynamic Coefficients Using Computational neural Networks*, Journal of Guidance, Control and Dynamics, v.16, n0.6, Nov-Dec. 1993
27. Maine, R.E. (1981), *Programmer's Manual for MMLE3. A General Fortran Program for Maximum Likelihood Parameter Estimation*. NASA TP-1690
28. Maine, R.E., Iliff, K.W. (1981), *The Theory And Practice Of Estimating The Accuracy Of Dynamic Flight-Determined Coefficient*, NASA RP 1077
29. Maine, R.E., Iliff, K.W. (1986), *Application Of Parameter Estimation To Aircraft Stability And Control, The Output-Error Approach*, NASA Reference Publication 1168
30. Malvestuto, F.F., Gale, L.J.Jr. (1947*), Formulas for Additional Mass Corrections to the Moment of Inertias of Airplanes*, NACA-TN 1187
31. Mathew, N.W., Pangeas, G.N. (1981), *HIMAT Aerodynamic Design And Flight Test Experience*, AIAA Paper 81-2433, Nov 1981
32. Milne, Garth (1992), *State-Space Identification Toolbox, For Use With Matlab*, The Mathworks
33. Mohammad, M (1995*), Identification of Turboprop Thrust From Flight Test Data*, Phd Dissertation, Delft University Press, ISBN:90-9009058-4
34. Mulder, J.A., Sridar, J.K., Breeman, J.H.(1994), *Identification of Dynamic Systems-Application to aircraft*. Part 2: Nonlinear Analysis and Manoeuvre Design. AGARD-AG-300, Vol.3. Part 2
35. Newman, D.M., Wong, K.C., (1995), *An Atmospheric Disturbance Model for Small Remotely Piloted Vehicle Simulation and Analysis*, Proceeding of the 2nd pacific International Conference on Aerospace Science and Technology (PICAST2), Melbourne March 1995, Vol.2, Page 579-583
36. Plaetschke, E., Schulz, G. (1979), *Practical Input Signal Design* : Parameter Identification, AGARD-LS-104, paper 3, 29 Oct.-2 Nov.
37. Pope, Alan (1947), *Wind Tunnel Testing*, John Wiley & Sons, New York
38. Raisinghani ,Singh, Jatinder, S.C. (1993), *Aileron And Sideslip-Induced Unsteady Aerodynamic Modelling For Lateral Parameter Identification*, Journal of aircraft, vol.30, no.4, July-Aug,
39. Reed, R.Dale (1974), *RPRV'S: The First And Future Flights*, Astronaut. & Aeronaut. Vol.12, No.4, April 1974

40. Roskam, J., (1985), *Component Weight And Estimation*, Airplane Design Part V, Roskam Aviation and Engineering Coorp.
41. Roskam, J., (1987), *Aiplane Design Part VI: Preliminary Calculation of Aerodynamics, Thrust and Power Characteristics*, Roskam Aviation and Engineering, Ottawa, Kansas
42. Ross, J.A. (1979), *Application Of Parameter Identification Techniques To Analysis Of Flight Data*, Progress in Aerospace Science, Vol.18, p.325-350.
43. Smetana, F.O. (1984), *Computer Assisted Analysis of Aircraft Performance Stability and Control*, McGeaw-Hill Book Court, N.Y, ISBN 0-07-058441-9
44. Sofyan, E., Bil, C., Danaher, R., (1996*), Aircraft Model Flight Test for Parameter Identification*, Proceeding of the 2nd ISASTI (International Symposium on Aeronautical Science and Technology in Indonesia), 27 July 1996, Jakarta, Indonesia, vol.1, page 118-129
45. Sofyan, E., Danaher, R., Thompson, L., Bil, C., (1995*), A Half Scale MAFV (Multi-Purpose Autonomous Flight Vehicle) Flight Test Program*, Proceeding of the 7th IASE (The Indonesian Aerospace Students in Europe), 12-14 July 1995, Manchester, England
46. The Wackett Centre (1995), *Airborne CO_2 Analyser Development for MAFV Jabiru*, Internal Memorandum, The Wackett Centre for Aerospace Design & Technology, Tel:86-3090, 15 December 1995
47. Thompson, L.A., Abanteriba, S. and Bil, C. (1993), *A Multi-purpose Autonomous Flight Vehicle System*, Proceedings of the 5th Australian Aeronautical Conference, Melbourne, 13 - 15 September 1993.
48. Valentinis, F., Bil, C., Riseborough, P.(1996), *Development and Trials of an Autonomous Flight Control System for UAVs*, Paper to be presented at the ICAS 1996 in Italy
49. Ward, Donald,T. (1993), *Introduction to Flight Test Engineering*, Elsevier Science Publisher, ISBN 0-444-881476
50. Wingrove, R.C. (1973), *Quasi Lineriazation Technique For Estimating Aircraft States From Flight Data*, Journal of Aircraft, vol.10, no.5, p.303-307
51. Wolowicz, C.H., Yancey, R.B (1974), *Experimental determination of Airplane Mass and Inertial Characteristics*, NASA TR R-433, October 1974
52. Wong, K.C.; Newman, D.M. (1989), *Exploratory Study Into The Use Of A Remotely Piloted Vehicle (RPV) For Aerodynamic Research*, Proceeding of The Australian Aeronautical Conference 1989, Melbourne, 9-11 Oct.1989, p.27-30
53. Yip, L.P.,Ross, H.M., Robelen, D.B. (1992), *Model Flight Test Of A Spin-Resistant Trainer Configuration*, Journal of Aircraft, vol.29, no.5, Sept-Oct
54. Young, Shin-en, Kneen, John (1995*), Data Acquisition Systems of The Multi Purpose Autonomous Flight Vehicle*, Project Report at the Department of Aerospace Engineering and Computer System Engineering RMIT, November 1995

APPENDIX 1: SENSOR CHARACTERISTICS USED IN THE TELEMASTER T240 FLIGHT TEST PROGRAM

No	Quantity measured	Transducer	Range	Static sensitivity	Resolution	Rms measurement error (% of full range)
1	Longitudinal acceleration	Accelerometer, Setra systems model 141	± 6g		±0.05g	
2	Lateral acceleration	Accelerometer, Setra systems model 141	± 6g		±0.05g	
3	Vertical acceleration	Accelerometer, Setra systems model 141	± 6g		±0.05g	
4	Pitching velocity	Rate piezo gyro, NE J-1000	±250°/s	2.29	±2°/s	1.1
5	Yawing velocity	Rate piezo gyro, NE J-1000	±250°/s	2.42	±2°/s	1.1
6	Rolling velocity	Rate piezo gyro, NE J-1000	±250°/s	2.50	±2°/s	0.8
7	Angle of attack	Flow vane, potensio type Murata LP06M3R1HA	-50° to 60^0	4.41	±0.4°	0.7
8	Angle of sideslip	Flow vane, potensio type Murata LP06M3R1HA	-50° to 40^0	4.13	±0.4°	1.9
9	Elevator deflection	Control position transducer, potensio type RS 173-574	-50° to 30^0	3rd order calibration	±0.2°	0.9
10	Rudder deflection	Control position transducer, potensio type RS 173-574	-60° to 30^0	3rd order calibration	±0.2°	0.6
11	Right aileron deflection	Control position transducer, potensio type RS 173-574	±20°	3rd order calibration	±0.2°	1.2
12	Left aileron deflection	Control position transducer, potensio type RS 173-574	±20°	3rd order calibration	±0.2°	0.4
13	Airspeed	Differential pressure sensor, SENSYM SCC05DN	0 to 65 m/s (0-10 inc H2O)	0.12 inc H2O	±0.8 m/s°	
14	Engine rotational speed	Hall effect IC.Switch RC 307-446	0-25000 rpm		10 rpm	

No	Quantity measured	Transducer	Max applied voltage or current	Normally applied voltage or current	Resistance	Zero offset	Others
1	Longitudinal acceleration	Accelerometer, Setra systems model 141		10 Volt , 5 mA	9 K Ohm	< ± 25 mV	$\xi = 0.7$ $\omega n = 350$ Hz
2	Lateral acceleration	Accelerometer, Setra systems model 141		10 Volt , 5 mA	9 K Ohm	< ± 25 mV	$\xi = 0.7$ $\omega n = 350$ Hz
3	Vertical acceleration	Accelerometer, Setra systems model 141		10 Volt , 5 mA	9 K Ohm	< ± 25 mV	$\xi = 0.7$ $\omega n = 350$ Hz
4	Pitching velocity	Rate piezo gyro, NE J-1000		4.8-6V, 80 mAh			dynamic range 0-720°/s
5	Yawing velocity	Rate piezo gyro, NE J-1000		4.8-6V, 80 mAh			dynamic range 0-720°/s
6	Rolling velocity	Rate piezo gyro, NE J-1000		4.8-6V, 80 mAh			dynamic range 0-720°/s
7	Angle of attack	Flow vane, potensio type Murata LP06M3R1HA	10 volt	6 volt	5 K Ohm		max rotational torque = 5 gr.cm
8	Angle of sideslip	Flow vane, potensio type Murata LP06M3R1HA	10 volt	6 volt	5 K Ohm		max rotational torque = 5 gr.cm
9	Elevator deflection	Control position transducer, potensio type RS 173-574	10 mA		5 K Ohm		
10	Rudder deflection	Control position transducer, potensio type RS 173-574	10 mA		5 K Ohm		
11	Left aileron deflection	Control position transducer, potensio type RS 173-574	10 mA		5 K Ohm		
12	Left aileron deflection	Control position transducer, potensio type RS 173-574	10 mA		5 K Ohm		
13	Airspeed	Differential pressure sensor, SENSYM SCC05DN	1.5 mA	1.0 mA	5 K Ohm	0 ± 20 mV	
14	Engine rotational speed	Hall effect IC.Switch RC 307-446	25 V	4.5 to 24V (6mA)			

APPENDIX 2: SENSOR ERROR ANALYSIS

1. Linear acceleration measurement

A. Transducer error.

Transducer error for the accelerometer is modelled as bias error and scale error. These errors are determined from the calibration.

B. Kinematics error.

Any cg offsets and misalignments produce errors in acceleration measurements. These errors are calculates as follows (Laban 1994):

Cg-Offset error

$$a_{x_{cg}} = a_{x_{measured}} + (x_{cg} - x_{ax})(q^2 + r^2) - (y_{cg} - y_{ax})(pq - \dot{r}) - (z_{cg} - z_{ax})(pr + \dot{q})$$

$$a_{y_{cg}} = a_{y_{measured}} + (y_{cg} - y_{ay})(r^2 + p^2) - (z_{cg} - z_{ay})(qr - \dot{p}) - (x_{cg} - x_{ay})(qp + \dot{r})$$

$$a_{z_{cg}} = a_{z_{measured}} + (z_{cg} - z_{az})(p^2 + q^2) - (x_{cg} - x_{az})(rp - \dot{q}) - (y_{cg} - y_{az})(rp + \dot{p})$$

x_{ax}, y_{ax} , and z_{ax} are longitudinal accelerometer positions.
x_{ay}, y_{ay} , and z_{ay} are lateral accelerometer positions.
x_{az}, y_{az} , and z_{az} are vertical accelerometer positions.

Misalignment error

$$a_{cg} = \begin{bmatrix} 1 & -y_0 & q_0 \\ y_0 & 1 & -j_0 \\ -q_0 & j_0 & 1 \end{bmatrix} . a_{measured}$$

Where ψ_0, θ_0, and φ_0 are yaw, pitch and roll misalignments.

Since the kinematics acceleration error is a systematic error, it can therefore be minimised by locating the three accelerometers as close as possible to the centre gravity.

2. Angular rate measurement

A. Transducer error.

The averages of 5 deg/s transducer error for the rate gyros were obtained from the calibration on the rate table.

B. Kinematics error.

The kinematics error due to misalignment is given as;

$$w_{cg} = \begin{bmatrix} 1 & -y_0 & q_0 \\ y_0 & 1 & -j_0 \\ -q_0 & j_0 & 1 \end{bmatrix} . w_{measured}$$

3. Airflow direction measurement

From Laban (1994, page 216) the vane dynamics is given as:

$$I_v \ddot{a}_{shaft} + (\frac{1}{2} \rho V^2 S_v Cl_{v_a} l_v) \frac{l_v \dot{a}_{shaft}}{V} + (\frac{1}{2} \rho V^2 S_v Cl_{v_a} l_v).(a_{shaft} - a_{vane}) = 0$$

The lift curve-slope $Cl_{v\alpha}$, can be approximated as;

$$Cl_{v_a} = \frac{A_v}{2 + \sqrt{4 + A_v^2}} . 2p$$

From the above 2nd order approximation, the damping and natural frequencies of the vane are;

$$w_0 = \sqrt{\frac{S_v Cl_{v_a} l_v}{I_v}.0.5rV^2} \qquad x = \sqrt{\frac{S_v Cl_{v_a} l_v^3}{8I_v}.r}$$

A simpler low frequency approximation to the vane dynamic can sometime be useful, and is given in a lag time form as follows;

$$a_{shaft}(t) = a_{vanet}(t + t_{vane})$$

$$t_{vane} = \frac{2}{w_0} = 2.\sqrt{\frac{I_v}{S_v Cl_{v_a} l_v}}.p_{impact}^{-0.5}$$

The a *and* b *vanes for the half-scale model has the following characteristics:*

Aspect ratio A_v = 2.66
Area S_v = 9.68 cm^2
Arm length l_v = 5.2 cm
Mass = 3.84 grams
Inertia I_v = 15.3 $gr.cm^2$

Calculation at v=15 m/s, gives a vane natural frequency of 108 rad/s, and damping of 0.19. The approximate time delay, t *is 19 msec.*

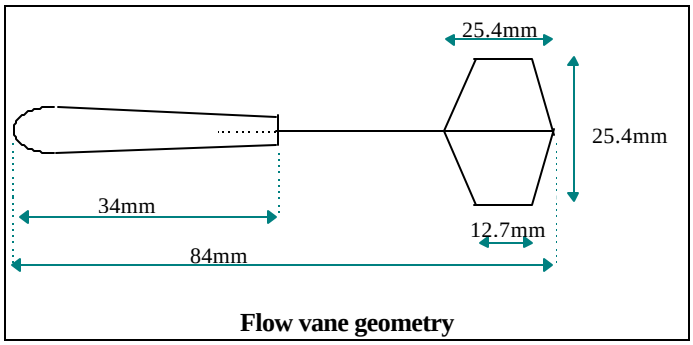

Flow vane geometry

Flow-Vane sources of errors:

A. Aerodynamic position error, due to flow perturbation in the presence of nose or body. Hence, the local angle will not represent the free stream flow directions. The flow vanes in this project were located far from the nose (twice the fuselage diameter), hence this error is assumed to be negligible.

B. Kinematics error, due to offset vane locations from the centre of gravity. This offset location produces angular velocities which affect the flow angle measurements.

$$a_{vane} = arc\tan\frac{V_z}{V_x}$$

$$b_{vane} = arc\tan\frac{V_y}{V_x}$$

Where V_x, V_y and V_z represents velocities relative to the air.

Then both the aerodynamic position error and kinematics error can be formulated as;

$$a_{vane\ location} = arc\tan\frac{V_z + (\Delta V_z)_{a/c\,induced} + q(x_{vane} - x_{cg})}{V_x + (\Delta V_{xz})_{a/c\,induced} - q(z_{vane} - z_{cg})}$$

$$= a_{cg\ location} + \Delta a_{cg\,induced} + q\frac{x_{vane} - x_{cg}}{V}$$

$$b_{vane\ location} = arc\tan\frac{V_y + (\Delta V_y)_{a/c\,induced} - r(x_{vane} - x_{cg}) + p(z_{vane} - z_{cg})}{V_x + (\Delta V_{xz})_{a/c\,induced} - q(z_{vane} - z_{cg})}$$

$$= b_{cg\ location} + \Delta b_{cg\,induced} - r\frac{x_{vane} - x_{cg}}{V} + p\frac{z_{vane} - z_{cg}}{V}$$

In a typical doublet manoeuvre, the T240 may experience a maximum pitch rate of 2.0 rad/s (from simulation). If the vanes are located at 1 meter forward of the c.g, this introduces kinematics error of $q(X_{vane}-X_{cg}/V)$*, which corresponds to a* 4^0 *error in angle of attack.*

C. Vane boom error, due to the present of boom support at the vicinity of the vanes. The vane-boom effect is normally obtained from wind tunnel calibration of the installed boom-vanes system.
Approximation using potential flow theory is given as;

$$\alpha_{vane} = [1 + K_{\alpha}]\alpha_{vane\ location}$$

$$\beta_{vane} = [1 + K_{\beta}]\beta_{vane\ location}$$

Where the correction K_{α}, and K_{β} are;

$$K_{\alpha} = K_{\beta} = \frac{1}{r_{nane\ \max} - r_{vane\ \min}} \cdot \int_{r_{vane\ \min}}^{r_{vane\ \max}} \left(\frac{r_{boom}}{r} \right)^2 dr$$

For the T240 vanes;
r boom = 0.7 cm
$r_{vane\ min}$ = 4 cm
$r_{vane\ max}$ = 9 cm
The correction values K_a, and K_b calculated to be 0.0136 (1.36% of boom error).

D. Static vane alignment error.
M.Laban (1994)commented that there seems to be no need to accurately measure the vane misalignments. This error can be combined with the induced flow distortion error, and simply stated as;

$$\alpha_{vane} = \alpha_{body\ axis} + \Delta\alpha_{alignment}$$

$$\beta_{vane} = \beta_{body\ axis} + \Delta\beta_{alignment}$$

E. Alignment error due to fuselage and boom bending.
This error can be calculates as;

$$\varepsilon = \left(\frac{\partial \varepsilon}{\partial f_z} \right) f_z + \left(\frac{\partial \varepsilon}{\partial \dot{q}} \right) \dot{q}$$

where

$$\frac{\partial \varepsilon}{\partial f_z} = \frac{1}{6}\sqrt{2}\left(\frac{\rho}{E} \right)\left(\frac{l}{r} \right)^3 \left(\frac{r}{\eta} \right)$$

$$\frac{\partial \varepsilon}{\partial f_z} = -\frac{1}{8}\sqrt{2}\left(\frac{\rho}{E} \right)\left(\frac{l}{r} \right)^3 \left(\frac{l\,r}{\eta} \right)$$

For the T240, the alignment error due to fuselage and boom bending is calculated below:

	Fuselage	**Vane boom**
Length, l (meter)	1.55	0.45
Diameter, r (meter)	0.18	0.003
Structural efficiency, η	10%	100%
Stiffness, E (N/m^2)	$72x10^9$	$72x10^9$
Density, ρ (Kg/m^3)	2800	2800
Offset from Cg, Δx (meter)	0	1
	$\varepsilon=5.13x10^{-6}\ f_z - 4.16x10^{-6}(dq/dt)$	$\varepsilon=9.28x10^{-5}\ f_z+\Delta x\ (dq/dt) - 3.13x10^{-5}(dq/dt)$
for max f_z = 25 m/s		0.006^0 due to the fuselage
and (dq/dt) = 5 rad/s^2	$\varepsilon=0.157^0$	0.151^0 due to the boom

Assessment of the flow vane for the T240.

The table below compares several existing flow vanes;

	Velocity (m/s)	Natural freq (rad/s)	Damping
Sydney University RPV	-	170	-
Swearingen Metro II	100	102	0.05
T240 model	15	108	0.19

Source of errors for the T240 flow vanes;

Error source	Magnitude	Comment
Flow perturbation	assumed negligible	Verify with the press. distribution at the nose.
Kinematics	max. 4^0	Determinate error
Vane boom	max 1.4 % (0.5^0 for $\pm 30^0$ range)	less than data acquisition resolution
Static alignment		obtain from wind tunnel calibration
Boom bending	0.16^0	neglected for the T240 model

The vane design is acceptable, since its damping is relatively high and its natural frequency is well above aircraft's mode (ω_{SPO} is typically < 18 rad/s). The expected error from the vane systems is small, and remains inside the required resolution of the sensor (which is $\pm 1^0$). Note that the kinematics error is quite significant and should be accounted for during the analysis of flight test data.

4. Air pressure measurement

A. Aerodynamic position error, due to the presence of the nose or body. This error normally dominates the static pressure errors. However, since the static pressure is located far away from the nose in the T240 configuration, then this error is assumed to be negligible.

B. Kinematics position error, due to the offset position from the cg. The kinematics error for the total pressure measurement is given as;

$$P_t = P_s + \frac{1}{2}\rho (V_{cg} + \Delta P_{pitot})^2$$

$$\approx P_{t_{cg}} + \rho V_{cg} \Delta V_{pitot}$$

$$\approx P_{t_{cg}} + \frac{P_s}{RT_s} V_{cg}[(Y_{pitot} - Y_{cg})r - (Z_{pitot} - Z_{cg})q]$$

for the T240;
ΔZ= 4 cm; q_{max} = 2 rad/s, V= 30 m/s, produces kinematics error of ΔP= -3 Pascal. (4.35x10^{-4} psi).

C. Probe error.

Probe error in total pressure can be neglected (Wuest, 1980) as long as the flow angle is less than 10 degree. However, probe error in static pressure is significant, and this includes error due to shear and error due to flow interference. Flow friction along the probe, ahead of static pressure transducer, reduces the static pressure ΔP, and is given as;

$$\Delta P_{shear} = [0.0576.\,\mathrm{Re}^{-1/5}.\, fn(\frac{d}{V}, \sqrt{\frac{\tau}{\rho}}, \frac{l}{d})].\, P_{impact}$$

The value of fn(...) depends on the design of the orifice and the wall characteristics. A severe value of fn(..)=2.5 is taken for the T240. At Reynold number 3.45×10^5 , at V=30 m/s and viscosity of 1.456×10^{-5}, the shear error is calculated as $\Delta P_{shear} = 0.016\ P_{impact}$. (or 1.6% impact pressure).

This error is caused by the interference between flow in and out of the orifice with the external flow.

For calculations in a flow interference error, refer to ESDU 85011.

D. Pressure tubes error.

This error includes change in pressure inside the tube which is caused by acoustic effect, air friction, and rotational speed of the aircraft. Present theoretical methods for determining this error is not reliable (M.Laban, 1994). A typical value of 3 msec delay per one meter tube length is normally assumed.

E. Pressure traducers error.
For electric transducer, this error is normally small and can therefore be neglected.

Airspeed measurement.

The airspeed value (V) is obtained indirectly from the measurement of static pressure (Ps), total pressure (Pt), air temperature (Ts), and is related as follows;

$$P_t = p_s\left[1+\frac{g-1}{2gRT_s}V^2\right]^{\frac{g}{g-1}}$$

where $\gamma = 1.4$ (vary very little with humidity, γ is also insensitive to V value).
$R = R_{\text{dry air}} = 287.05$ J/Kg.K. The value of R depends on the dew point temperature. Assuming a constant value of R, produces a speed uncertainty of $\Delta V=0.5$ m/s at temperature of 20 ^{0}C (Laban 1994).

Airspeed sensitivity due to changes in air parameters are given as;

$$\Delta V = \frac{1}{2}V\frac{\Delta R}{R}$$

$$\Delta V = \frac{1}{2}V\frac{\Delta T_S}{T_S}$$

T in Kelvin

Suppose an error of 2 degrees in temperature measurement at an airfield (say, T=18^{0}C) to measure aircraft's velocity of 30 m/s. This temperature measurement error is equivalent to uncertainty in speed measurement of $\Delta V=0.1$ m/s. In addition, A 10 degree variation in due point, which corresponds to $\Delta R=5$ J/Kg.K, produce uncertainty in speed measurement of $\Delta V=0.26$ m/s

For low-speed flight;

$$v = \sqrt{\frac{2(p_t - p_s)}{r}}$$

The actual calibration of the airspeed sensor is carried out in the wind tunnel.

5. Control surface deflection measurement

1. Transducer error.
This error is obtained from the calibration.

Control surfaces	errors (deg)	% full scale
Right elevator	0.35	0.9
Rudder	0.34	0.6
Right aileron	0.51	1.2
Left aileron	0.16	0.4

2. Mechanical linkage error.
This error is caused by the elasticity, lag, and imperfection of the mechanical linkages connecting the two sides of the control surfaces. Due to this error, it becomes impossible to have a perfectly symmetrical movement of the left and right control surfaces. Ideally, deflection sensors should be placed on all control surfaces. However, due to limited number of channels available, only left and right ailerons are measured separately.

In this project, since the linear accelerometers were not working, then no angular rate correction can be performed. Kinematics errors for angle of attack and sideslip were corrected. From the error analysis above, other low vane errors can be neglected.

APPENDIX 3: CHARACTERISTICS OF THE TELEMASTER T240 MODEL

Wing	Value
Area (cm^2)	8300
Span (cm)	226
Chord (cm)	35
Swept angle (deg)	0
Dihedral angle (deg)	2
Aspect ratio	6.8
Taper ratio	1
Setting incidence (degree)	11
Downwash angle (degree)	0
Efficiency	0.8
Max thickness ratio (at position)	0.13 (0.3c)
LE distance from the nose (cm)	37.5
2-D lift curve slope (per degree)	
2-D drag curve slope (per degree)	

Tailplane	Value
Area (cm^2), excluding elevator	1550
Span (cm)	86
Chord (cm)	18
Swept angle (deg)	0
Dihedral angle (deg)	0
Aspect ratio	2.4
Taper ratio	1
Setting incidence (degree)	11
Downwash angle (degree)	0
Efficiency	
Max thickness ratio (at position)	0.14 (0.4)
LE distance from the nose (cm)t	134.5
2-D lift curve slope (per degree)	
2-D drag curve slope (per degree)	

Vertical fin	Value
Area (cm^2), including rudder	820
Span (cm)	39
Chord (cm)	30
Swept angle (deg)	60
Dihedral angle (deg)	0
Aspect ratio	1.1
Taper ratio	0.8
Setting incidence (degree)	0
Downwash angle (degree)	0
Efficiency	
Max thickness ratio (at position)	
LE distance from the nose (cm)	134.5
2-D lift curve slope (per degree)	
2-D drag curve slope (per degree)	

Aileron	Value
Area of each aileron (cm^2)	550
Span (cm)	55
Chord (cm)	10
Swept angle (deg)	0
Dihedral angle (deg)	0
Aspect ratio	5.5
Taper ratio	1
Inboard station (% half span)	44.7
Outboard station (% half span)	100

Elevator	Value
Area of each elevator (cm^2)	180
Span (cm)	36
Chord (cm)	5
Swept angle (deg)	0
Dihedral angle (deg)	0
Aspect ratio	7.2
Taper ratio	1
Inboard station (% half span)	5
Outboard station (% half span)	95

Rudder	Value
Area (cm^2)	490
Span (cm)	39
Chord (cm)	13
Swept angle (deg)	0
Dihedral angle (deg)	0
Aspect ratio	3
Taper ratio	
Inboard station (% half span)	0
Outboard station (% half span)	100

Flap	Value
Area of each flap (cm^2)	348
Span (cm)	43.5
Chord (cm)	8
Swept angle (deg)	0
Dihedral angle (deg)	0
Aspect ratio	5.4
Taper ratio	1
Inboard station (% half span)	6
Outboard station (% half span)	44.7

ENGINE AND PROPELLER CHARACTERISTICS	Value
Engine type	Irvine-150
Power	22 cc
Idle rpm	1700
Full throttle rpm	8000-12000
Type	Fixed pitch
Diameter (mm)	360
Mean chord (mm)	30
Hub diameter (mm)	70
Pitch (mm)	14

DISTANCES	Value
Fuselage length (cm)	155
Fuselage width (cm)	18
Centre of gravity, Xcg (cm)	52
Vertical centre of gravity, Zcg (cm)	+1.5
C.g to tailplane quarter chord (cm)	140-Xcg
C.g to wing quarter chord (cm)	46-Xcg
C.g to wing a.c (chordwise in cm)	46-Xcg
C.g to wing a.c (vertical in cm)	14-Zcg
C.g to thrust axis (cm)	0
Nose to wing quarter chord (cm)	46
Nose to tail quarter chord (cm)	140
Wing to tail quarter chord (cm)	94
Vertical distance from wing to tail (cm)	8

APPENDIX 4: FLIGHT TEST SENSOR CALIBRATIONS

Results of the flight test sensor calibrations are presented in figures A4-1 to A4-11. Each figure contains 2 different graphs; the top graph shows the experimental result and its fitted curve, the bottom graph shows the corresponding calibration error.

Channel allocations and calibration results are shown below:

Channel no	Sensors	Calibration	Standard deviation (% full scale)	Mean	Figure no
1	spare				
2	Rate gyro 1	1.4283X-216.88	1.0005 (0.27)	1.345×10^{-14}	A4-1
3	Rate gyro 2	1.5342X-234.38	1.1977 (0.30)	-3.527×10^{-14}	A4-2
4	Rate gyro 3	-1.3555X+170.84	3.9375 (1.14)	3.4639×10^{-14}	A4-3
5	Accelerometer				
6	Accelerometer				
7	Accelerometer				
8	spare				
9	spare				
10	Airspeed	$(1890.3X-3544.6)^{0.5}$	1.7(2.6)	9.2667×10^{-13}	A4-4
11	Yaw vane	0.41327X-57.99	0.7515 (0.74)	-0.962×10^{-14}	A4-5
12	Angle of attack vane	-0.43511X+63.768	0.6745 (0.66)	1.228×10^{-14}	A4-6
13	Left aileron	$-2.767\times10^{-6}X^3+1.3356\times10^{-3}X^2-4.477\times10^{-3}X-18.115$	0.1747 (0.58)	-1.790×10^{-15}	A4-7
14	Right aileron	$2.2612\times10^{-6}X^3-9.3349\times10^{-4}X^2-7.5499\times10^{-2}X-21.917$	0.5094 (1.2)	5.9164×10^{-15}	A4-8
14 (optional)	Flap	$-2.5549\times10^{-6}X^3+5.9816\times10^{-4}X^2+1.9118\times10^{-1}X-5.4749$	0.4075 (1.02)	2.6412×10^{-15}	A4-9
15	Elevator	$-1.0155\times10^{-5}X3+3.1717\times10^{-3}X^2+5.9756\times10^{-2}X-33.208$	0.2096 (0.5)	-0.7905×10^{-15}	A4-10
16	Rudder	$-6.1266\times10^{-6}X^3+2.4028\times10^{-3}X^2+9.3398\times10^{-2}X-45.87$	0.3346 (0.6)	1.5258×10^{-15}	A4-11
17	Engine rotational speed	256*channel 17 + channel 18			
18	Engine rotational speed	256*channel 17 + channel 18			

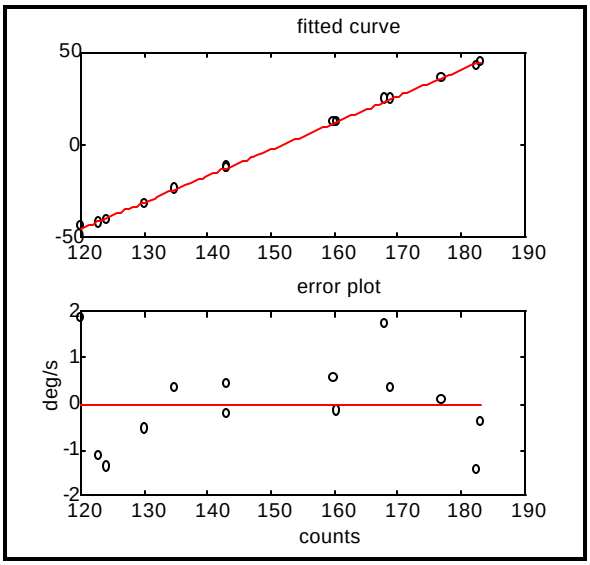

Figure A4- 1: Yaw Rate Gyro (Chn 2) Calibration

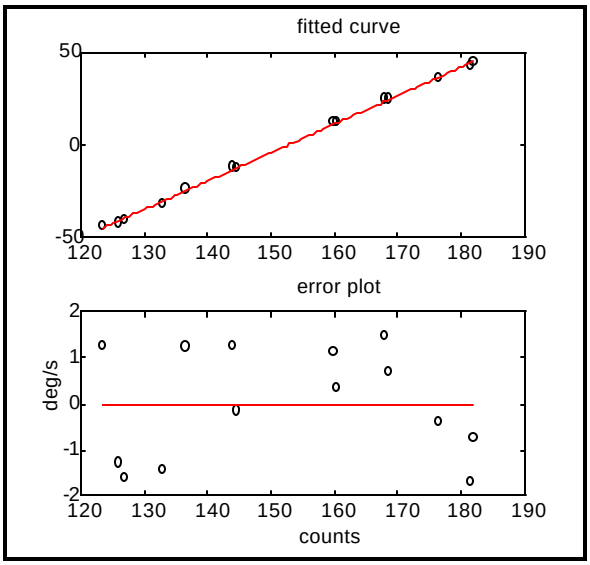

Figure A4- 2: Pitch Rate Gyro (Chn 3) Calibration

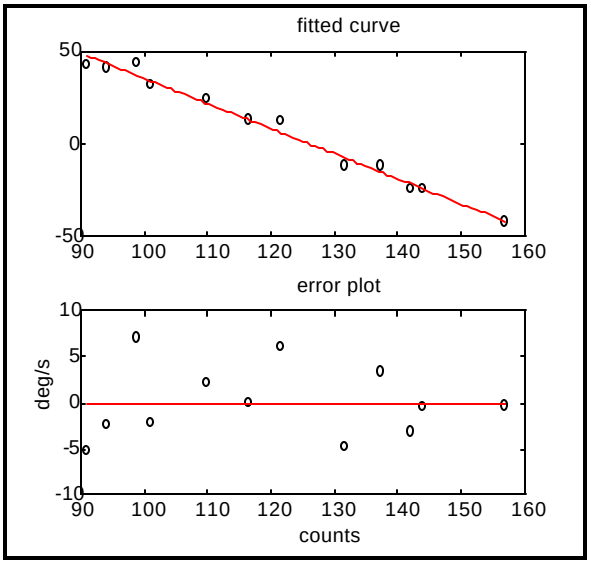

Figure A4- 3: Roll Rate Gyro (Chn 4) Calibration

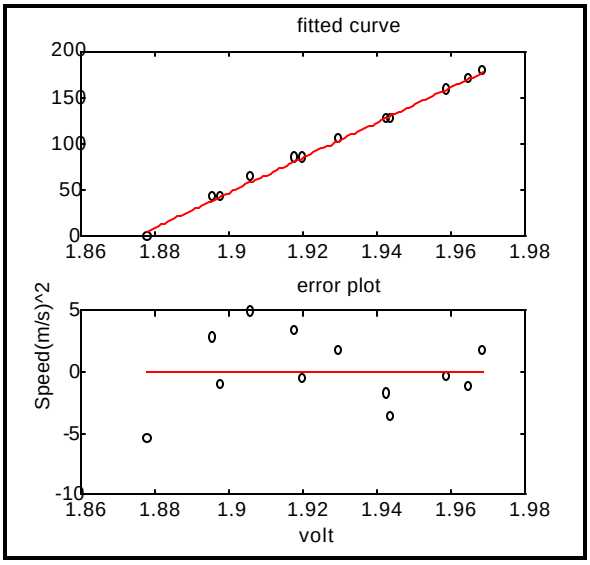

Figure A4- 4: Airspeed Sensor Calibration

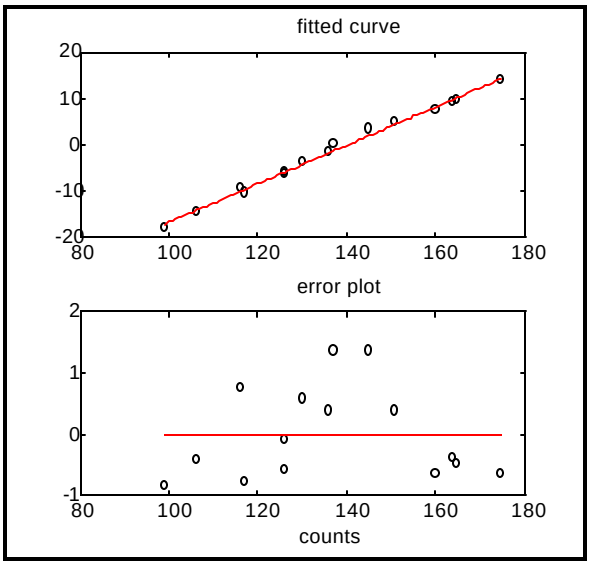

Figure A4- 5: Yaw Vane Calibration

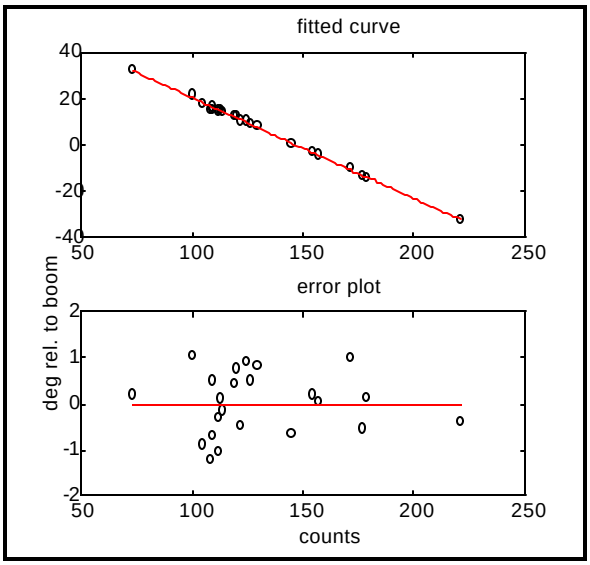

Figure A4- 6: Angle of Attack Calibration

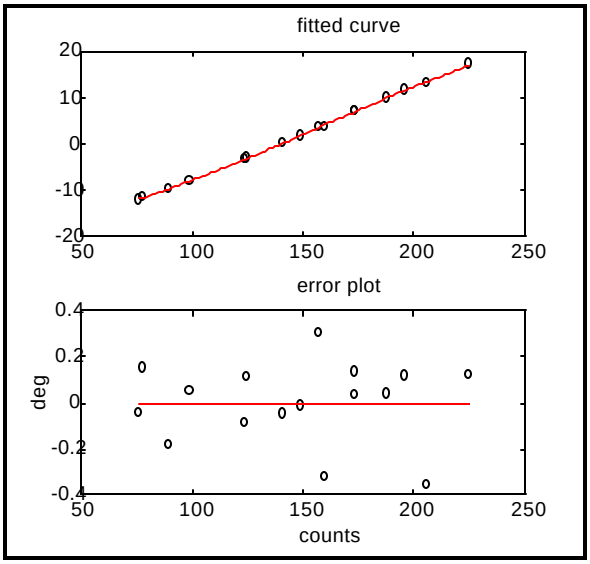

Figure A4- 7: Left Aileron Calibration

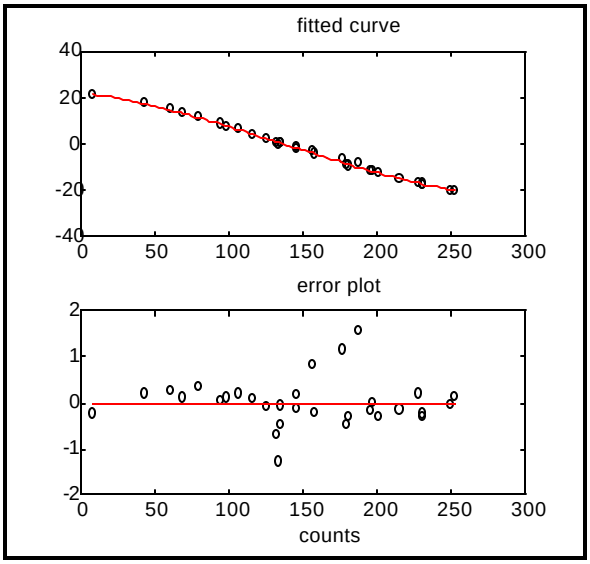

Figure A4- 8: Right Aileron Calibration

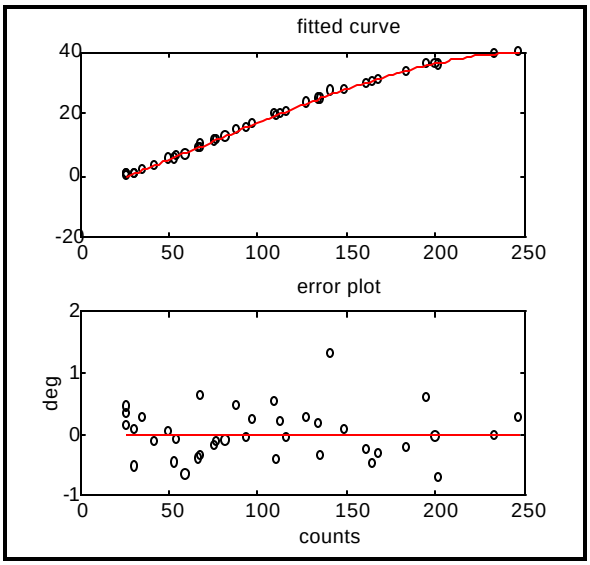

Figure A4- 9: Flap Calibration

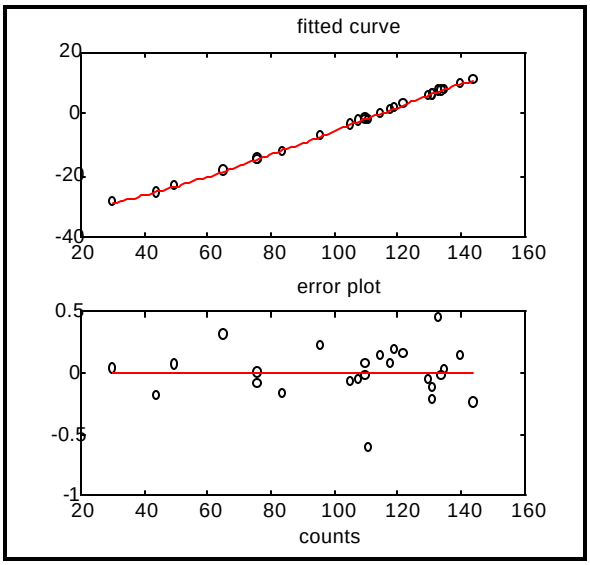

Figure A4- 10: Right Elevator Calibration

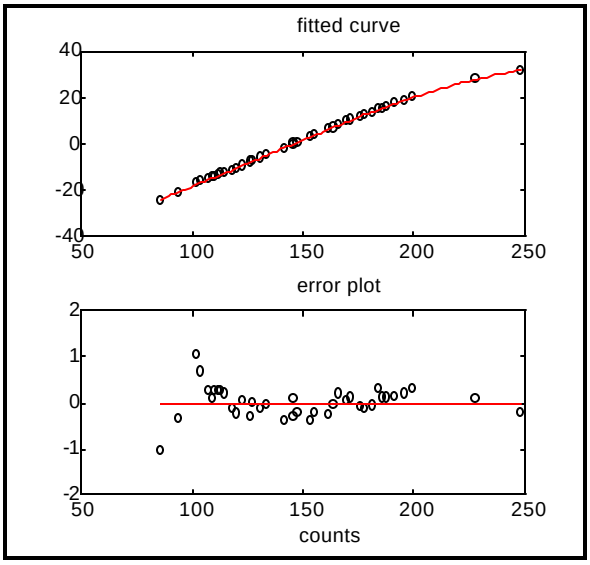

Figure A4- 11: Rudder Calibration

APPENDIX 5: FLIGHT TEST SOFTWARE DESCRIPTION

Input and output variables in the subprogram m files.

M file	Input variables		Output variables
		optional	
londyn.m		u	u alpha q alphadot qdot
latdyn.m		u	ua ur beta p r betadot pdot rdot
lslongui.m	u alpha q	alphadot qdot	u alpha q alphadot qdot alpha_est q_est Cz Cm Cz_est Cm_est P_est
lslatgui.m	ua ur beta p r	betadot pdot rdot	ua ur beta p r betadot pdot rdot Cy Cl Cn Cy_est Cl_est Cn_est P_est beta_cal p_cal r_cal STD
mllongui.m	u alpha q	alphadot qdot	u alpha q alpha_est q_est P_est CRB
mllatgui.m	ua ur beta p r	betadot pdot rdot	ua ur beta p r beta_est p_est r_est P_est CRB
preprocess.m	Vax Vay Vaz Vp Vq Vr Vdc Vdal Vdar VdR Vrps Vdyn Vstat Valpha Vbeta		axcg aycg azcg pcg qcg rcg dc da dR rps thrust vcg alphacg betacg

APPENDIX 6: TESTINGS

1. Engine test.

Test specification:

Engine type : RC-80, approx. 1.7 Hp
Propeller diameter : 14 inches
Pitch : 6 inches
Engine speed range : 0 - 9000 rpm
Air speed range : 0 - 25 m/s

Apparatus:

- A thrust balance, with the thrust calibration: Thrust (Newton) = 1.9833 x (balance reading) - 0.454. The accuracy of the balance is approximately 0.2 Newton.
- A pitot static tube and an inclined manometer, with SG=0.785, and inclination of 36 degrees. The wind tunnel speed is calculated as $v = \sqrt{2x9.81x\sin(36)xSGx\Delta H}$, where H is the manometer reading in mm.
- A digital tachometer, with engine speed reading in rpm (revolution per minute), where rpm=100x(displayed value on the tachometer).
- JR remote control system.

Note : To avoid overheating inside the wind tunnel, the engine exhaust is channelled out of the wind tunnel through a flexible hose.

Measurements.

No	Manometer readings (mm)	Tachometer readings	Balance readings	Airspeed (m/s)	Engine speed (rpm)	Thrust (N)	Advance ratio J=v/(nD)	Thrust coefficient Ct=T/(ρ n^2 D^4)
1	0	3.8	4.1	0	3800	7.6763	0	0.067529
2	6	3.8	3.5	7.348469	3800	6.4865	0.297509	0.057063
3	16	3.8	1.6	12	3800	2.7188	0.48583	0.023918
4	0	5.0	4.7	0	5000	8.8661	0	0.045051
5	0	5.0	4.5	0	5000	8.4695	0	0.043035
6	12	5.0	4.4	10.3923	5000	8.2712	0.319763	0.042028
7	12	5.0	3.9	10.3923	5000	7.2797	0.319763	0.03699
8	18	5.0	3.1	12.72792	5000	5.6933	0.391628	0.028929
9	28	5.0	2.2	15.87451	5000	3.9086	0.488446	0.01986
10	0	7.4	11.6	0	7400	22.5488	0	0.052308
11	10	7.4	10.2	9.486833	7400	19.7726	0.197231	0.045868
12	32	7.4	8.0	16.97056	7400	15.41	0.352818	0.035748
13	62	7.4	4.1	23.62202	7400	7.6763	0.491102	0.017807
14	0	9.0	17.5	0	9000	34.2485	0	0.053711
15	12	9.0	16.2	10.3923	9000	31.6706	0.177646	0.049668
16	28	9.0	14.3	15.87451	9000	27.9029	0.271359	0.043759
17	60	9.0	10.9	23.2379	9000	21.1607	0.397229	0.033186
18	0	4.3	4.0	0	4300	7.478	0	0.051376
19	0	2.5	2.5	0	2500	4.5035	0	0.091533

Results:

Thrust model:

Ct = 0.065 - 0.089 J, or Thrust = $1.84x10^{-3}$ n^2 - $6.46x10^{-3}$ V n (At sea level, where ρ = 1.225 Kg/m^3).
where J = v / nD, and Thrust = ρ n^2 D^4 Ct
D = Propeller diameter = 0.39 meter, n = rotational speed in rev/s.
The data is fitted with the standard deviation of 1 Newton

2. Centre of gravity determination

The distance between the two support points, d=1250mm.

Thickness (mm)	equivalent theta	Rm(kg)	Rn(Kg)	W(kg)	tan(theta)	Rnd/wcos
0	0	9.0085	1.3	10.3085	0	0.157637
24	1.100228	9.0487	1.26	10.3087	0.019204	0.152812
50	2.292612	9.0968	1.21	10.3068	0.040032	0.146865
105	4.818878	9.195	1.11	10.305	0.084298	0.135121
151	6.938786	9.2755	1.03	10.3055	0.121691	0.125855
177	8.141042	9.3285	0.98	10.3085	0.143041	0.120044
202	9.300463	9.3723	0.94	10.3123	0.163752	0.115459
0	0	9.01	1.3	10.31	0	0.157614
147	6.754109	9.2717	1.04	10.3117	0.118422	0.126951
167	7.678238	9.3015	1.01	10.3115	0.134809	0.123544
105	4.818878	9.1885	1.11	10.2985	0.084298	0.135206
80	3.669708	9.1522	1.16	10.3122	0.064131	0.140899
55	2.522014	9.1066	1.2	10.3066	0.044043	0.145679
	Total	9.181215	1.126923	10.30814		

Result:

xcg : 15.74cm from the datum, ie 47.5 cm behind the nose

zcg : 25.79cm from the datum, ie 14 cm above ref. point.

3. Moment of inertia determination

Pitching moment		**Roll**		**Yaw**	
ly = 0.14 m M = 10.3 kg b = 2.26 m L = 1.55 m		l_x = 0.1m R_r = 0.662m		l_y = 0.44 m R_y = 0.2475 m	
no oscillation	*time (s)*	*no oscillation*	*time (s)*	*no oscillation*	*time (s)*
10	19	10	22	10	21
10	19	10	21	10	21
10	19	10	22	10	21
10	19	10	21	10	21
10	19	10	21	5	10
15	29	5	10	5	10
15	28	8	17	8	17
15	29	8	17	8	7
15	28	8	17	9	19
12	23			9	19
12	23				
12	23				
Average Period	1.904167	Average period	2.119444	Average period	1.945679

Results:

Rolling inertia I_{xx} = 1.15 Kgm^2

Ptiching inertia I_{yy} = 1.30 Kgm^2

Yawing inertia I_{zz} = 1.28 Kgm^2

Appendix 7: Flight test procedures and the collected records

Sample record of flight data

Test name	: Longitudinal dynamic			Input Manoeuvre	: Elevator doublet 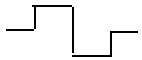
Test model	: Telemaster T240		Flap setting (deg)	: 0	
Date	: 13/6/96		Approx. Speed (m/s)	: 15	
T-O time : 13.00			Landing time	: 13.13	
Manoeuvre/ flight.no	: 1/3			Filename	: test2-1
T-O fuel (Kg)	: 0.25				
T-O weight (Kg)	: 11				
Cg (x,y,z) in cm	: 47.5,0,14				
Inertia (Kgm2)	: Ixx= 1.15	Iyy= 1.30		Izz= 1.28	Ixz= 0
Ground temp (deg C)	: 16			Ground pressure (mmHg)	: 76

Apparatus checklist:
1. Inclinometer.
2. Scales.
3. Spare vanes.
4. Metering tape.
5. Stopwatch.
6. Temperature and pressure measuring devices.
7. Laptop

Flight test procedure to perform dynamic manoeuvre.

Step no	D e s c r i p t i o n
1	Check all sensors are connected to the appropriate channels
2	Verify all switches are off
3	Switch the transmitter and receiver on
4	Switch the IMU and DAS on, the DAS light indicator should be blinking
5	Press the enable/disable DAS button
6	Click the gear control on the transmitter forward and then backward to check that the DAS records the data. The DAS indicator should stop blinking .
7	Connect the RS232 to the laptop.
8	Run the communication program (Telemate) to receive the data.
9	Initiate the log file to save the data into a file (press alt-L), and input filename.
10	Once the DAS indicator starts blinking again, unload data by pressing the unload button.
11	Close the file by pressing Alt-L
12	Repeat step 2 to 5
13	Taxi the aircraft into take off position on runway.
14	Take off.
15	Climb to altitude, then perform a turn. Prepare for doublet manoeuvre.
16	Maintain heading and wing level.
17	Click the gear control on the transmitter to start recording the flight data.
18	Throttle idle, perform doublet manoeuvre, throttle maximum.
19	Climb out.
20	Perform a turn and prepare for landing
21	Landing, then engine off.
22	Repeat step 7 to 11.

Records of flight data

(Also contained in the accompanying disc)

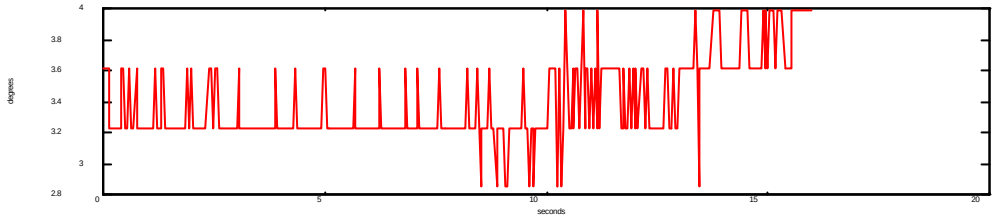

Elevator deflection

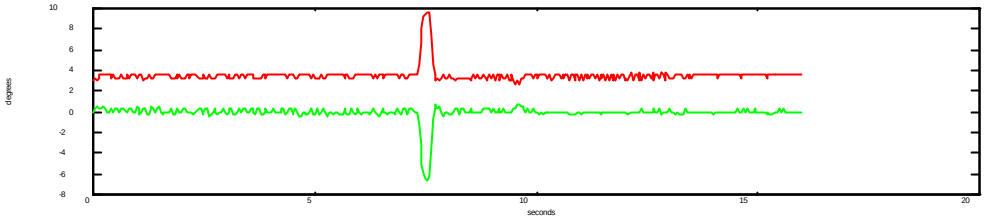

Aileron right (top) and aileron left (bottom) deflection

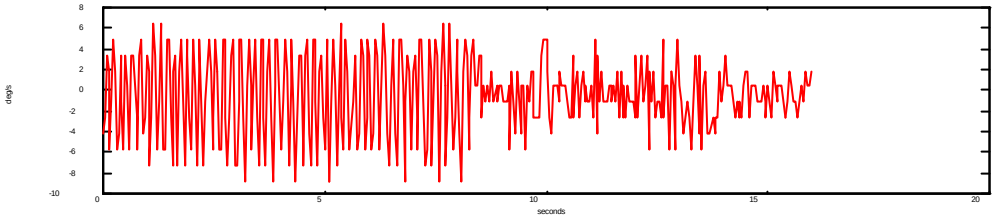

Pitch rate

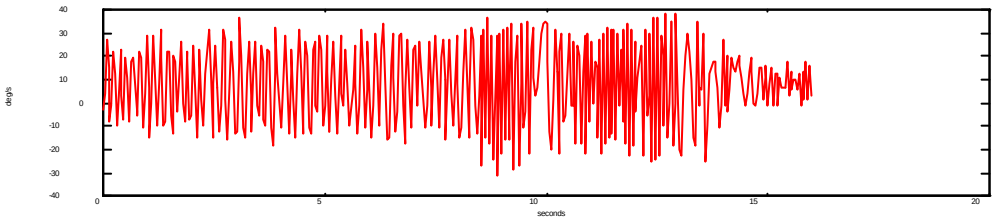

Roll rate

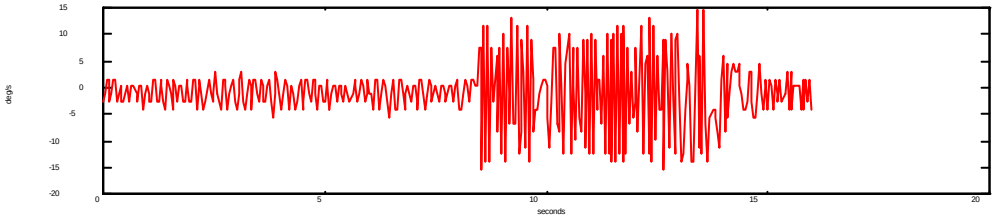

Yaw rate

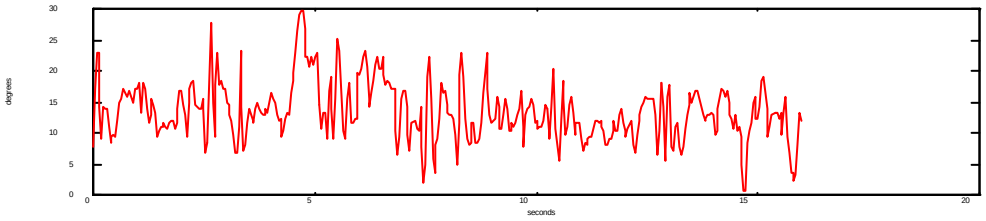

Angle of attack

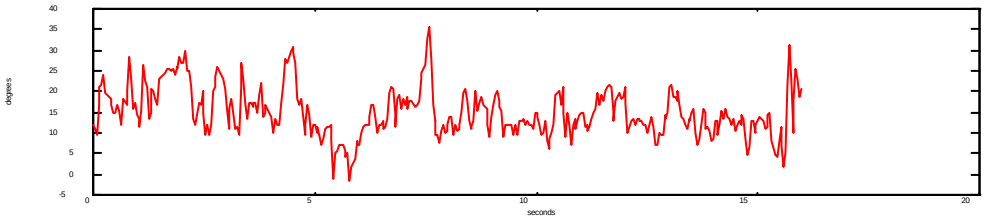

Sideslip angle

Figure A7- 1: Flight_1 records

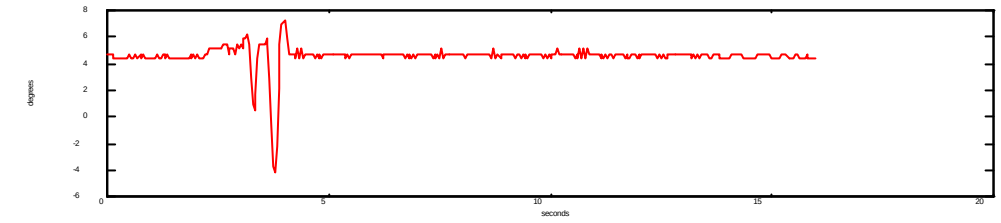

Elevator deflection

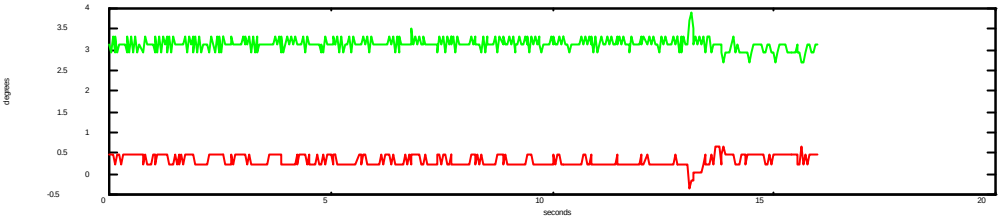

Aileron right (top) and aileron left (bottom) deflection

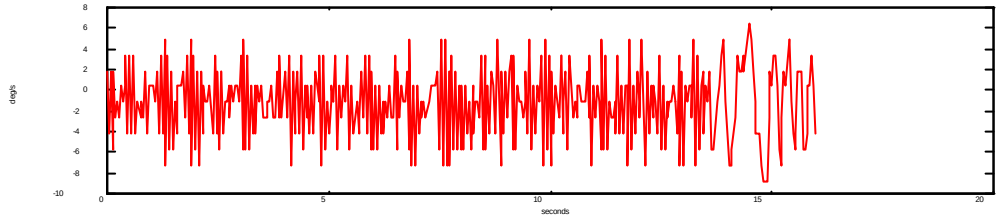

Pitch rate

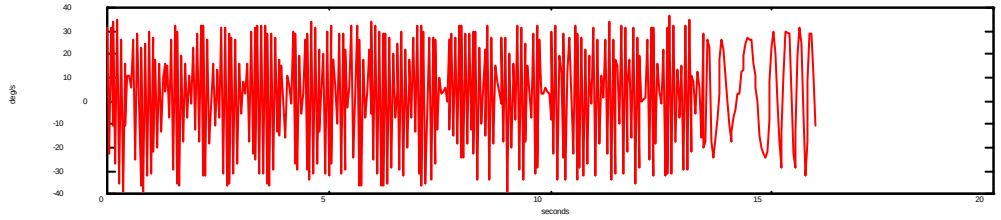

Roll rate

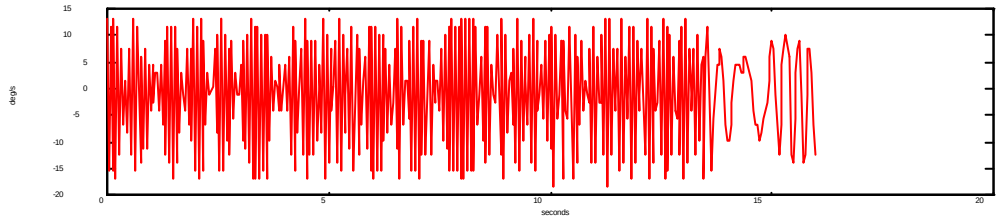

Yaw rate

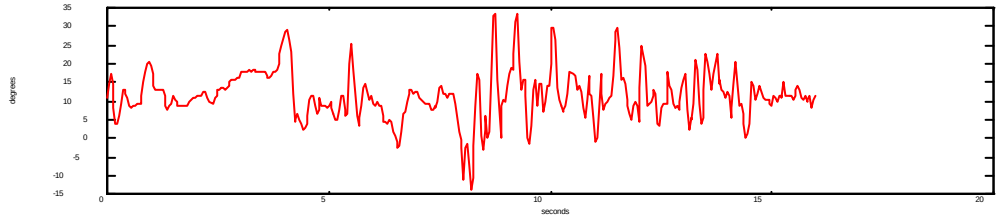

Angle of attack

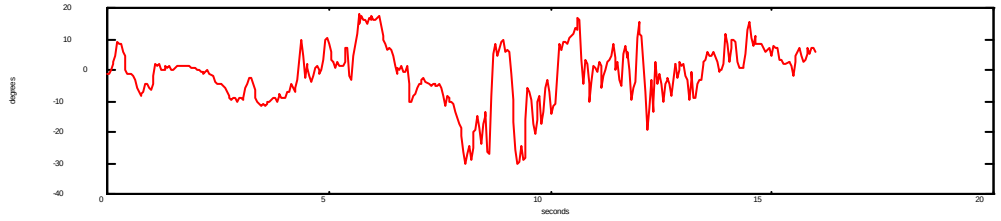

Sideslip angle

Figure A7- 1: Flight_2 records

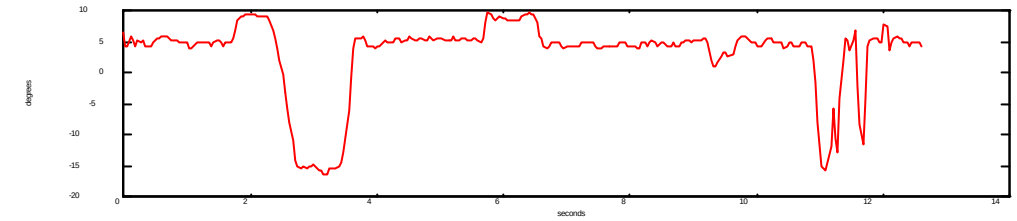

Elevator deflection

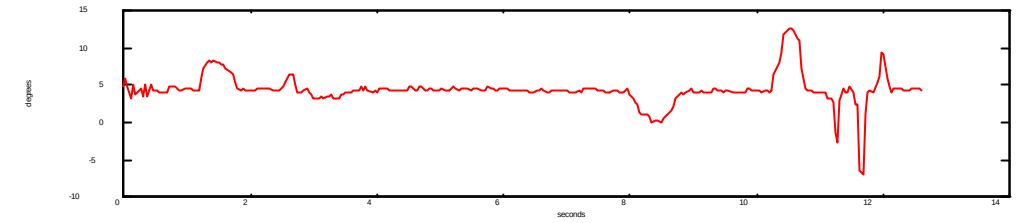

Right aileron deflection

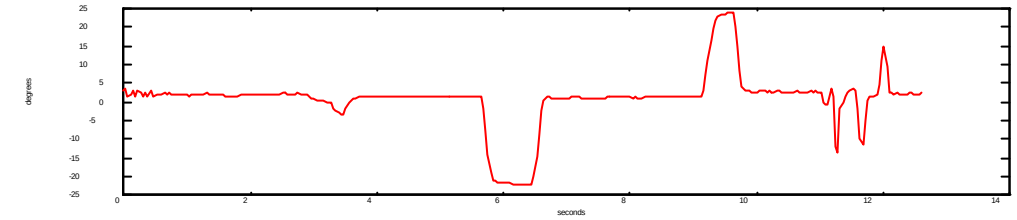

Rudder deflection

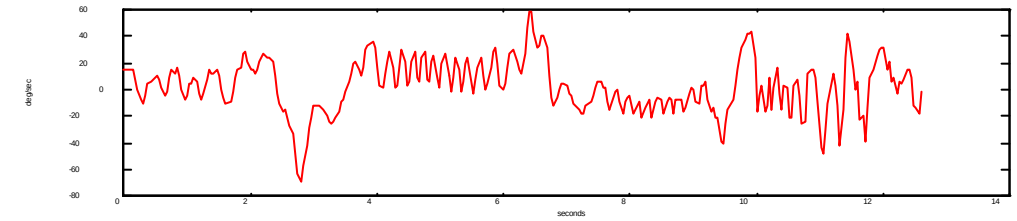

Pitch rate

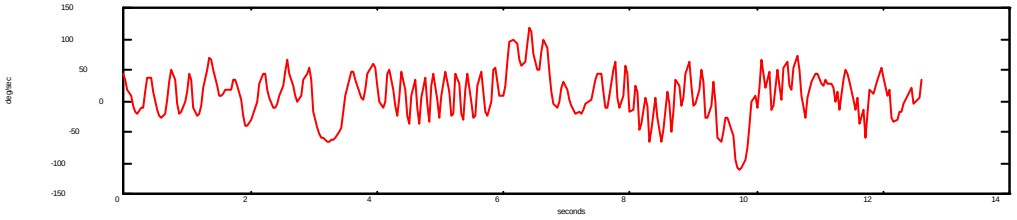

Roll rate

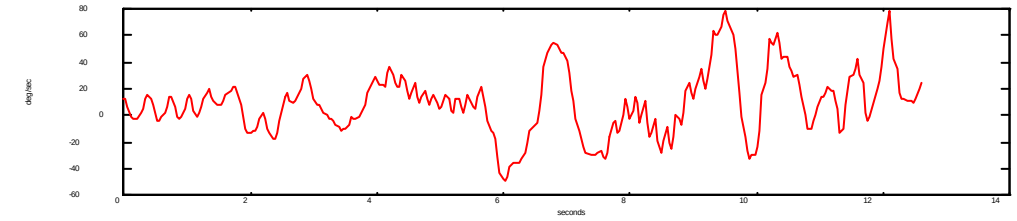

Yaw rate

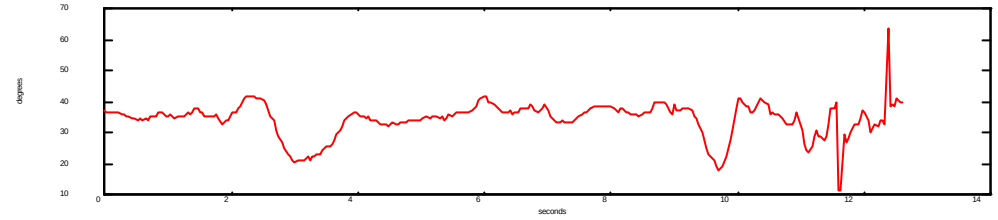

Angle of attack

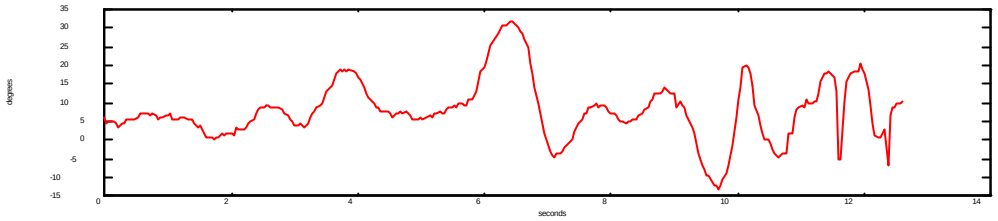

Sideslip angle

Figure A7- 2: Flight_3 records

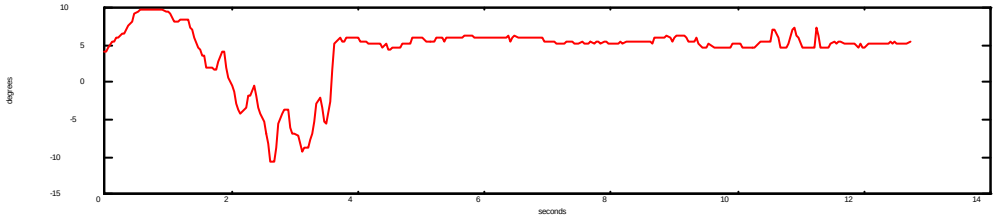

Elevator deflection

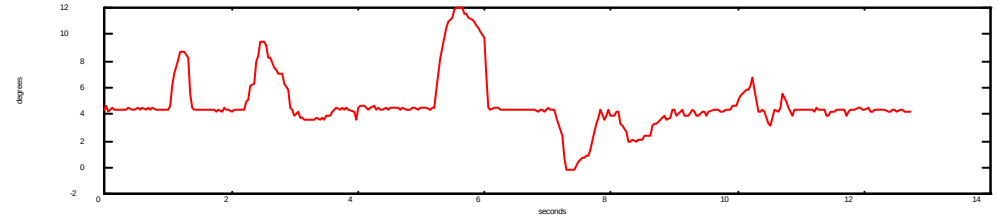

Right aileron deflection

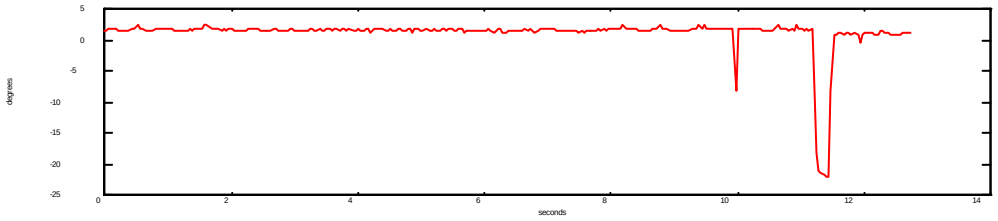

Rudder deflection

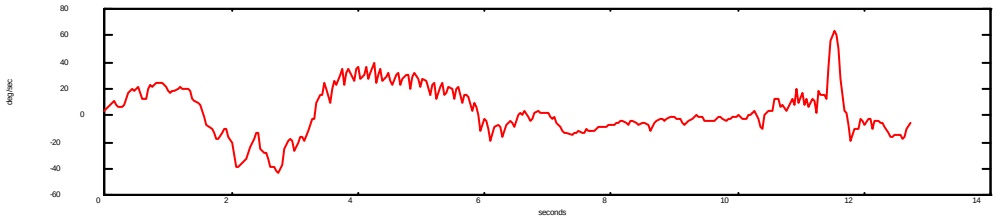

Pitch rate

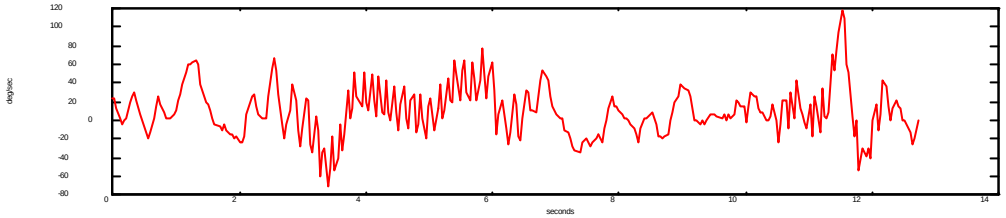

Roll rate

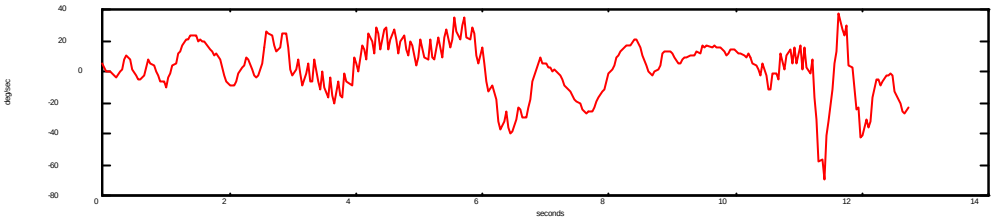

Yaw rate

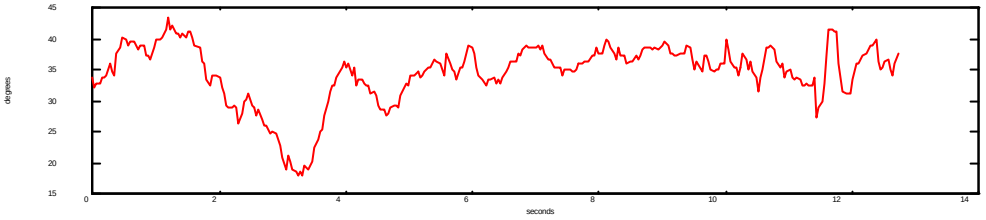

Angle of attack

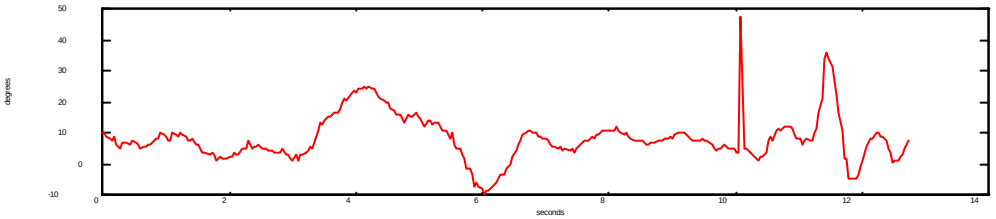

Sideslip angle

Figure A7- 3: Flight_4 records